NASA TECHNICAL NOTE

NASA TN D-4266

NASA TN D-4266

FLIGHT TEST OF A 15-FOOT-DIAMETER (4.6-METER) 120° CONICAL SPACECRAFT SIMULATING PARACHUTE DEPLOYMENT IN A MARS ATMOSPHERE

by Wayne L. Darnell, Allen B. Henning, and Reginald R. Lundstrom

Langley Research Center
Langley Station, Hampton, Va.

NATIONAL AERONAUTICS AND SPACE ADMINISTRATION • WASHINGTON, D. C. • DECEMBER 1967

NASA TN D-4266

FLIGHT TEST OF A 15-FOOT-DIAMETER (4.6-METER) 120° CONICAL SPACECRAFT SIMULATING PARACHUTE DEPLOYMENT IN A MARS ATMOSPHERE

By Wayne L. Darnell, Allen B. Henning,
and Reginald R. Lundstrom

Langley Research Center
Langley Station, Hampton, Va.

NATIONAL AERONAUTICS AND SPACE ADMINISTRATION

For sale by the Clearinghouse for Federal Scientific and Technical Information
Springfield, Virginia 22151 – CFSTI price $3.00

FLIGHT TEST OF A 15-FOOT-DIAMETER (4.6-METER) 120° CONICAL SPACECRAFT SIMULATING PARACHUTE DEPLOYMENT IN A MARS ATMOSPHERE

By Wayne L. Darnell, Allen B. Henning,
and Reginald R. Lundstrom
Langley Research Center

SUMMARY

An experiment was conducted in Earth atmosphere which simulated the deployment of an 85.3-foot-diameter (26.0-meter) ringsail parachute behind a spacecraft entering a Mars atmosphere when at an altitude of about 18 000 feet (5.5 kilometers). The spacecraft was a 120° cone having a base diameter of 15 feet (4.6 meters) and weighing 1687 pounds (765 kilograms). It was carried to an altitude of 130 300 feet (39.7 kilometers) above the Earth by a 26 000 000-ft^3 (736 240-m^3) balloon. After release from the balloon over the White Sands Missile Range, rockets propelled the spacecraft to a Mach number of 1.19 and a dynamic pressure of 6.4 lbf/ft^2 (306 N/m^2). The parachute was deployed by a parachute mortar. On-board instrumentation consisted of motion-picture cameras and a tape recorder which recorded the output from accelerometers and temperature sensors. Good data were obtained from all instrumentation. The parachute, which was deployed in a reefed condition, did not have sufficient drag to withdraw the instrumented payload from the spacecraft until it was disreefed. Temperatures measured at critical points in the spacecraft were within the desired operating range.

INTRODUCTION

For many decades a great interest has existed in the planet Mars. Because of its proximity to Earth, it is less difficult to study than most other planets and it also appears to have the best possibility of supporting life of any of the members of our solar system. Currently, it appears that the study of Mars can be furthered appreciably since rocketry has progressed to an extent where it is possible to send moderately sized instrumented payloads to the planet and guide them to a desired location. A rocket project designed to place an instrumented payload on the surface of Mars is NASA's Project Voyager. A description of the planetary entry problem for this mission may be found in reference 1.

One of the major problems of landing on Mars is to determine an acceptable method of decelerating a vehicle as it starts to enter the atmosphere of the planet. One proposed

method is to make the entry vehicle a high-drag body so that it will decelerate as it descends. After it has slowed down considerably and at an acceptable altitude above the surface a parachute would be deployed to reduce the velocity to a value where impact with the surface can be made without damage to the payload. Data on the Martian atmosphere obtained from Mariner IV indicate that the pressure at the surface of Mars is probably between 5 and 10 millibars instead of 10 millibars or greater as previously believed. Calculations show that entry velocities would be 12 000 to 16 000 ft/sec (3.7 to 4.9 m/sec). A spacecraft entering a 5-millibar atmosphere with these velocities produces a dynamic pressure of 5 to 6.5 lbf/ft^2 $(239 \text{ to } 311 \text{ N/m}^2)$ at an altitude of 15 000 to 20 000 feet (4.6 to 6.1 kilometers) and at a Mach number slightly above 1.

Reference 2, which is a widely accepted authority for parachute data, does not contain information concerning the opening characteristics of large parachutes in the transonic or supersonic Mach number range at such low dynamic pressures. Additional unknowns occur when the parachute is deployed in the wake of a bluff body such as a spacecraft.

The subject report contains a vehicle description, the flight test procedure, and performance of a test vehicle used for parachute deployment tests behind a spacecraft configuration at a Mach number of about 1.2 and an Earth altitude of 133 000 feet (40.5 kilometers) over the White Sands Missile Range, New Mexico. The spacecraft used was a 120° cone having a base diameter of 15 feet (4.6 meters). The parachute used for this test was an 85.3-foot (26.0-meter) constructed diameter ringsail parachute which is one of the candidates being considered for application to Voyager. The opening characteristics of the parachute used in this test are described in reference 3.

SYMBOLS

Measurements for this investigation were taken in the U.S. Customary System of Units. Equivalent values are indicated herein in the International System (SI) in the interest of promoting use of this system in future NASA reports. Details concerning the use of SI, together with physical constants and conversion factors, are given in reference 4.

A	body frontal area, feet^2 (meters^2)
A_L	longitudinal acceleration, g units
A_N	normal acceleration, g units
A_T	transverse acceleration, g units

C_D	drag coefficient
H	magnetic field strength (vector), milligauss (mG)
H_h	horizontal component of magnetic field strength (vector), milligauss (mG)
H_V	vertical component of magnetic field strength (vector), milligauss (mG)
M	Mach number
m	mass, slugs (kilograms, kg)
q	dynamic pressure, pounds/foot^2 (newtons/meter^2, N/m^2)
t	time, seconds
γ	flight-path angle, degrees

TEST CONDITIONS

The overall test plan consisted of deploying a parachute in the Earth's atmosphere at an altitude where the atmospheric pressure is the same as that expected to be encountered at the deployment altitudes on Mars. For a parachute deployment at transonic speeds the important quantities to be simulated are Mach number and dynamic pressure. Since maintaining full dynamic similarity for a scale model parachute presents some insurmountable problems, the parachute was made as close to the expected full scale as possible. Since rocket systems in the near future will be capable of sending several thousand pounds to Mars it was decided to make the parachute size for these tests as large as practical.

A study of possible configurations for the spacecraft, presented in reference 5, showed that a 120° cone was a very practical spacecraft shape for a Mars mission. It also appeared practical to incorporate an instrumented payload inside the spacecraft capable of being detached and to soft land only this instrumented payload instead of trying to soft land the entire spacecraft. The deployment of a parachute behind a blunt base object such as a 120° cone and the withdrawal of an instrumented payload from such a spacecraft therefore appeared to be conditions that should be duplicated insofar as possible.

The best current estimates of the Martian atmosphere from reference 6 indicate the probable limits of pressure at the surface to be between the 10-millibar (VM-3 or

VM-4) atmospheres and the 5-millibar (VM-7 or VM-8) atmospheres. These VM designations (the numerals indicate consecutive models) have been used in previous reports and designate theoretical Voyager-Mars engineering model atmospheres that may be encountered by the Voyager spacecraft (see ref. 6). Both reference 1 and unpublished data from Langley Research Center show that a spacecraft entering Mars atmosphere from a vehicle in orbit about Mars would have an entry velocity of between 12 000 and 16 000 ft/sec (3.7 and 4.9 km/sec). Corresponding entry angles would be approximately -7.5° and -15.5°. Results of calculations using these velocities and entry angles with the aforementioned predictions of the Mars atmosphere are presented as plots of dynamic pressure against Mach number in figure 1. A ballistic coefficient m/C_DA of 0.32 slug/ft^2 (50 kg/m^2) was used for this analysis as it was believed to be a reasonable value for a Voyager-type spacecraft. Lower values of the ballistic coefficient would cause the spacecraft to lose its velocity at a higher altitude. Values of Mars altitude are labeled in figure 1. It can be seen that the highest Mach number at a 17 000-foot (5.18-kilometer) altitude occurs with the VM-8 atmosphere where $M = 1.2$ and $q = 5.7$ lbf/ft^2 (273 N/m^2). It may also be noted that the curves of q against M fall within a rather narrow band even though they do include a wide altitude range.

METHOD OF TEST

Since a zero-pressure balloon (ref. 7) appeared to be the most feasible method of conducting this particular test, the NASA contracted with the Air Force Cambridge Research Laboratory to design, procure, and launch a balloon system capable of carrying a 1730-pound (785-kilogram) spacecraft to an altitude of 130 000 feet (39.6 kilometers). The resulting tandem balloon system utilized a 175 000-ft^3 (4960-m^3) launch balloon and a 26 000 000-ft^3 (736 240-m^3) main balloon. The launch balloon was made of a $\frac{1}{2}$-mil (12.7-micrometer) Mylar with dacron reinforcing threads (scrim) bonded to its surface and weighed 486 pounds (220.4 kilograms). The main balloon was made of a $\frac{1}{3}$-mil (8.4-micrometer) Mylar with dacron scrim and weighed 3304 pounds (1499 grams). A 100-foot-diameter (30.5-meter) parachute was inserted between the balloon and the load as a safety measure for the case of a balloon malfunction and to let down balloon instrumentation after spacecraft release. The main balloon was encased in a protective sleeve. The entire assembly was stretched out on an airplane runway and a measured amount of helium was valved into the launch balloon. The launch balloon was then allowed to lift up the encased main balloon and was restrained against the action of the wind by the mainstay. Directly beneath the safety parachute was the load bar from which was suspended the spacecraft, ballast hoppers capable of carrying 1200 pounds (544 kilograms) of fine iron granules, and instrumentation consisting of two command systems each having 9 channels. The load bar was suspended from a large mobile crane

at the time of launch. Figure 2 is a sequence of pictures showing (a) layout of the balloon, (b) inflation of the launch balloon, (c) the reel up of the system showing the main balloon in its protective casing and also the safety parachute, and (d) the balloon system just after launch. The balloon assembly was released from the mainstay and then from the crane with pyrotechnic releases at the time of launch. About one-fourth of the protective sleeve around the main balloon is stripped off at launch. As the system rises in altitude the lower air density atmosphere allows the helium to expand gradually through the transfer duct into the main balloon; this expansion tears off the remainder of the protective sleeve. The balloon then becomes a zero-pressure balloon.

The launch was made from Walker Air Force Base, New Mexico, which was about 100 miles (160.9 kilometers) east of the White Sands Missile Range (WSMR). The prevailing easterly wind above 100 000 feet (30.5 kilometers) during the summer period carried the balloon to the west. The winds were carefully monitored in advance to insure that the balloon would follow an acceptable ground track. At the proper location over the WSMR the spacecraft was released from the balloon load bar by using the command system.

The spacecraft was carried under the balloon with its longitudinal axis tilted upward at a 60° angle as shown in figure 3. After release the spacecraft was in free-fall for about 4 seconds. Then the mechanical timer, which was started by a lanyard pull at release, ignited the rocket motors. After rocket motor burnout a parachute was deployed. As the parachute opened it withdrew an instrumented payload from the spacecraft. This sequence of events is displayed in figure 3. On-board and ground-based instrumentation measured and recorded flight events and data. Post-flight recovery was made by WSMR and NASA personnel.

SPACECRAFT DESCRIPTION

The spacecraft consists of two integral parts called the aeroshell and the payload. The payload was a weighted instrument package that was withdrawn from the aeroshell by the test parachute. The following description presents the two parts individually.

Aeroshell

The aeroshell was a 15-foot-diameter (4.6-meter) 120° flat based cone with a nose radius of 5 inches (12.7 centimeters). A sketch of the spacecraft is presented in figure 4(a) and photographs are shown in figures 4(b) and 4(c). The aeroshell was constructed in sections or quadrants; each quadrant was of aluminum stringer construction with $\frac{1}{32}$-inch (0.8-millimeter) aluminum skin on the cone face and an annular sector of $\frac{1}{64}$-inch (0.4-millimeter) aluminum skin on the rear face. The center section of the aeroshell or the hub, to which the aeroshell quadrants are mounted, was of a welded

aluminum plate construction with a cylindrical compartment in the center for the payload. Around the payload compartment was a ring of 12 Falcon M58A2 solid-fuel rocket motors each modified with a 33.5° canted nozzle adapter. The canted nozzle permitted the thrust line of each rocket motor to pass near or through the center of gravity along the longitudinal axis. This alinement minimized angular disturbances to the spacecraft due to slight variations and asymmetries in thrust or burning time of the 12 rocket motors. Several static test firings were made at sea level and at a simulated flight altitude of 133 000 feet (40.5 kilometers). Typical thrust-time curves are shown in figure 5. These static tests showed that nozzle closures which maintained approximately a sea-level pressure inside the motors were needed for positive ignition.

The center of gravity was located within 0.020 inch (0.51 millimeter) of the spacecraft longitudinal axis. An illustration of the thrust line intersection with relation to the center of gravity of the complete spacecraft is shown in figure 6. In addition, misalinement in mounting the motors within the vehicle in the extreme case could cause the thrust vector to be displaced laterally about 0.046 inch (1.17 millimeter) from the center of gravity. Characteristics of weight, center of gravity, and estimated moment of inertia are presented in table I.

On the rear face of the aeroshell, two cameras, each with a field of view of 52° by 38° and a frame rate of 64 frames per second, were mounted looking rearward. These cameras were installed to photograph the ejection of the parachute bag, the opening of the parachute, and extraction of the payload from the spacecraft.

A C-band transponder mounted in the aeroshell was used for radar tracking. Antennas for transmission of the modulated C-band signal were placed in the nose of the aeroshell and on the camera bracket located on the rear face of the aeroshell. Two recovery beacons were positioned in the aeroshell to aid in its location and recovery after its impact on the range. The antennas for these recovery beacons consisted of four 9-inch (23-centimeter) lengths of music wire placed 90° apart on the rear face of the spacecraft.

Additional instrumentation consisted of 9 thermistors placed at various locations throughout the aeroshell. These thermistors were used to indicate any unusual temperature variation due to the extended time spent at high altitude before the spacecraft reached the free-fall point. The various locations of the thermistors are presented in table II. The temperature data were commutated and recorded on the on-board tape recorder in the payload section.

Two magnetic aspect sensors were mounted rigidly on the aeroshell frame. Both probes were situated so that they would lie in a common horizontal plane while the spacecraft was suspended in flight attitude under the balloon. The north (positive) pole of probe 1 was pointed in the direction of the spacecraft nose whereas that of probe 2 was

rotated 90° clockwise. The output from the magnetometer system modulated the signal of the C-band transponder which allowed the ground radar to reproduce the voltage outputs. These magnetometer readings were used to determine spacecraft pointing azimuth before release from the balloon for range safety considerations and as a radar tracking aid. Further details on this application of aspect magnetometers can be found in the appendix.

The spacecraft was attached to the balloon instrument bar by a tension rod which contained an explosively actuated tension rod separator. The spacecraft was held at some distance from the bar by a standoff truss that fitted into three mounting pads built into the aeroshell structure. Those pads were designed so that, when the tension rod separator was actuated by ground command, the spacecraft would fall from the standoff truss without any binding or tipoff. Figure 4(c) shows the balloon load bar and spacecraft with the tension rod attached and the standoff truss in place on the mounting pads.

Payload

The payload was cylindrical in shape with a smaller cylinder protruding slightly from one end and a frustum of a cone on the other end. It was constructed of welded magnesium plate designed to weigh approximately 600 pounds (272.2 kilograms) which included instrumentation and ballast, the ballast weighing approximately 325 pounds (147.4 kilograms). A sketch of the payload is presented in figure 7 and photographs are shown in figures 8(a) and 8(b). The actual physical characteristics of the payload are given in table I. The outside cylindrical surface of the payload was made of aluminum with cork and aluminum foil bonded to its surface for thermal protection. A teflon ring and magnesium strip runners were fitted between the payload and the inside hub surface to permit the payload to slide easily out of the hub when the parachute was opened. The payload was released from the aeroshell by an explosive nut attached to the stud on the front end of the ballast. The three major parts of the payload were the mortar and parachute assembly, instrumentation deck, and the ballast.

The mortar-parachute assembly was fitted into a compartment in the center of the payload along the longitudinal axis so that the parachute could be ejected out of the back of the payload. A sketch of the mortar-parachute assembly is shown in figure 9. When the powder charge was ignited the expanding gases escaped from the breech through the erodible orifice into the space behind the sabot. The erodible orifice was designed to give the desired pressure time history in the mortar tube during its operation. The results from test firings of the mortar are presented as pressure and thrust variation with time in figure 10. From these test firings the mortar muzzle velocity was found to be about 134 ft/sec (40.8 m/sec). The pressure in the mortar barrel pushed against a sabot which in turn pushed against the packed parachute bag to force the mortar cover

plate rivets to shear off. This sudden release of pressure ejected the mortar cover plate, parachute bag, and sabot from the mortar barrel. The cover plate was attached to the parachute bag. The sabot was attached to a breakaway tether that was fastened to the aeroshell hub. The tether imparted a sideways force to the sabot before breaking so that the sabot would not interfere with the parachute suspension lines. The complete parachute (canopy and suspension lines) was packed in the parachute bag with a density of 41.5 lbm/ft^3 (664 kg/m^3).

The parachute canopy used in this flight test had a diameter of 85.3 feet (26.0 meters) and was of a ringsail type with 13 sails. One sail row, the ninth from the crown, was removed to increase the parachute porosity. Seventy-two 78-foot (23.8-meter) suspension lines were attached to the canopy and joined together at the payload-bridle junction. Three 6-foot (1.8-meter) parachute bridles are attached to the payload. A sketch of the parachute is shown in figure 11. When the parachute was deployed it opened in a reefed condition because it was held by a reefing line threaded through rings in the parachute skirt. After the suspension lines were drawn out of the parachute bag, lanyards incorporated into suspension lines pulled the firing pins on four reefing line cutters which had 4-second delay fuses.

The payload instrumentation included three cameras, four accelerometers, five thermistors, a tape recorder, two recovery beacons, and two programers. One camera, with a field of view of 43.6° by 33°, looked out of the front of the payload through a hole in the ballast to record the payload leaving the aeroshell and ballast release, and to observe possible ground identification points for payload motion studies. Another camera, with a field of view of 52° by 38°, looked out the side of the payload to observe the horizon for payload motion studies. These two cameras ran at a film rate of 16 frames per second. The third camera was a high-speed camera, with a field of view of 65° by 48.4°, which looked out of the back of the payload and recorded the ejection and opening of the parachute at the rate of 500 frames per second. All on-board cameras had a timing code superimposed on the film. Of the four accelerometers, two with a range of ±50g and ±100g measured the longitudinal acceleration, one with a range of ±5g measured the normal acceleration, and the other with a range of ±5g measured the transverse acceleration. Five thermistors, labeled channels 10 to 14 in table II, were located in the payload. The measurements from the accerometers and all the thermistors were recorded by a tape recorder placed in the instrument deck of the payload. The event timing and the camera timing were also recorded by the tape recorder. Two radio beacons were installed in the payload to aid in the recovery after the payload had impacted on the ground. Four antennas for these beacons were spring wires that extended perpendicularly to the side of the payload. (See fig. 8.) Duplicate programers were installed in the payload section to initiate the various events in their proper sequence and were

started by a lanyard pull when the spacecraft was dropped from the balloon load bar. The nominal sequence of events set into the programer is given in table III.

The ballast was a solid steel cone frustum that weighed 323 pounds (146.5 kilograms). A conical hole was machined into the ballast for camera viewing. Photographs of the ballast attached to the payload are shown in figure 8. The same type of explosive nut used to separate the payload from the aeroshell separated the ballast from the payload. The ballast was dropped at a predetermined time in order to change the descent rate of the parachute and load.

ACCURACY

The estimated accuracy of the data from the spacecraft on-board instrumentation together with the accuracy of measured quantities from radar and theodolite position data are presented herein. The following best estimate represents the known accuracy of some components, experience from the use of other components, and scatter in the data.

An excellent check point for the accelerometers existed immediately after the spacecraft was released from the balloon. During this period of free fall the spacecraft was extremely close to being in a zero g condition and the data were calibrated to this point. The errors in accelerometer readings are as follows:

Longitudinal acceleration during thrust	±0.3g
Longitudinal acceleration other than thrust period	<±0.2g
Normal or transverse acceleration	<±0.05g

The temperature measurements are believed to be accurate within ±5° C.

The space position data were determined by a modified FPS-16 radar set and by theodolite. From the scatter in the data and the agreement between the two methods it is believed that the position data were measured to within ±25 feet (7.6 meters).

The velocity with respect to the ground was obtained by differentiating the space position. The winds at altitude were determined with an Arcas sounding rocket. The spacecraft velocity was determined from the ground speed and measured wind data. It is believed that at a velocity of 1200 ft/sec (366 m/sec) the velocity is accurate to about ±30 ft/sec (±9.1 m/sec), at 600 ft/sec (182.9 m/sec) the velocity is accurate to about ±20 ft/sec (±6.1 m/sec), and at 150 ft/sec (45.7 m/sec) the accuracy is ±15 ft/sec (±4.6 m/sec).

Local atmospheric conditions were measured with a rawinsonde up to 128 000 feet (39 kilometers). The density above 128 000 feet (39 kilometers) was obtained by extrapolating these data; the U.S. Standard Atmosphere, 1962 (ref. 8) was used as a guide for the

extrapolation. The measured density from 110 000 to 128 000 feet (33.5 to 39 kilometers) was consistently 10 percent higher than values from the U.S. Standard Atmosphere, 1962. Measurements of density at this altitude are believed to be within ±5 percent. The combined errors in density and velocity will produce an error in dynamic pressure near its maximum value of about ±12 percent.

The possible error of 5^{o} C in the measurement of ambient temperature causes an error of about 1 percent in the determination of the speed of sound. This temperature accuracy together with the velocity accuracy mentioned previously resulted in a probability of the Mach number being within ±3 percent near maximum Mach number (M = 1.2) and about ±4 percent at M = 0.6.

The magnetometers used to produce spacecraft azimuth data are believed to have provided results which were accurate to within 6^{o}. However, pitching motions, which may have been felt by the spacecraft at very low amplitude, could increase azimuth data to unpredictable values. After surveying the post-flight magnetometer data it appeared that the amount of pitching motion was quite small and that errors attributable to this source should not exceed 6^{o}. The overall accuracy of the magnetometer results appeared to be within $\pm 12^{o}$. Additional remarks concerning magnetometer errors will be found in the appendix.

RESULTS AND DISCUSSION

The results obtained from the flight test of the balloon launched spacecraft for investigating parachute deployment in planetary atmospheres are presented herein. Since the balloon and spacecraft are two separate entities combined so that the balloon acts as a launching platform for the spacecraft, their data will be presented separately. The analysis of the parachute data is beyond the scope of this report, but some of the data are shown herein as results obtained from the satisfactory operation of the various components of the overall configuration. Further details on the operation and performance of the parachute used in this investigation may be found in reference 3.

Balloon

The wind profile was measured at both the balloon launch site and at WSMR to determine in advance that the balloon would drift over the desired section of WSMR. Particular emphasis was placed on the wind velocity and direction at the expected equilibrium or float altitude. The launch was made from Walker Air Force Base, New Mexico, at 7:17 a.m., MST on August 30, 1966. Figure 12, which is an altitude time history of the balloon flight, shows that the balloon had an average rise rate of about 1230 ft/min (375 m/min) up to 100 000 feet (30.5 kilometers). The rise rate then

gradually decreased until a float altitude of about 126 500 feet (38.6 kilometers) was reached. Ballast was then metered out over a 30-minute period and the float altitude increased to 130 300 feet (39.7 kilometers) just before spacecraft release. The ballast was retained until late in the flight because the winds were more favorable at the lower altitude. The balloon ground track presented in figure 13 shows the change in direction from approximately 255° azimuth to 270° azimuth after the balloon had climbed to 130 000 feet (39.6 kilometers). Figure 12 shows that dropping 1200 pounds (544 kilograms) of ballast increased the float altitude by approximately 3800 feet (1158 meters). Figure 14 shows the balloon as observed from an aeroshell camera immediately after the spacecraft had passed the balloon during its upward flight.

After release of the spacecraft, the main balloon ruptured. The ruptured balloon, safety parachute, and instrument bar became entangled and fell to Earth thus destroying all the balloon instrumentation and equipment. The exact time of the rupture is not known but the camera film indicated it was between 41 and 55 seconds after spacecraft release. Earlier release of the balloon instrumentation and safety parachute was not made in order to avoid additional radar targets in the vicinity of the test.

Magnetometer Data

Readings from the magnetometers were made intermittently for spacecraft pointing azimuth determinations beginning 14 minutes before the release of the spacecraft from the balloon. At this time balloon ballast release had just been concluded. The spacecraft azimuth data covering this period are presented in figure 15. Three slightly differing processes were used to obtain these data. Voltmeter data were read and reduced manually during the flight; magnetic tape and oscillograph data were recorded for postflight reduction and study. Magnetic tape data are considered the best of the three so that the estimated curve generally favors these data in figure 15.

The spacecraft appeared to be in an oscillatory rotation about its axis of suspension under the balloon. The periods of these oscillations average about 280 seconds showing angular velocities as great as 90° per minute. Little damping of the spacecraft oscillations can be seen in the three cycles present. At the time of spacecraft release the pointing azimuth was determined by the magnetometers to be approximately 116°.

The high spacecraft turning rates apparent in the data had not been anticipated and azimuth calculating procedures had not been geared to accommodate them. Consequently, useful predictions of the spacecraft azimuth at release were not available for the use of the radar operators. It is believed that rotational motions induced on the suspended spacecraft system resulted from moments produced during balloon ballast release. The dropping of balloon ballast should take place further in advance of the spacecraft release to allow a longer damping period to exist in order to reduce both the amplitude and

angular rate of twisting. It is believed that earlier balloon ballast release and faster spacecraft pointing azimuth calculating methods will make it feasible to use the magnetic aspect sensor to predict spacecraft azimuth on similar flights in the future.

Spacecraft Performance

When the balloon system had reached its final float altitude and had traveled approximately halfway across WSMR, a command from the ground activated the tension rod separator and the spacecraft was released from the balloon load bar. The altitude of the spacecraft at the time of release was 130 300 feet (39.7 kilometers). As the spacecraft dropped away from the load bar the programer and instrument recorder were started by two lanyards attached to the load bar. Release time (the time at which the programers and instrument recorder were started) is considered zero time and all data presented herein are referred to this time. The sequence of events as recorded from payload instrumentation and camera data are presented in table III. Differences between the nominal and flight event times are probably due in part to the fact that the lanyards had different amounts of slack so that they disconnected at slightly different times. Some of the events recorded in table III were not actuated by the programer but were sufficiently significant to be mentioned herein. From the flight test instrumentation records it is shown that at 3.67 seconds after spacecraft release the rocket motors fired and propelled the spacecraft to test velocity and an increased altitude. At 6.98 seconds the parachute mortar fired and the parachute bag was ejected. At 7.61 seconds, the time indicated for parachute line stretch, the parachute suspension lines were completely out of the parachute bag. The payload separation nut was fired at 7.75 seconds which unfastened the payload from the aeroshell. After line stretch the canopy emerged from the parachute bag. From observation of the parachute bag in the pictures taken from the aeroshell cameras it was determined that the parachute canopy was completely out of the bag by 7.99 seconds. When the parachute opened to its reefed condition the payload was expected to be withdrawn from the aeroshell, but apparently the opening of the reefed chute in the wake of the blunt body of the spacecraft did not produce enough force to pull the payload completely out of the aeroshell. However, the force produced by the reefed opening of the parachute did withdraw the payload enough to electrically disconnect the payload from the aeroshell at 8.56 seconds. Motion-picture film from the on-board cameras indicated that after disreefing the payload began to come out of the aeroshell at 13.83 seconds and had completely cleared the aeroshell at 14.18 seconds. The ballast was released from the payload at 29.74 seconds. This sequence of events presents a background for the detailed flight data that follow. Radar and cinetheodolite data are combined to give the complete trajectory.

Trajectory.- When the spacecraft was released from the balloon system the angle of elevation was expected to remain near 60^{o} during the 4-second free fall. The altitude

time history from release to 180 seconds is presented in figure 16 and the velocity time history for the same period of time is presented in figure 17. The velocity presented is true airspeed as determined by differentiating the radar position data and modifying it to account for the effect of wind. Two curves are shown after aeroshell-payload separation, one for the aeroshell and one for the payload-parachute combination. In order to better evaluate the events during the prime test time, an expanded view of altitude and velocity is presented in figure 18 from 0 to 24 seconds. Comparison of the actual flight trajectory with the nominal trajectory is made and various events are marked. The variation of drag coefficient with Mach number used in the nominal trajectory calculations was estimated from unpublished data and is presented in figure 19. It should be noted in figure 18 that the nominal curves show the payload-parachute system separating from the aeroshell at 8.5 seconds when the parachute opened in its reefed condition. As previously stated, separation did not occur until about 14.2 seconds or after the parachute had disreefed. The maximum velocity obtained was about 50 ft/sec (15.2 m/sec) lower than expected and occurred at a higher altitude. A plot of altitude variation with velocity for the aeroshell and payload-parachute is shown in figure 20.

The variation of flight-path elevation angle with time is plotted in figure 21 from 0 to 32 seconds. This plot shows that at 4 seconds the flight-path angle is greater than 60° which indicates some pitch-up of the spacecraft during free fall and possibly pitch-up from rocket motor misalignment during rocket motor burning. The flight-path angle of the payload-parachute combination decreased rapidly after separation because of the large drag of the parachute and the decreased weight of the parachute load. Apogee of the payload-parachute occurred at about 23 seconds. At 29.74 seconds when the ballast was released, the flight-path angle was approximately -72°. The roll rate of the spacecraft for the first 20 seconds as observed on the motion-picture film from the aeroshell cameras was approximately 4 revolutions per minute.

The variation of altitude with horizontal range for the early part of the aeroshell and payload-parachute trajectory is presented in figure 22. Since the aeroshell and payload-parachute fell at low velocities the high-altitude winds influenced their trajectories. Their flight paths were constantly changing with the variation in wind speed and direction as they descended through the various wind layers. The ground track of the aeroshell and payload-parachute is presented in figure 23. The areas of impact show the result of the drift caused by the winds. The complete ground track of the payload-parachute is not shown because it was not tracked beyond 180 seconds.

The variation of Mach number and dynamic pressure with time for the aeroshell and payload-parachute is presented in figure 24 from 0 to 24 seconds which is the prime data period. A crossplot of these data is compared with the nominal values and is shown as the variation of dynamic pressure with Mach number in figure 25. Pertinent flight

events are pointed out on both curves. The maximum Mach number of the spacecraft was 1.19 and the maximum dynamic pressure obtained was 6.4 lbf/ft^2 (306 N/m^2). These conditions correspond to those anticipated at about 15 000 feet (4570 meters) above Mars in the 5-millibar (VM-8) atmosphere. The mortar fired at a Mach number of about 1.16 and the parachute opened to the reefed condition at a Mach number of about 1.06 and a dynamic pressure of about 4.7 lbf/ft^2 (225 N/m^2). This condition simulated reefed canopy opening in a 5-millibar (VM-8) atmosphere at approximately 18 000 feet (5490 meters) above Mars. The parachute-opening dynamic pressure and Mach number conditions were lower than expected because of the slightly lower velocities obtained. These flight data and the tentative Mars atmosphere entry corridor from figure 1 are combined and presented in figure 26 to compare the regime of the required and obtained data. This figure shows that it is possible to obtain the required data in or near the entry corridor by using this system of balloon launched spacecraft.

Acceleration.- The data obtained from the accelerometers from 3.0 to 29.7 seconds are presented in figure 27. From 0 to 3.0 seconds no data are presented since all the accelerometers read essentially zero. Data beyond 29.7 seconds were unavailable because the accelerometers were damaged by the explosive nut which released the payload ballast.

Figure 27(a) presents the accelerations during the rocket motor thrusting period. A slight thrust misalignment is indicated by the readings on the normal and transverse accelerometers particularly near rocket burnout. The rocket motors appeared to have a very gradual thrust tail-off and were producing some thrust even after mortar firing; therefore, the deceleration level before mortar firing is not a true indication of spacecraft drag. The parachute mortar fired at $t = 6.98$ seconds (fig. 27(b)), and produced a high sharp peak on all accelerometer traces.

From 7.06 to 7.61 seconds the suspension lines were being withdrawn from the parachute bag. It was estimated from preflight ground tests that the force needed for this was on the order of 65 to 135 pounds (289 to 601 newtons). At 7.61 seconds line stretch occurred indicating that the suspension lines were completely withdrawn from the parachute bag. The ensuing longitudinal deceleration variations were believed to be produced as the individual sails were pulled from the parachute bag. The low deceleration peak at 7.73 seconds is believed to have occurred when that part of the canopy where a sail was omitted was pulled from the bag. The payload separation nut fired at 7.75 seconds producing a shock felt by all the accelerometers. This freed the payload to move longitudinally in the aeroshell. At about 7.95 seconds the parachute was fully extended and the bag had freed itself from the parachute. The bag was observed to be free by the aeroshell cameras at 7.99 seconds. (See table III.)

The parachute bag traveled from the mortar muzzle to the canopy crown, a distance of 129 feet (39.3 meters), in 0.97 second for an average velocity with respect to the spacecraft of 133 ft/sec (40.5 m/sec).

After 7.95 seconds there was a gradual increase in longitudinal deceleration as the parachute attempted to open to its reefed condition. At about 8.50 seconds the drag of the parachute was enough to start payload movement. The electrical connection between the payload and aeroshell was disconnected at 8.55 seconds. Between this point and 8.88 seconds it appears that the payload became wedged in the aeroshell and no further withdrawal of the payload occurred at this time. As the parachute fluttered around in the wake in its reefed condition from $t = 8.88$ to 12.84 seconds it varied its pull on the spacecraft and variable oscillations were sensed by the longitudinal accelerometer. It is believed that the lip of the payload was out of the aeroshell cavity so that small normal and transverse motions were possible.

At approximately 12.84 seconds the reefing lines were cut and disreefing began. As the parachute opened, the pull on the payload increased as is seen by the increased longitudinal deceleration in figure 27(c). Sporadic movements of the payload occurred up to 13.76 seconds. Definite payload movement was detected by the aeroshell cameras at 13.83 seconds. Observation from one of the payload cameras shows that the payload was completely free of the aeroshell by 14.18 seconds. After the payload was free of the aeroshell the sporadic vibrations ceased but some sinusoidal oscillations continued for a short time and ceased as the parachute emerged from the wake of the aeroshell. An analysis of the parachute data is presented in reference 3.

Parachute system.- Some photographic data are presented herein in order to illustrate the results of the mortar firing and the parachute opening. Figure 28 shows the views from aeroshell camera 1 of (a) the parachute bag leaving the mortar, (b) the canopy emerging from the parachute bag, (c) the inflation of the reefed canopy, and (d) the payload leaving the aeroshell with an almost fully inflated parachute. Figure 29 presents a similar sequence of photographs at different flight times taken from aeroshell camera 2 and shows (a) the parachute bag leaving the mortar, (b) the parachute bag and sabot during sabot separation, (c) the parachute opening to the reefed condition, and (d) the parachute fully disreefed after the payload has left the aeroshell. These two figures illustrate the successful deployment and opening of the parachute at transonic speed and low dynamic pressure.

Atmospheric data.- Wind velocity data were obtained from an atmospheric sounding rocket and a rawinsonde balloon which together covered the entire data range of the flight. Temperature and pressure data however were obtained only by rawinsonde which gave no data above 128 800 feet (39.3 kilometers). Data above this altitude were obtained by extrapolating the rawinsonde data with the U.S. Standard Atmosphere, 1962 as a guide.

The pressure and temperature data used for reduction of data in this report are presented in figures 30(a) and 30(b). It may be observed that the altitudes corresponding to the measured pressures are about 2000 feet (610 meters) higher than would be indicated by the U.S. Standard Atmosphere, 1962.

Temperature data.- Temperature measurements were made at selected places throughout the spacecraft in order to find out what effect the long period of time from balloon launch to spacecraft release had on the internal temperature of various components. Some of the vital components such as batteries and cameras had thermostatically controlled heaters to keep the temperature of the components in their best operating range. The location of the various thermistors is given in table II. The temperature readings recorded from these thermistors are tabulated in table IV. Temperature data from aeroshell thermistors 1 to 9 were recorded from spacecraft release time until the payload was electrically disconnected from the aeroshell. Data from payload thermistors 10 to 14 were recorded from spacecraft release time until the recorder was turned off. Most of the temperatures remained constant throughout the recording time except those of the rocket motor cases (thermistors 1 to 4) which rose after rocket motor thrusting because of propellant residue burning inside the empty cases. The temperature of the skin on the outer edge of the aeroshell (thermistor 7) was high and rose slightly probably because of exposure to direct radiation from the sun during the time it was suspended beneath the balloon.

Aeroshell and payload recovery.- In figure 23 the impact points of the aeroshell and the payload-parachute are indicated. These points are widely separated because both objects were carried by local winds during the descent. Figure 31 shows a photograph of the aeroshell as it was found at the point of impact. The aeroshell landed in a marshy area. The nose of the aeroshell was extensively damaged, although the major part of the structure showed little or no damage. Neither the aeroshell cameras nor the film in the cameras received any injury. The payload-parachute landed on a mountain side. The area of impact was rugged and somewhat inaccessible, therefore no photographs were taken of the payload at its impact point. The parachute and payload were recovered with little damage to either. Photographs taken after payload recovery are presented in figure 32. The cameras and tape recorder were not damaged and all planned data were obtained.

CONCLUSIONS

The flight test of a 15-foot-diameter (4.6-meter) 120° conical spacecraft was conducted by using a large zero-pressure balloon as a launch platform. The balloon lifted the spacecraft to 130 300 feet (39.7 kilometers). After the spacecraft was released from the balloon, rockets propelled it to the desired Mach number and dynamic pressure. At

these conditions a parachute was deployed to simulate deployment conditions during a Martian entry. The following conclusions were drawn from this experiment:

1. The 26 000 000-ft^3 (736 240-m^3) balloon performed well as a launch platform for the test. It carried the spacecraft to an altitude of 130 300 feet (39.7 kilometers) where the pressure was 3.2 millibars.

2. The structural and mechanical design of the spacecraft was proven to be satisfactory. All instrumentation as well as pyrotechnic devices performed as expected. The on-board cameras and the tape recorder were recovered from the impacted aeroshell and payload without damage to themselves or their flight data.

3. The rocket motors propelled the spacecraft to a maximum Mach number of 1.19 and dynamic pressure of 6.4 lbf/ft^2 (306 N/m^2). This condition corresponded to entry into a 5-millibar (VM-8) Martian atmosphere when at approximately 15 000 feet (4570 meters) above the Martian surface.

4. The ringsail parachute canopy opened in a reefed condition at a Mach number of 1.06 and a dynamic pressure of 4.7 lbf/ft^2 (225 N/m^2). This condition simulates reefed canopy opening in a 5-millibar (VM-8) atmosphere at approximately 18 000 feet (5490 meters) above Mars.

5. The parachute opening in the wake of the spacecraft did not have sufficient drag to withdraw the instrumented payload from the aeroshell until parachute disreefing.

6. On-board cameras produced good quality motion-picture films which clearly documented the performance of the parachute mortar and the behavior of the parachute throughout deployment. From this evidence it was shown that the mortar ejected the parachute in the manner required and provided more than the required minimal muzzle velocity.

7. Measurements of the temperature of various components and at selected places in the spacecraft showed that the temperatures were within the desired operating range.

8. A system employing two aspect magnetometers to predict the pointing angle of the spacecraft at the time of release could not perform this function satisfactorily because of rather large amplitude rotary oscillations caused by the late dropping of balloon ballast.

It is believed that a faster readout and data reduction method and also the dropping of the balloon ballast earlier in the flight could make this method useful on future flights.

Langley Research Center,
National Aeronautics and Space Administration,
Langley Station, Hampton, Va., July 27, 1967,
709-08-00-01-23.

APPENDIX

MAGNETIC ASPECT SENSORS

Radar tracking requirements on the spacecraft indicated the need for forecasting the general direction in which it would be propelled after its release from the balloon. It was determined that knowledge of the spacecraft pointing azimuth (aspect angle) to within 13^{o} would be sufficient. In addition it was believed that for a normal balloon-spacecraft flight the spacecraft pitching motions would be very small in the period just prior to spacecraft release. With these considerations the simplified aspect magnetometer system was chosen to meet the need for spacecraft pointing azimuth data.

In this installation both probes are expected to sense only the horizontal component of the Earth magnetic field. The magnetic field characteristic of the area of WSMR is diagramed in figure 33. It should be noted that the magnetic field vector H of figure 33(a) dips approximately 61^{o} (inclination) at an azimuth of approximately 12.5^{o} (declination).

The electronics of each probe produce a voltage essentially linear with the field strength sensed. The voltage field-strength curve for the type of magnetic aspect sensor used on the spacecraft was approximately linear. The resulting variation of pointing azimuth (degrees clockwise from magnetic north) with horizontal field strength and hence with voltage output is the simple cosine curve of figure 34. It will be noted, however, that the curve is double-valued, thus a choice of two azimuths for each voltage is produced. This double value is to be expected since the magnetic probe will sense the same field strength for a given angle to magnetic north regardless of whether it is on the east or west side. To overcome this ambiguity two probes can be used at right angles to each other in the horizontal plane to provide a "match." This arrangement can be used to show that one of the two indicated azimuth values of probe 1, plus the 90^{o} difference between probes, must match one of the two indicated azimuth values of probe 2. This fact is illustrated in figure 35 where probe 2 is located 90^{o} clockwise from probe 1. When probe 1 voltage reads 3.34 volts the azimuths indicated are either 20^{o} or 340^{o}. Simultaneously probe 2 reads 2.00 volts indicating that it is pointing at an azimuth of either 110^{o} or 250^{o}. The matching set of azimuths is obviously 20^{o} for probe 1 and 110^{o} for probe 2. This is the only set out of the four values in which probe 2 is advanced 90^{o} clockwise from probe 1, which is the required condition. If probe 1 were positioned in the spacecraft with its north pole pointing toward the spacecraft nose, the spacecraft azimuth would be 20^{o} from magnetic north for this case.

In the spacecraft installation the output of the magnetometer system was used to modulate the signal of the on-board C-band tracking transponder. This modulation

provided a real-time telemetry link with the ground-based radar during operation of the remotely controlled C-band transponder. During the flight the magnetometer voltages were reproduced at the radar station and forwarded to the control room for monitoring of the spacecraft azimuth. These voltages were also recorded on magnetic tape and strip charts for postflight use.

Calibration

Local anomalies in the earth magnetic field will produce small deviations from the field-strength azimuth angle plot of figure 34. In addition the magnetic probes and associated electronics may produce small nonlinear effects over the range considered. For these reasons a calibrated ground test curve was considered necessary.

To provide the truest spacecraft azimuth variation with magnetometer voltage, calibrations were made on the spacecraft during ground preflight checkout. The spacecraft was rotated through 360^{o} while suspended under the load bar in its normal flight attitude. Flight electronics were used to produce and telemeter the results to the on-site instrument van for readout. The reproduced voltage output of each magnetometer system was plotted with corresponding spacecraft azimuth. The values were adjusted for temperature and magnetic field strength changes at 130 000 feet (39.7 kilometers). The resulting curves are shown in figure 36. In this set of curves, probe 2 azimuth values have been arbitrarily shifted 90^{o} counterclockwise. This condition allows spacecraft pointing azimuths indicated by both magnetometer voltages to be read directly from the curves. The matching set is now more quickly evident. In addition, the amount of disagreement between values in the matching set can be used to judge the reliability of the data.

It is readily evident that each magnetometer is most sensitive along the straighter portion of its calibration curve. Generally one magnetometer azimuth is on a more sensitive portion of its curve than the other. This sensitivity forms a basis for choosing which of the two values to accept when differences occur in the matched set values.

Error Analysis

The errors involved in the production of spacecraft azimuth data from the magnetometer system can be relegated to three areas. These are (1) the accuracy and precision of the instrumentation involved, (2) the ability of the calibration curve to represent the correct azimuth to voltage relationship during flight, and (3) the amount of pitching of the spacecraft.

The error involved in the use of instrumentation is believed to be less than ± 0.04 volt. The effect of this voltage error in terms of one magnetometer azimuth

reading is $\pm 3^{\circ}$ except when near the maximum or minimum voltage points. (See fig. 36.) The use of two magnetometers 90° apart always insures that one of the two azimuth values in the matched set will not fall within 45° of the maximum or minimum voltage points.

Uncertainties involved in making the calibration and fairing the calibration curves amounted to $\pm 3^{\circ}$ in addition to those mentioned previously.

Significant errors can be produced in the spacecraft azimuth determinations if the plane of the magnetometers is tilted from the horizontal because of spacecraft pitching. The amount of this error will depend on the azimuth of the particular magnetometer and the amount it is tilted. The maximum azimuth error occurs when a magnetometer is pitched about an axis perpendicular to the direction in which it is pointing and is zero when pitched about an axis in line with the direction in which it is pointing. The largest amount of tilt considered probable during the period of the flight under consideration is 2°. Using 2° as the maximum amount of tilt and considering the maximum error condition result in a probable error in azimuth of about $\pm 6^{\circ}$.

The total error resulting from the combined effects of calibration errors, instrument errors, and spacecraft pitching should not exceed $\pm 12^{\circ}$.

REFERENCES

1. Thompson, R. P.: The Practical Problem of Landing on Mars. Astronaut. Aeron., vol. 4, no. 7, July 1966, pp. 66-73.

2. American Power Jet Co.: Performance of and Design Criteria for Deployable Aerodynamic Decelerators. ASD-TR-61-659, U.S. Air Force, Dec. 1963.

3. Whitlock, Charles H.; Bendura, Richard J.; and Coltrane, Lucille C.: Performance of a 26-Meter-Diameter Ringsail Parachute in a Simulated Martian Environment. NASA TM X-1356, 1967.

4. Mechtly, E. A.: The International System of Units - Physical Constants and Conversion Factors. NASA SP-7012, 1964.

5. Anon.: Comparative Studies of Conceptual Design and Qualification Procedures for a Mars Probe/Lander. Volume V: Subsystem and Technical Analyses – Book 2: Aeromechanics and Thermal Control. AVSSD-0006-66-RR (Contract NAS 1-5224), AVCO Corp., May 11, 1966.

6. Stone, Irving: Atmosphere Data to Alter Voyager Design. Aviation Week and Space Technol., vol. 83, no. 21, Nov. 22, 1965, pp. 66-67, 69.

7. Payne, James C.: Balloon Development for the Planetary Entry Parachute Program. Proceedings, Fourth AFCRL Scientific Balloon Symposium, James F. Dwyer, ed., AFCRL:67:OO75, Spec. Rept. No. 57, U.S. Air Force, Jan. 1967, pp. 11-18.

8. Anon.: U.S. Standard Atmosphere, 1962. NASA, U.S. Air Force, and U.S. Weather Bur., Dec. 1962.

TABLE I.- PHYSICAL PROPERTIES OF SPACECRAFT, AEROSHELL, AND PAYLOAD

Item	Weight, lbm (kg)	Center of gravity from cone apex, in. (cm)	Estimated moment of inertia in pitch, slug-ft^2 (kg-m^2)	Estimated moment of inertia in roll, slug-ft^2 (kg-m^2)
Spacecraft at release	1686.8 (765.1)	35.19 (89.38)	198.0 (268.5)	228.0 (309.2)
Spacecraft at rocket burnout	1303.8 (591.4)	32.85 (83.44)	187.0 (253.6)	208.0 (282.1)
Aeroshell without payload	697.8 (316.5)	39.24 (99.67)	139.0 (188.5)	203.0 (275.3)
Payload before parachute ejection	606.0 (274.9)	25.49 (64.74)	30.1 (40.8)	5.4 (7.3)
Instrument package without parachute, ballast, and miscellaneous parts	193.3 (87.7)	37.03 (94.06)	9.7 (13.2)	2.4 (3.3)
Parachute (inflated)	81.1 (36.8)	1036.62 (2633.01)	1820.0 (2468.3)	1220.0 (1654.6)
Ballast	323.0 (146.5)	13.66 (34.70)	1.4 (1.9)	2.7 (3.7)
Miscellaneous parts lost after mortar firing and parachute inflation (includes mortar cover, sabot, and parachute bag)	8.6 (3.9)	------ (------)	----- (-----)	----- (-----)
Payload with ballast during descent	516.3 (234.2)	22.24 (56.49)	20.2 (27.4)	5.1 (6.9)
Payload without ballast during descent	193.3 (87.7)	37.03 (94.06)	9.7 (13.2)	2.4 (3.3)
Payload-parachute system with ballast during descent	597.4 (271.0)	160.09 (406.63)	----- (-----)	----- (-----)
Payload-parachute system without ballast during descent	274.4 (124.5)	332.45 (844.42)	----- (-----)	----- (-----)

TABLE II.- THERMISTOR LOCATIONS

Thermistor	Function	Location
1	Rocket motor temperature	On side over a grain valley near forward end of rocket motor case farthest from balloon
2	Rocket motor temperature	On side over a grain peak near rear end of rocket motor case farthest from balloon
3	Rocket motor temperature	On side over a grain valley near rear end of rocket motor case nearest balloon
4	Rocket motor temperature	On side over a grain peak near forward end of rocket motor case nearest balloon
5	Aeroshell nose cap temperature	Inside of nose cap on aeroshell on side of spacecraft nearest balloon
6	Aeroshell hub temperature	On side of aeroshell hub nearest balloon
7	Aeroshell skin temperature	On rear face edge of aeroshell on side of spacecraft nearest balloon
8	Aeroshell camera temperature	Inside camera box on outside of camera opposite end from lens
9	Aeroshell battery box temperature	Inside battery box near center close to thermostat
10	Instrument compartment temperature	Near base of tape recorder
11	Instrument compartment temperature	Between payload skin and instrument compartment structure on side nearest the balloon
12	High-speed camera temperature	On outside edge of camera
13	Pyrotechnic battery temperature	On outside of battery box
14	Pyrotechnic battery temperature	On outside of battery box

TABLE III.- TIME AND SEQUENCE OF EVENTS

Event	Time, seconds		
	Nominal	Flight measurement	
		Instrumentation	Cameras
Release from balloon	0		
Rocket motor ignition	4.0	3.674	3.68
Mortar firing	7.5	6.983	6.99
Parachute line stretch	---	7.612	----
Payload separation nut firing	7.9	7.751	----
Parachute bag observed free	---	----	7.99
Payload-spacecraft electrical disconnect	---	8.556	----
Payload movement detected	---	13.0 to 14.4	13.83
Payload completely clears aeroshell	---	----	14.18
Ballast ejection	30.0	29.745	29.84

TABLE IV.- THERMISTOR MEASUREMENTS

Time, sec (*)	Degrees centigrade for thermistor –								
	1	2	3	4	5	6	7	8	9
0.95	16.12	20.23	18.70	25.39	35.04	38.87	83.30	18.53	18.75
1.60	15.16	19.18	17.74	24.47	33.54	36.90	81.92	17.37	17.37
2.25	15.79	20.01	18.49	24.91	34.39	37.63	83.68	17.41	18.04
2.90	15.49	20.04	18.52	25.38	34.64	38.38	85.20	17.28	17.92
3.55	15.16	19.80	18.30	24.76	35.17	38.24	85.21	17.54	18.35
3.77	16.25	20.29	18.74	25.56	35.33	37.96	88.97	17.59	18.39
3.99	16.92	21.01	19.55	26.39	36.40	39.10	89.94	18.20	18.74
4.21	16.60	21.04	19.58	25.96	35.33	38.91	86.67	17.41	17.98
4.42	15.78	20.33	18.79	25.94	34.93	37.31	86.18	17.40	18.04
4.63	17.16	21.58	20.21	26.75	36.32	39.31	89.97	17.84	17.91
4.85	17.61	21.74	20.40	26.61	36.00	38.92	87.63	17.76	18.40
5.06	16.99	20.73	19.63	26.65	35.34	37.98	89.93	17.69	17.84
5.28	18.23	22.26	21.01	27.41	35.79	39.31	86.14	18.09	17.99
5.50	17.64	22.48	21.27	26.61	36.33	40.60	90.38	18.70	18.33
5.72	18.45	23.17	20.55	28.35	34.70	39.89	93.30	17.95	18.18
5.95	18.79	24.78	21.03	27.54	34.64	38.86	86.63	17.20	17.12
6.17	18.29	27.49	22.58	27.37	35.76	38.01	88.99	17.48	18.19
6.40	19.13	30.90	23.32	27.96	35.01	39.31	88.06	17.43	17.66
6.61	18.65	34.78	23.89	27.82	34.46	38.65	87.08	17.72	17.63
6.84	18.61	39.85	25.73	26.85	34.06	37.21	81.92	16.79	17.21
7.07	19.67	45.26	29.04	28.84	36.19	39.31	90.93	18.00	18.39
7.29	20.87	51.79	31.14	29.09	34.78	37.77	89.03	16.81	17.54
7.51	22.79	59.83	34.11	31.71	35.56	38.40	92.31	17.31	18.43
7.73	----	66.19	36.79	33.73	35.32	39.68	90.95	17.89	17.88
7.95	26.57	74.63	41.43	36.61	36.21	40.94	94.71	18.38	18.84
8.17	26.88	73.77	42.77	37.47	34.90	38.72	93.75	17.89	18.59
8.39	29.60	81.59	45.18	38.83	35.75	40.68	92.34	18.36	18.02

*Zero time is vehicle release time from balloon.

TABLE IV.- THERMISTOR MEASUREMENTS – Continued

Time, sec (*)	Degrees centigrade for thermistor –				
	10	11	12	13	14
0.95	21.30	21.48	33.77	19.29	20.49
1.60	20.22	19.98	32.41	18.23	19.37
2.25	20.28	20.33	33.48	19.07	20.26
2.90	21.04	20.54	32.31	18.58	19.74
3.55	21.22	20.65	34.05	18.51	19.67
3.77	20.79	20.26	32.20	18.14	19.27
3.99	21.31	20.94	33.53	18.69	19.85
4.21	20.68	21.05	33.37	18.63	19.79
4.42	20.42	19.93	32.35	18.27	19.41
4.63	20.62	20.80	32.73	18.05	19.18
4.85	20.61	20.51	33.39	18.90	20.08
5.06	20.64	20.18	34.52	18.58	19.74
5.28	20.21	20.15	32.15	18.22	19.36
5.50	21.32	21.14	34.45	19.64	20.87
5.72	20.32	20.94	33.96	18.17	19.76
5.95	20.22	20.36	32.31	17.72	18.56
6.17	20.91	20.59	32.69	18.62	19.78
6.40	20.12	19.88	33.01	18.65	19.81
6.61	20.75	20.40	32.26	18.36	19.51
6.84	19.73	19.51	31.26	18.06	19.10
7.07	21.44	20.99	33.87	18.82	20.09
7.29	20.16	20.84	32.76	18.68	19.94
7.51	20.59	20.41	33.46	19.31	20.52
7.73	20.42	20.39	32.64	18.44	19.59
7.95	21.66	21.25	34.61	19.31	20.52
8.17	21.33	20.88	33.46	18.88	20.06
8.39	22.21	22.05	35.40	19.55	20.77
8.68	21.36	20.91	33.25	18.99	20.17
8.90	20.93	21.07	33.86	19.06	20.25
9.12	20.82	20.39	33.05	18.77	19.94
9.33	21.09	21.06	33.17	18.71	19.88
9.55	20.76	20.60	33.17	18.28	19.42
9.77	20.61	20.61	33.34	18.64	19.80
9.99	20.66	20.49	32.29	18.26	19.40

*Zero time is vehicle release time from balloon.

TABLE IV.- THERMISTOR MEASUREMENTS – Continued

Time, sec (*)	Degrees centigrade for thermistor –				
	10	11	12	13	14
10.21	21.21	20.91	33.75	18.32	19.47
10.43	20.47	20.83	33.66	18.58	19.84
10.64	21.68	21.54	34.06	19.33	20.53
10.86	20.94	20.71	33.59	18.39	19.54
11.07	20.66	20.48	32.92	18.61	19.78
11.29	21.13	21.02	34.38	18.58	20.11
11.50	21.07	20.86	33.01	18.43	19.58
11.71	20.69	20.80	33.62	18.47	19.62
11.92	20.73	20.46	32.76	18.68	19.94
12.14	20.85	20.69	33.71	19.15	20.35
12.35	20.53	20.34	32.73	18.74	19.91
12.57	21.20	21.09	33.50	19.09	20.28
12.78	20.85	21.26	34.67	19.23	20.43
12.99	20.45	20.99	33.59	18.48	19.63
13.20	20.57	20.76	32.53	18.08	19.21
13.42	20.62	20.34	33.01	19.08	20.27
13.63	21.21	21.02	33.80	18.84	20.02
13.84	21.11	21.36	33.73	19.34	20.54
14.05	20.64	20.65	33.23	18.50	19.84
14.26	20.51	20.50	32.94	18.29	19.43
14.47	20.96	20.63	33.60	18.75	19.92
14.68	20.91	20.68	33.98	18.96	20.15
14.89	20.72	20.37	33.23	18.67	19.84
15.10	21.22	21.48	33.34	18.94	20.12
15.73	20.82	20.48	33.10	18.52	19.67
16.35	21.34	21.34	33.28	18.98	20.16
16.96	20.49	20.76	33.10	18.17	19.31
17.57	20.55	20.36	32.60	18.06	19.19
18.19	20.98	20.94	32.96	18.52	19.67
18.81	20.92	21.25	33.03	18.88	20.15
19.42	20.44	20.33	32.90	18.47	19.71

*Zero time is vehicle release time from balloon.

TABLE IV.- THERMISTOR MEASUREMENTS – Concluded

Time, sec (*)	Degrees centigrade for thermistor –				
	10	11	12	13	14
20.03	21.12	20.73	32.89	18.92	20.11
20.63	21.42	20.70	33.37	18.89	20.06
21.24	20.25	20.39	32.64	18.36	19.50
21.84	20.96	21.29	33.12	18.83	20.10
22.45	20.76	20.60	32.17	18.62	19.78
23.05	20.18	20.59	32.26	18.45	19.60
24.26	20.38	20.74	32.54	18.31	19.46
24.86	20.46	20.35	33.07	18.57	19.73
25.45	20.53	20.33	32.47	18.03	19.25
26.05	20.59	20.32	32.89	18.28	19.42
26.64	20.75	20.49	32.55	18.88	20.15
27.23	20.74	20.66	33.68	18.52	19.67
27.81	21.05	20.65	33.66	18.76	20.39
28.39	21.04	20.92	33.55	19.26	20.37
28.97	20.41	20.38	31.95	18.69	19.85
29.57	20.63	20.36	32.74	18.67	19.83
30.18	20.70	21.28	33.25	18.38	19.53
34.93	20.70	20.72	32.63	18.65	19.82
39.95	20.82	20.85	33.39	18.86	20.04
44.95	20.97	20.94	32.99	18.94	20.12
49.90	21.42	21.45	32.79	19.15	20.43
55.01	21.21	21.20	33.55	19.26	20.56
59.92	20.97	21.02	32.80	18.93	20.11
65.00	21.42	21.34	32.60	19.05	20.24
69.91	21.18	21.17	33.08	19.06	20.25
74.99	20.68	21.07	32.13	18.72	19.98
80.08	20.88	20.74	32.22	18.84	20.02
84.95	21.30	21.59	32.56	18.68	19.93
90.01	21.54	21.68	33.32	19.36	20.56
95.05	21.33	21.35	31.67	18.96	20.14
100.09	20.82	21.22	31.52	18.69	19.85
104.94	20.94	20.99	31.90	18.47	19.71
109.99	21.44	21.37	32.63	18.57	19.73

*Zero time is vehicle release time from balloon.

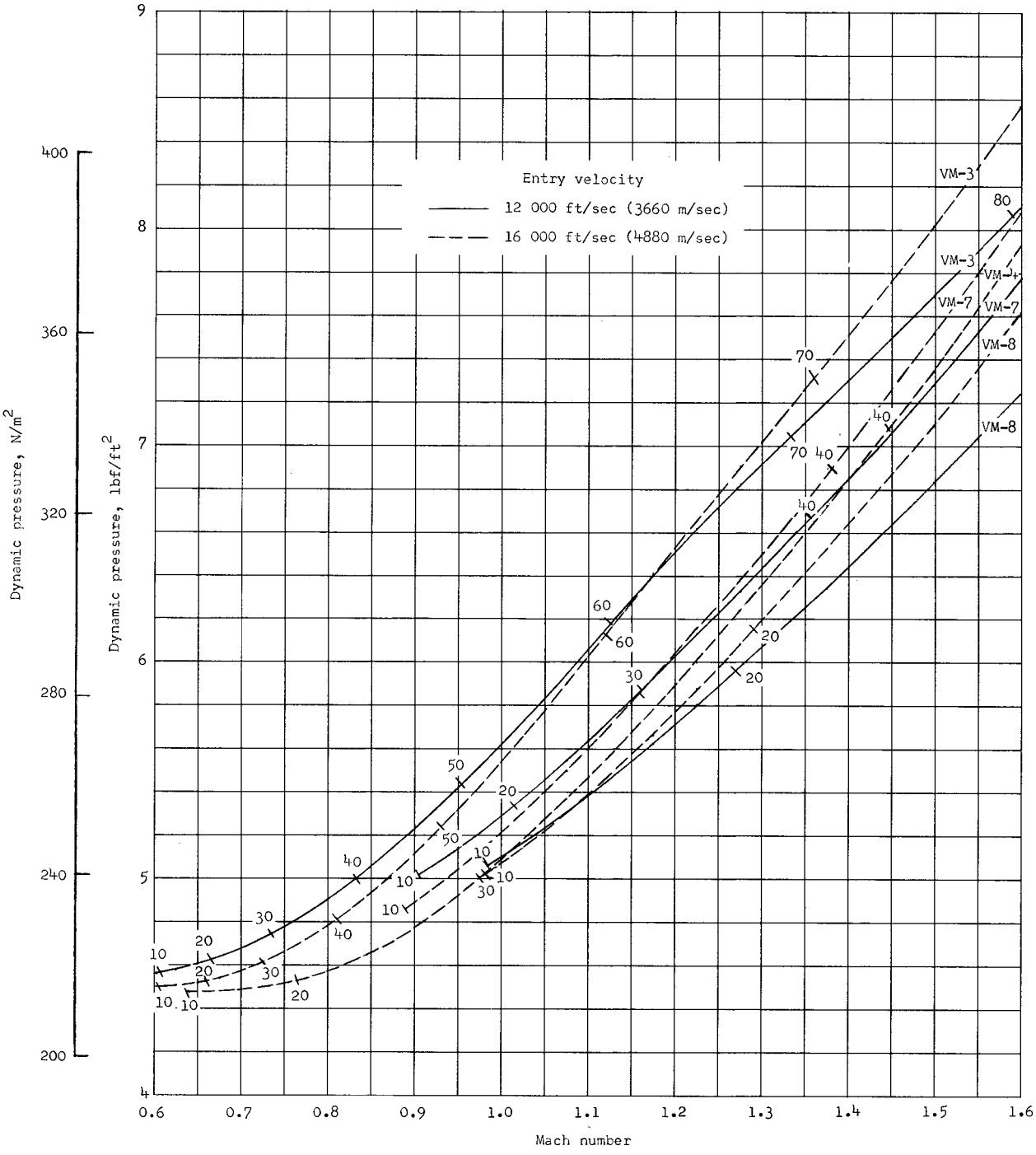

Figure 1.- Dynamic pressure variation with Mach number for entry into four tentative Mars atmospheres at two velocities. Tick marks denote altitude above the surface of Mars in thousands of feet (1000 ft = 0.3048 km).

(a) Layout of balloon and safety parachute prior to inflation.

Figure 2.- Launch procedure. L-67-6636

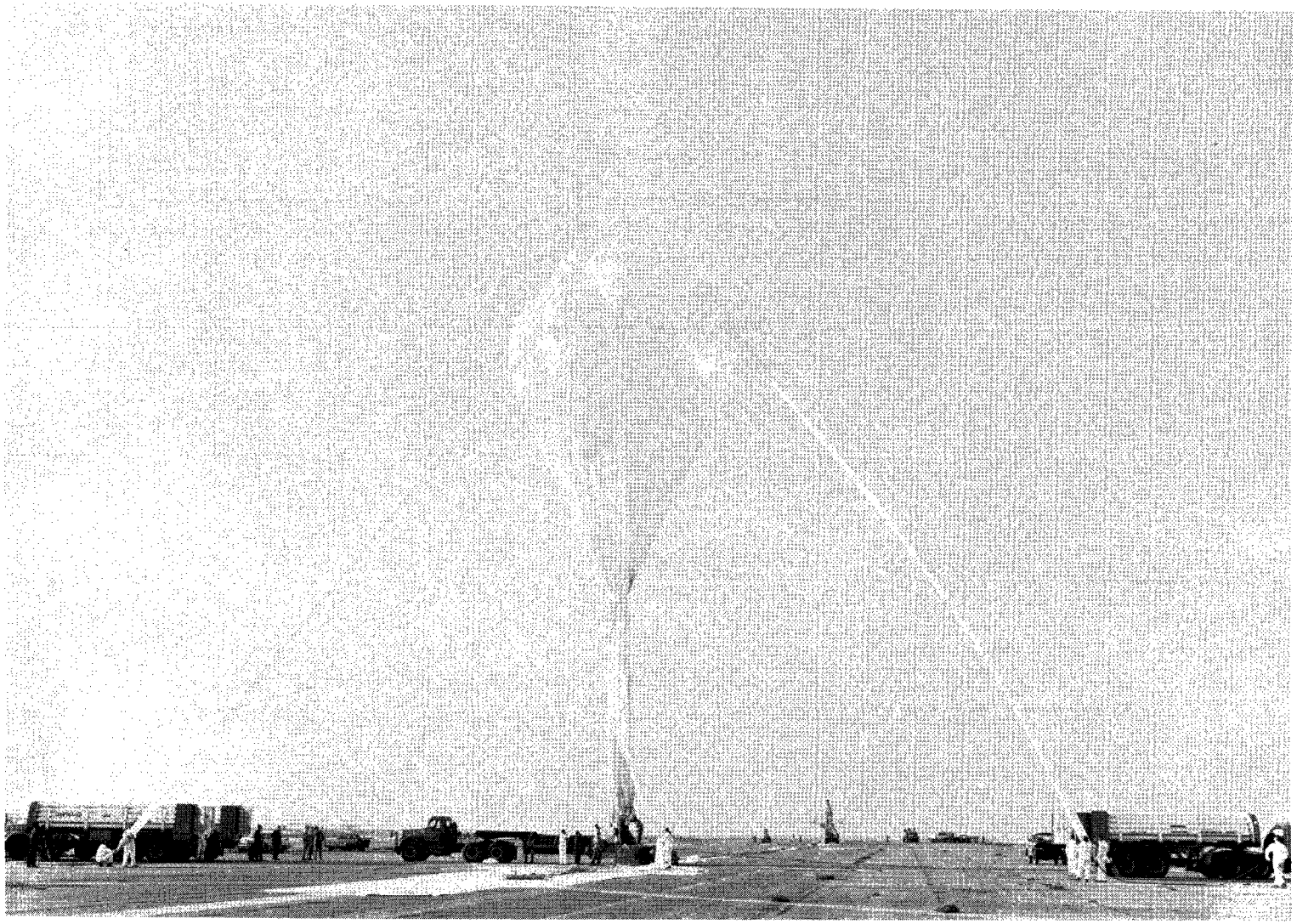

(b) Start of inflation of launch balloon.

Figure 2.- Continued.

L-67-6637

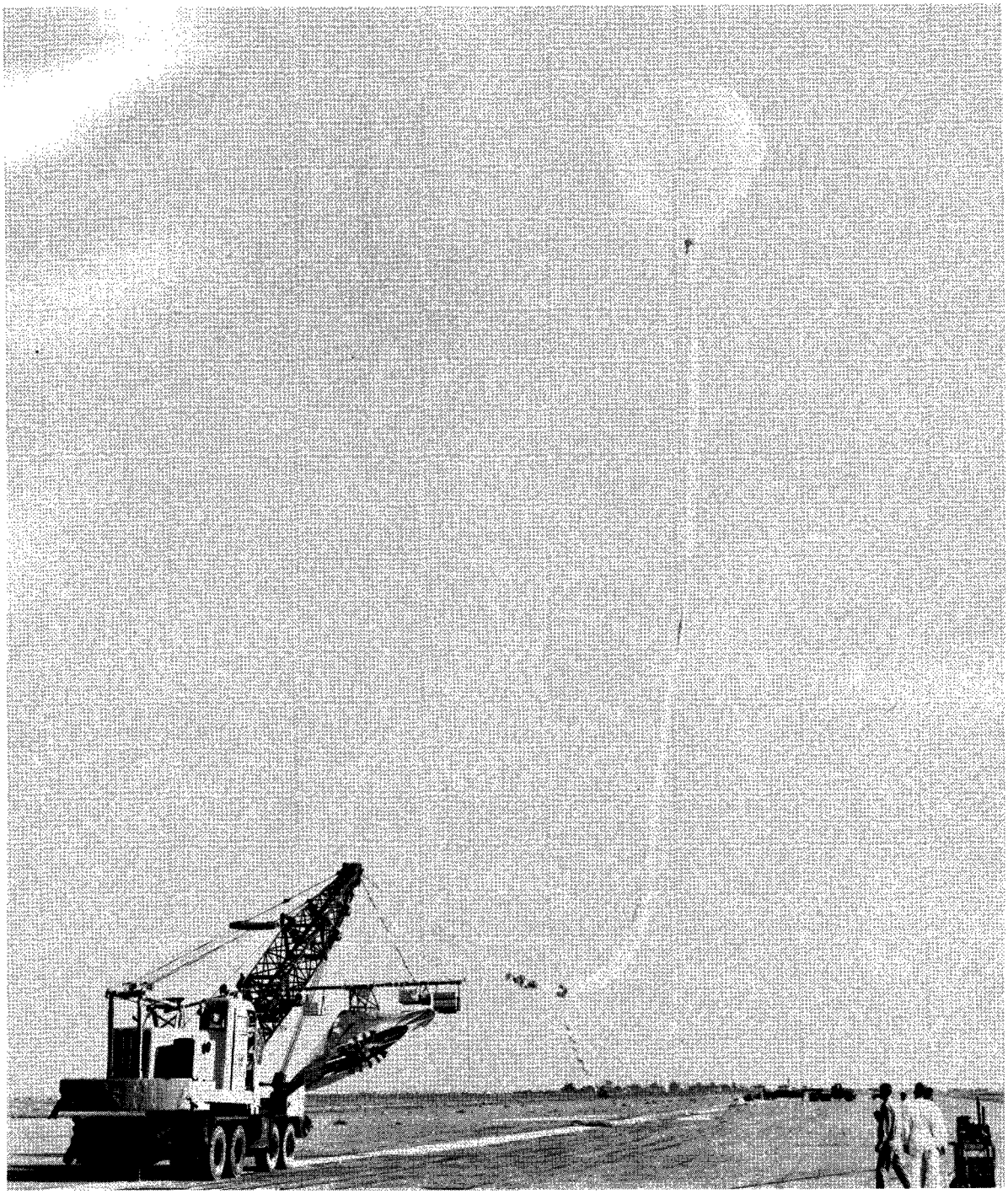

(c) Reel up of balloon system just prior to launch.

Figure 2.- Continued.

L-67-6638

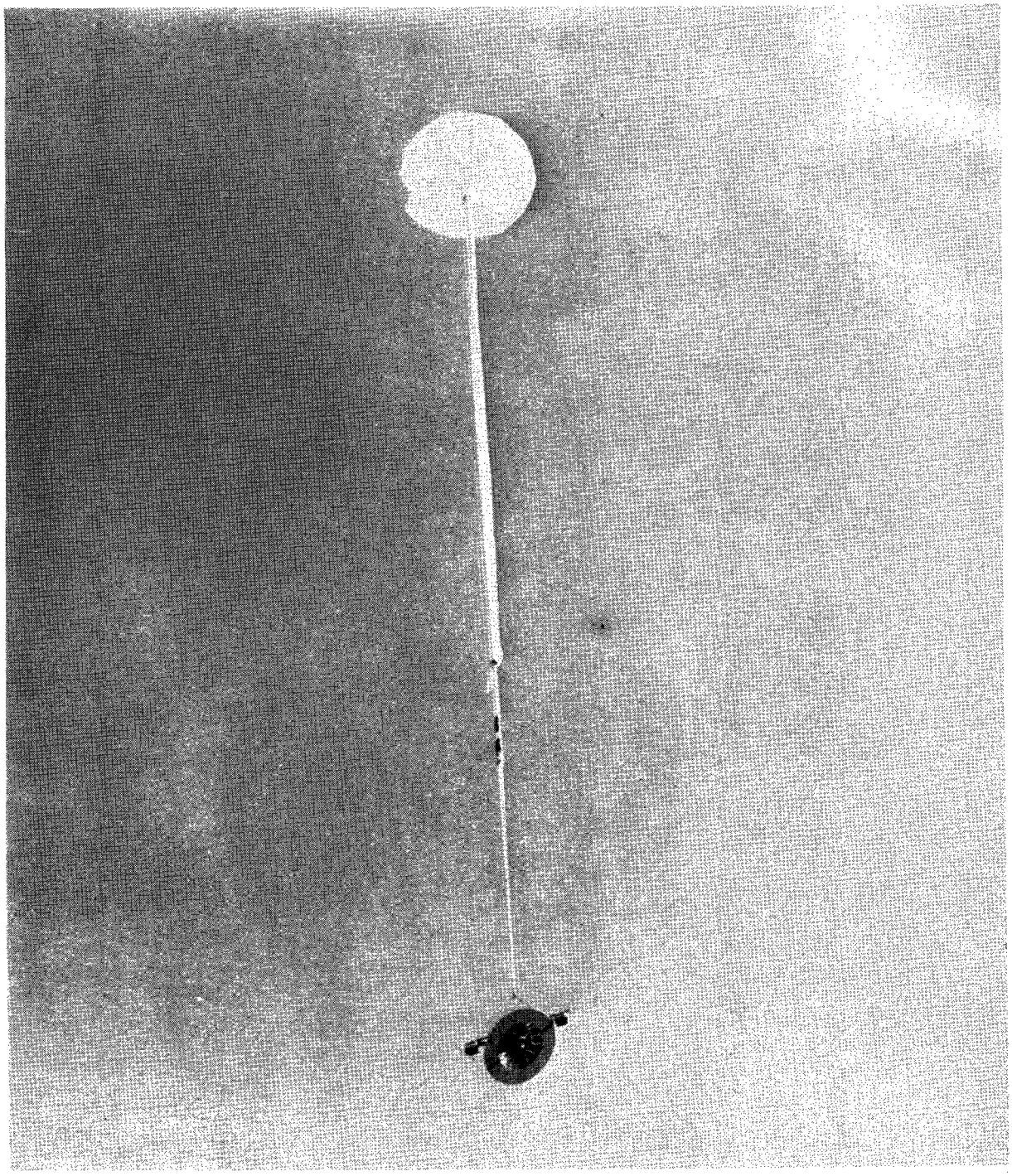

(d) Balloon system after release.

Figure 2.- Concluded.

L-67-6639

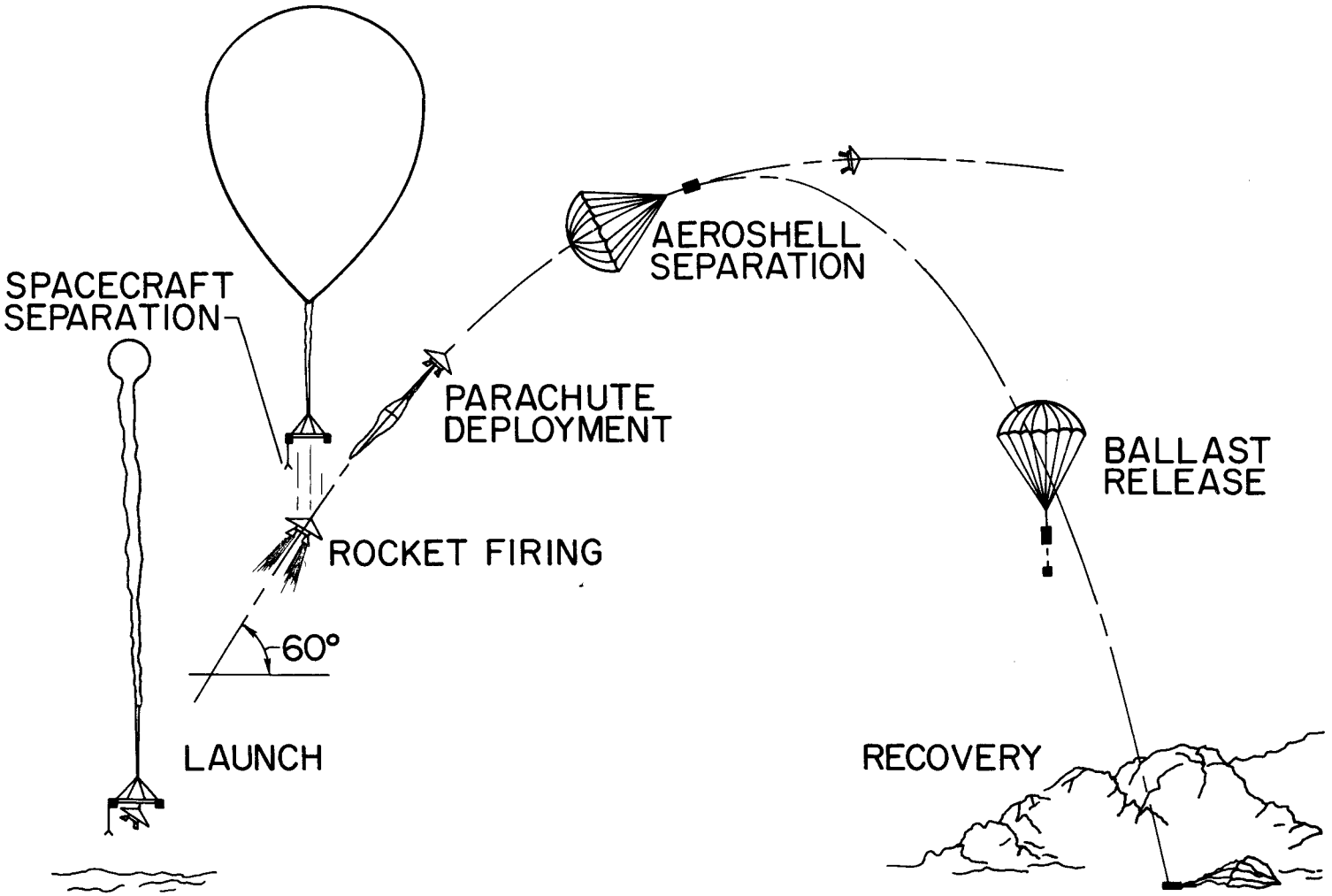

Figure 3.- Flight-test sequence of balloon-launched system.

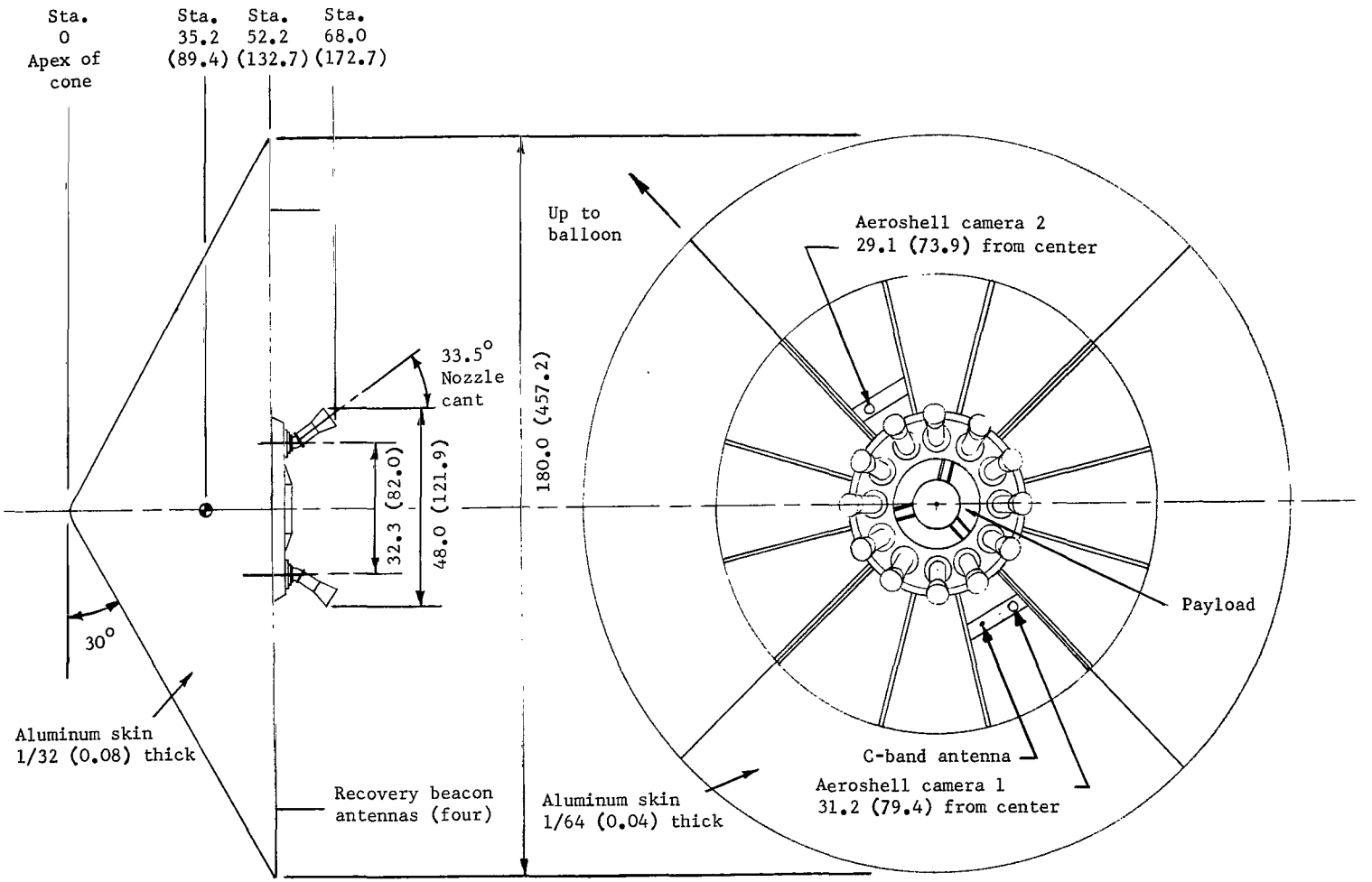

(a) Sketch of spacecraft, side and rear view. All dimensions and stations are in inches (cm).

Figure 4.- Details of spacecraft configuration.

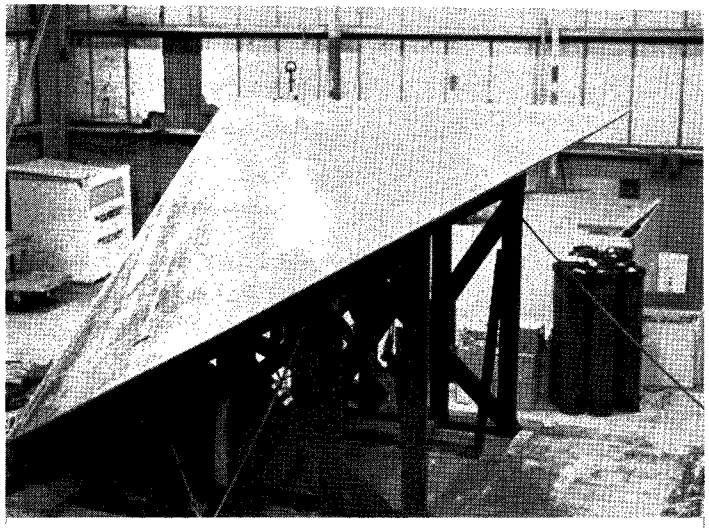

Side view

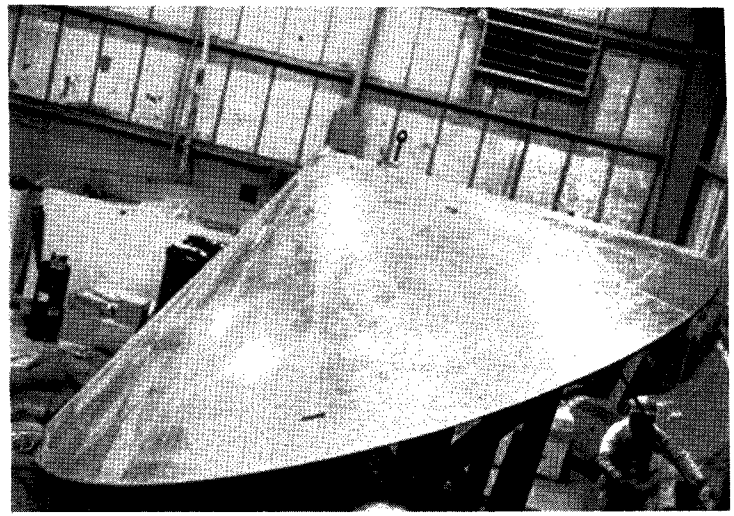

Three-quarter side view

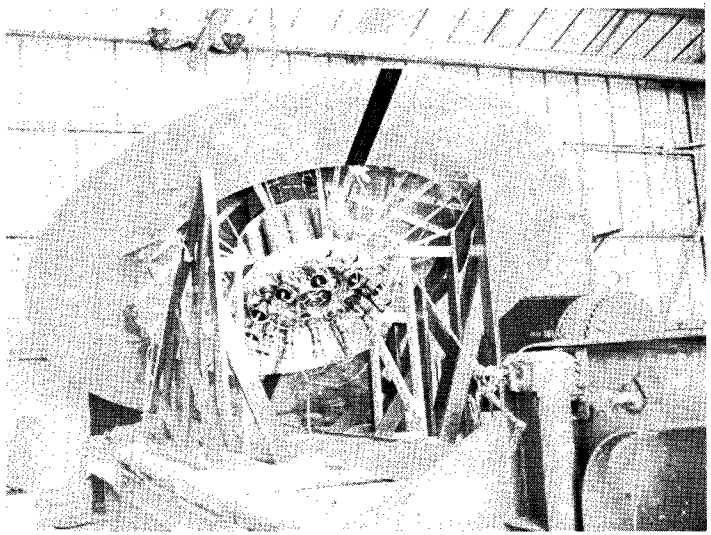

Three-quarter rear view

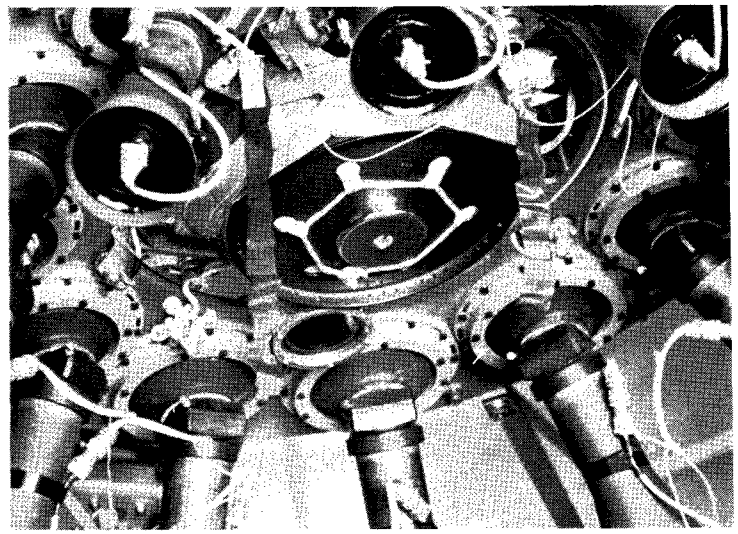

Closeup of rocket nozzle and payload

(b) Photographs of spacecraft.

Figure 4.- Continued.

L-67-6640

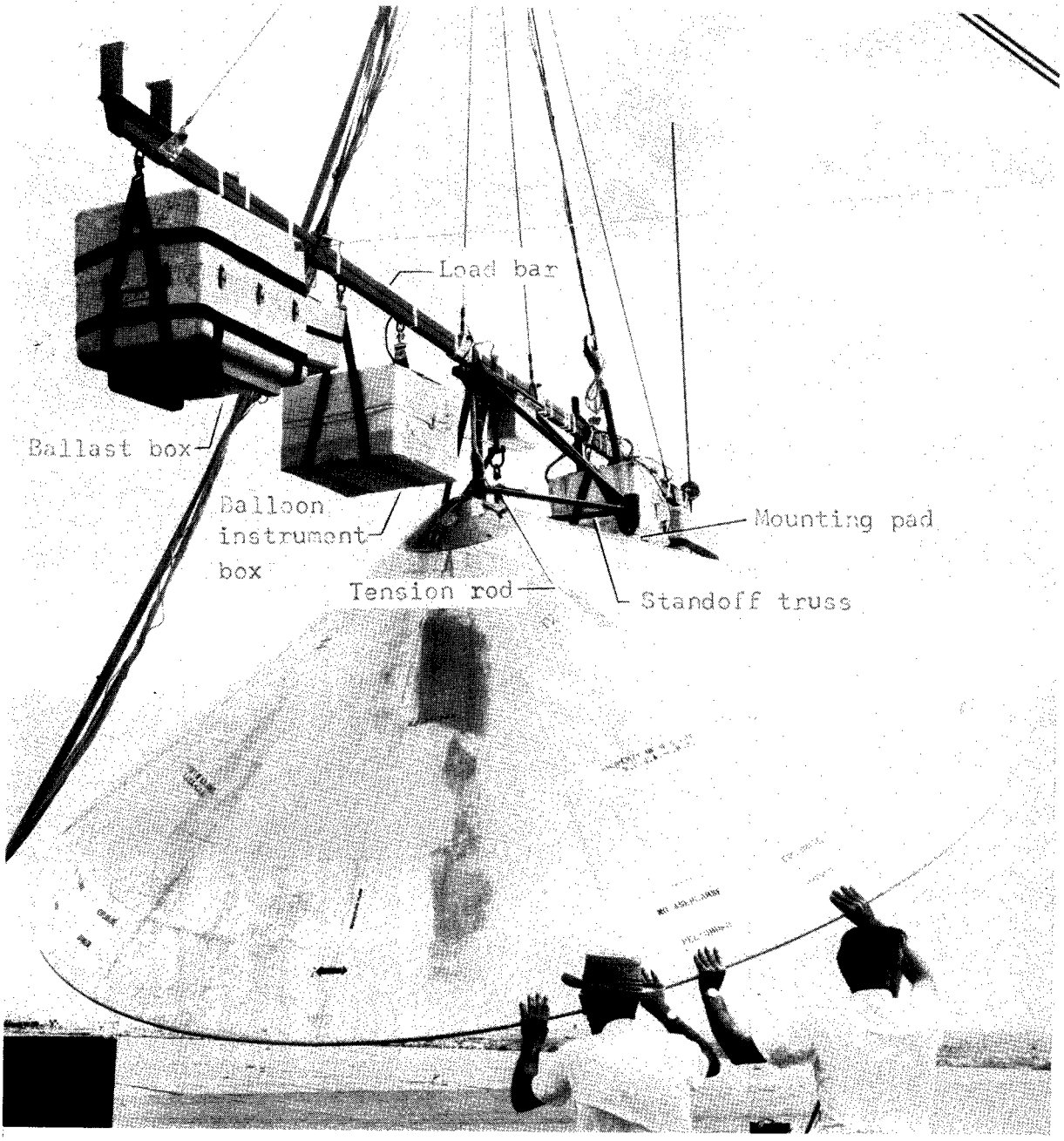

(c) Photograph of spacecraft attached to balloon load bar.

Figure 4.- Concluded. L-67-6641

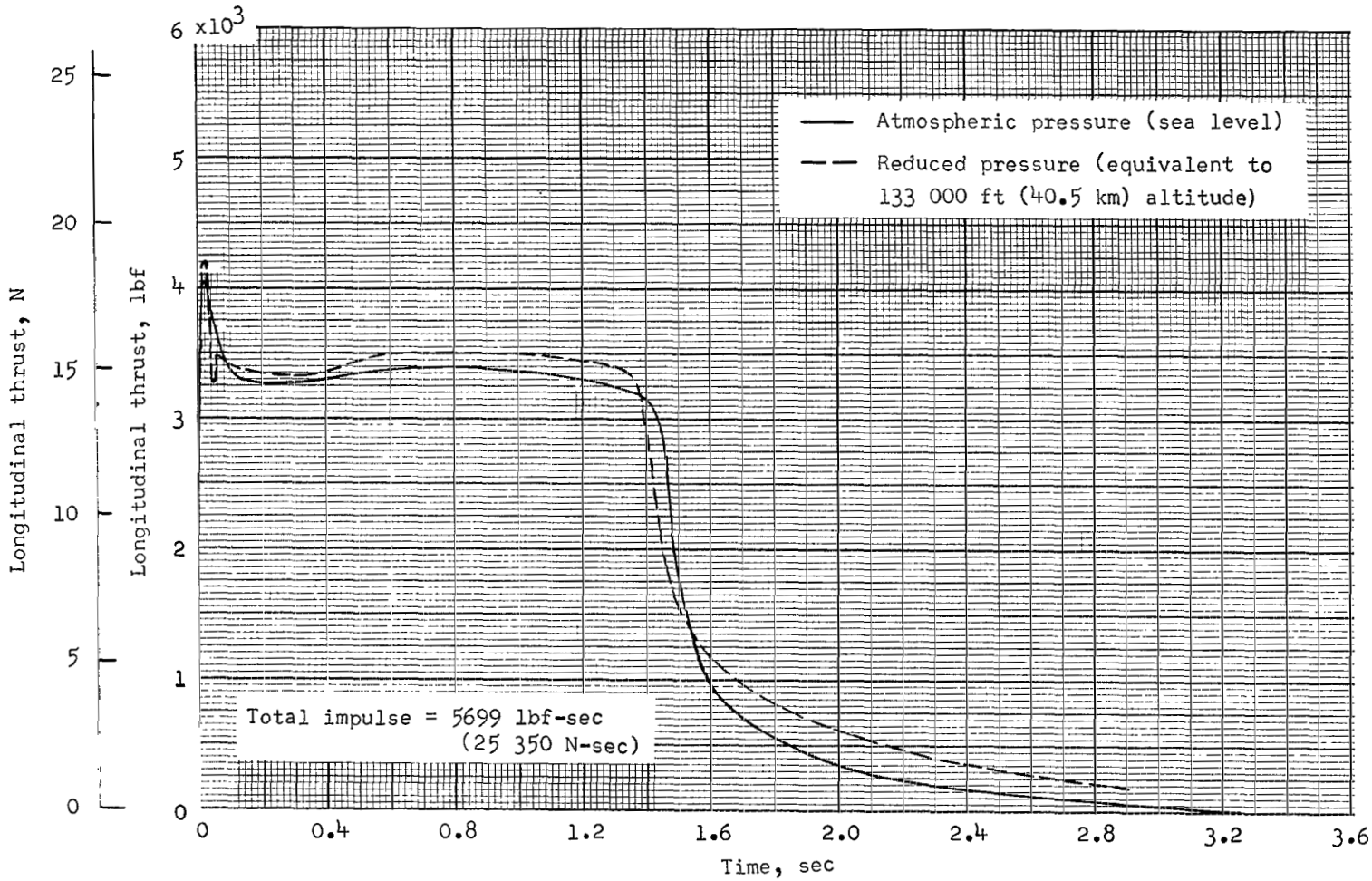

Figure 5.- Variation of longitudinal thrust with burning time for two static firing tests on typical M58A2 rocket motors with 33.5° canted nozzles.

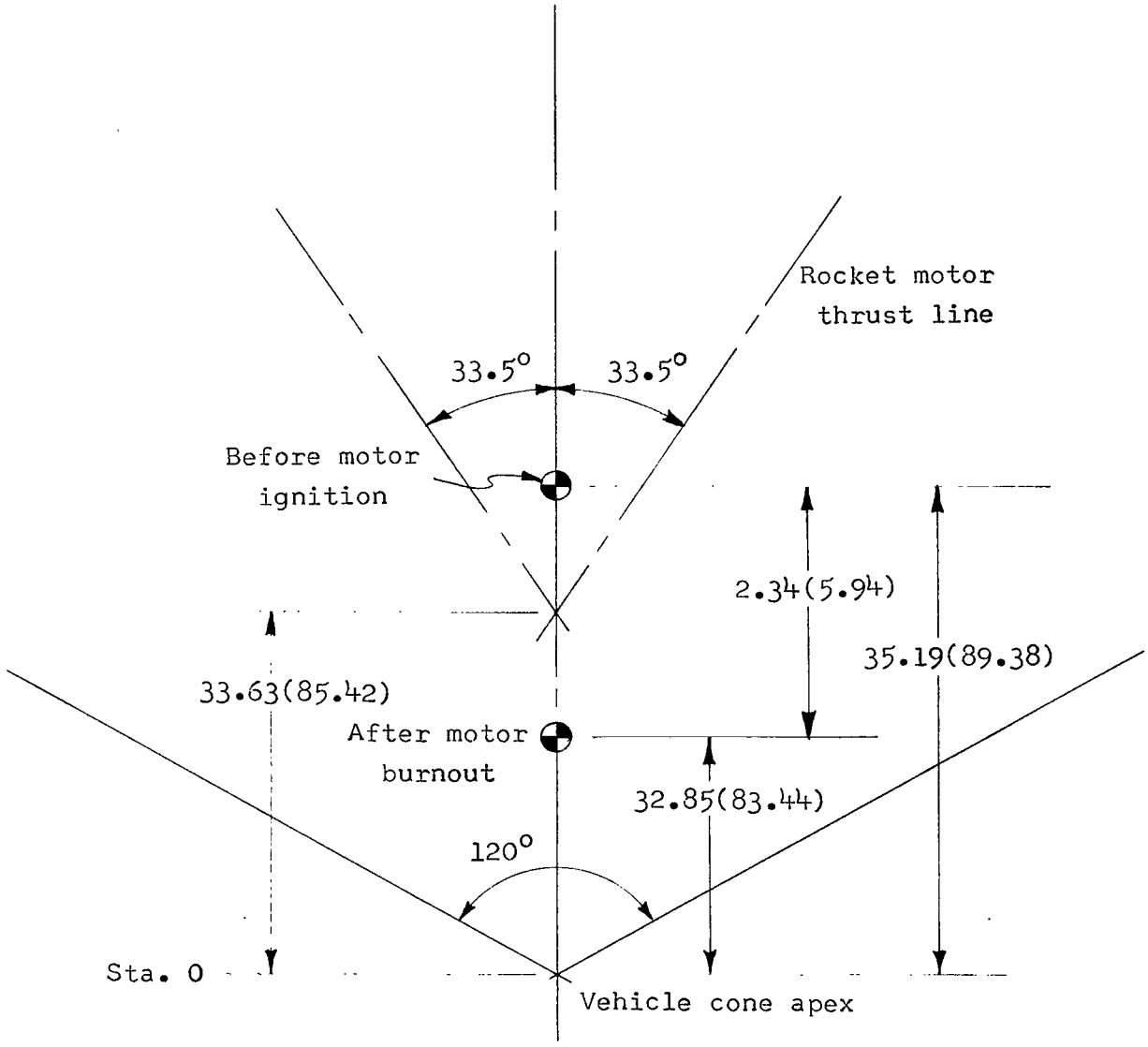

Figure 6.- Sketch of center-of-gravity positions with respect to rocket thrust line intersections. (Illustration not to scale. Dimensions are in inches (cm).)

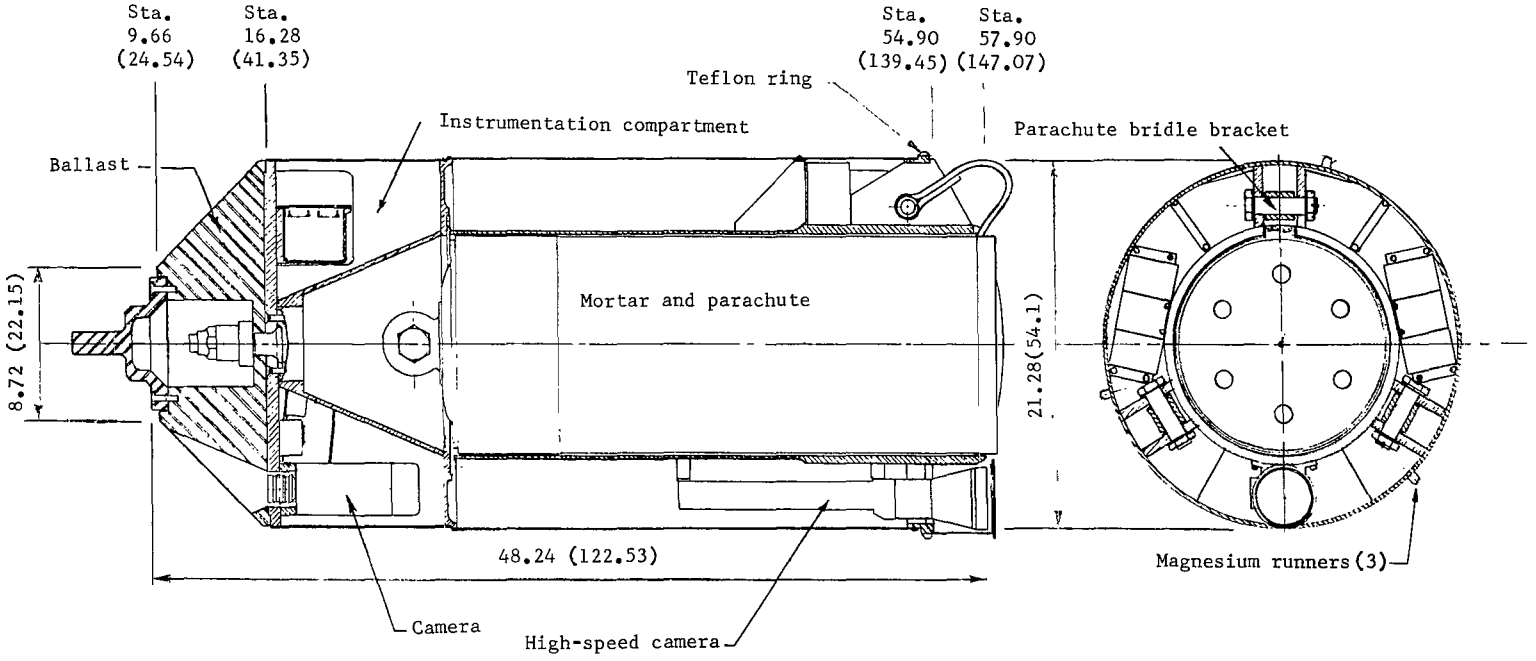

Figure 7.- Cross-section sketch of payload. All dimensions and stations are in inches (cm).

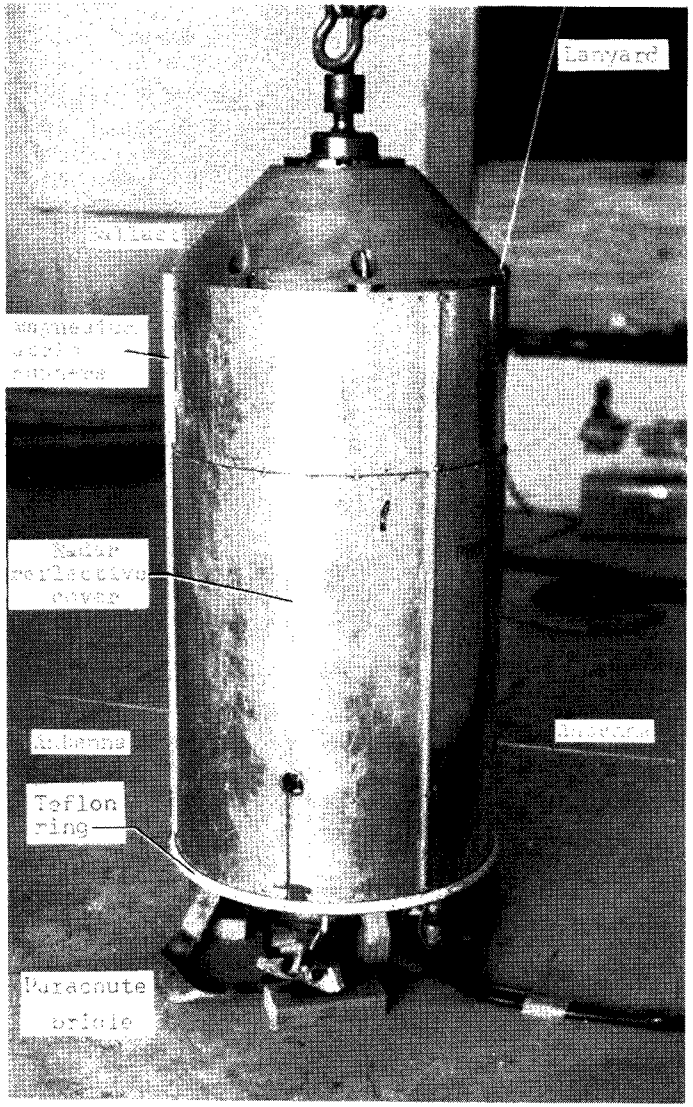

(a) With external cover.

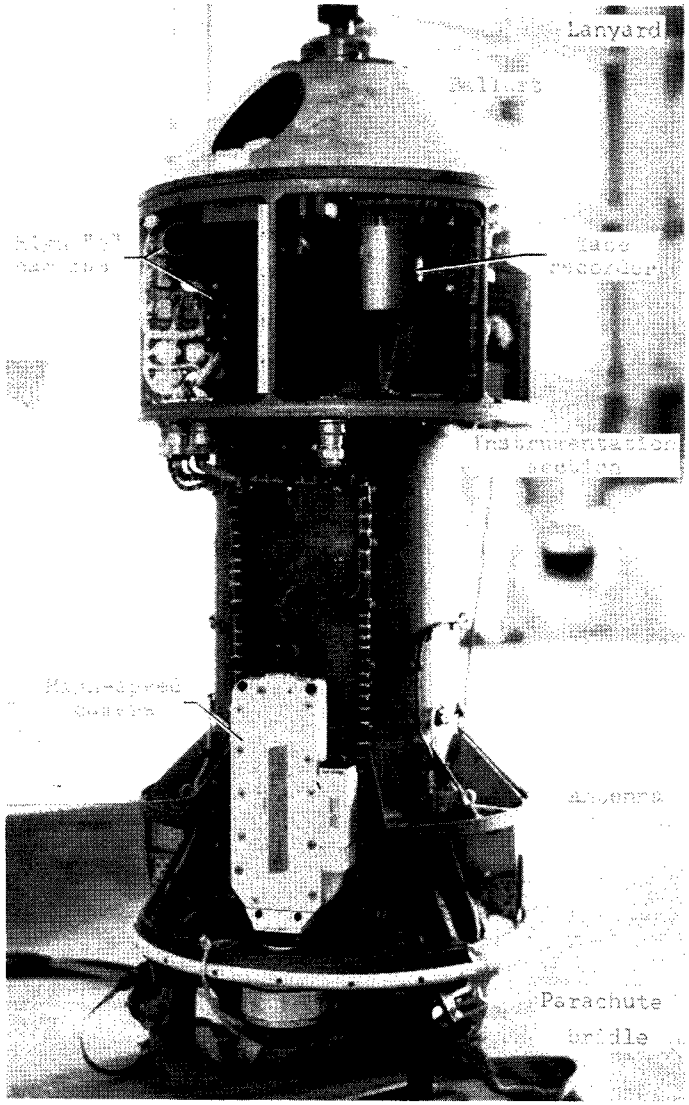

(b) Without external cover.

Figure 8.- Photographs of payload.

L-67-6642

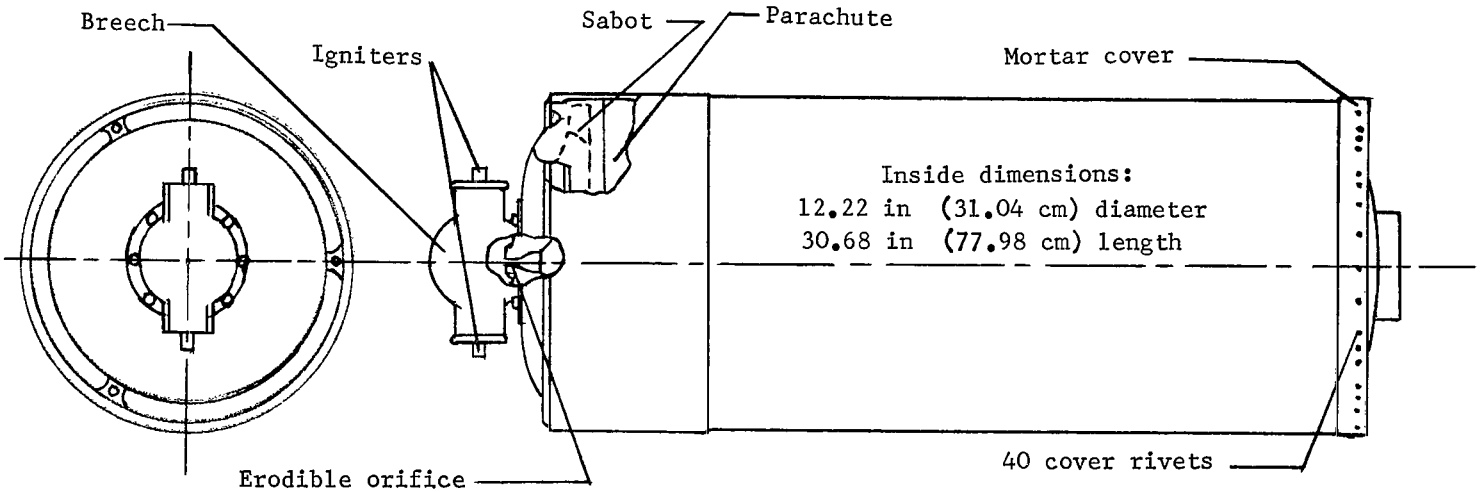

Figure 9.- Sketch of mortar-parachute assembly.

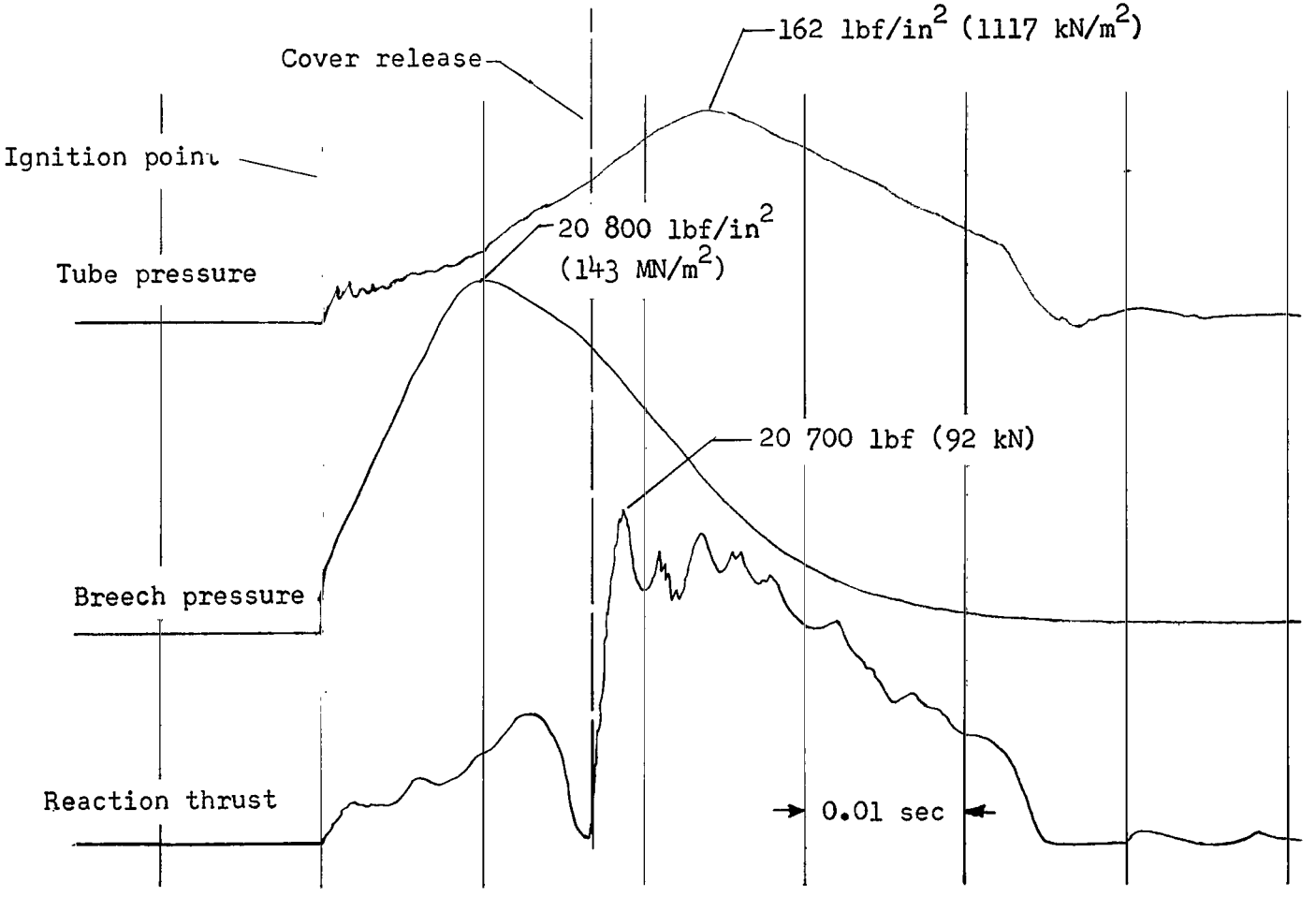

Figure 10.- Mortar test firing as shown by high-speed strip chart recording.

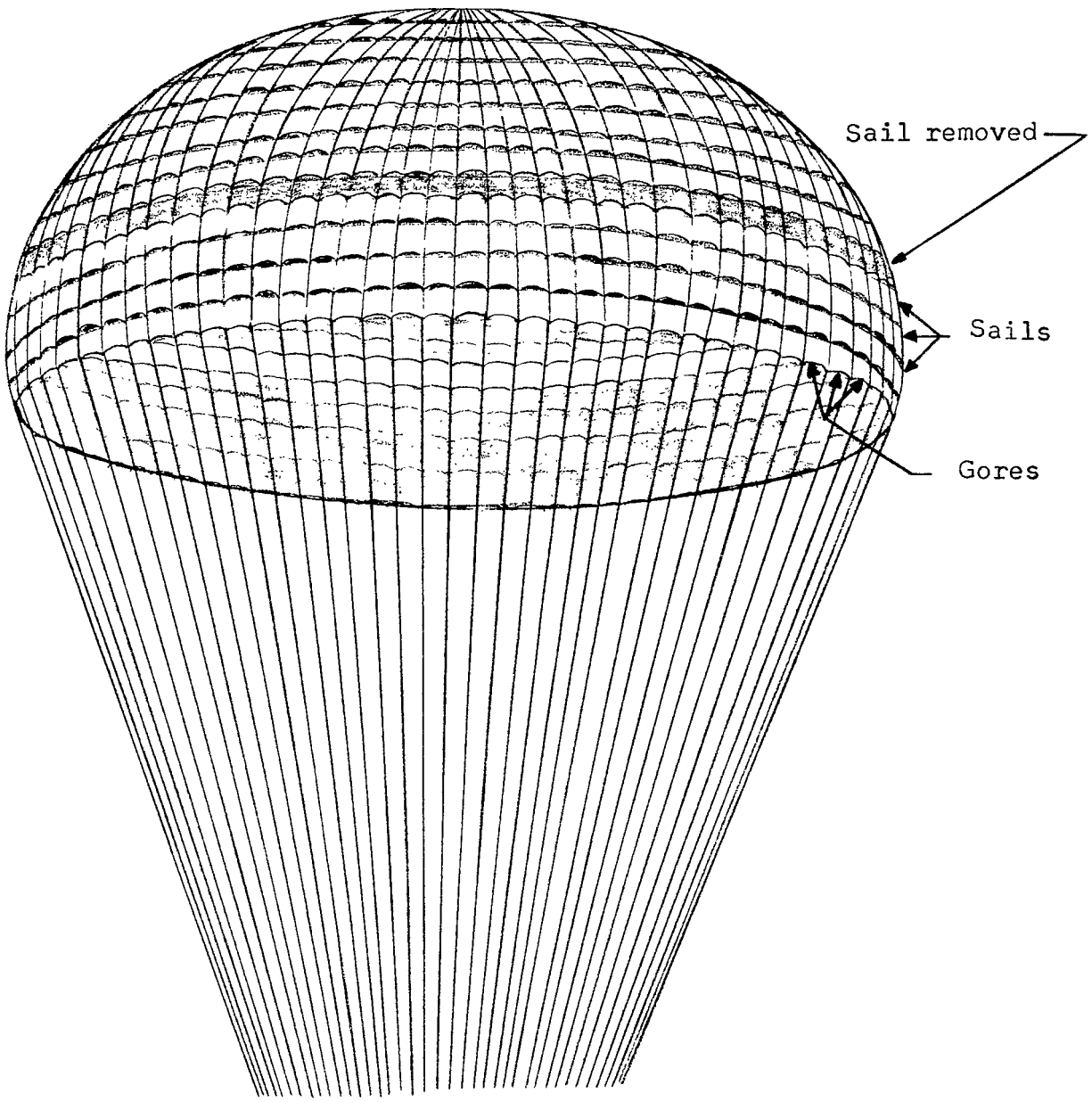

Figure 11.- Ringsail canopy configuration.

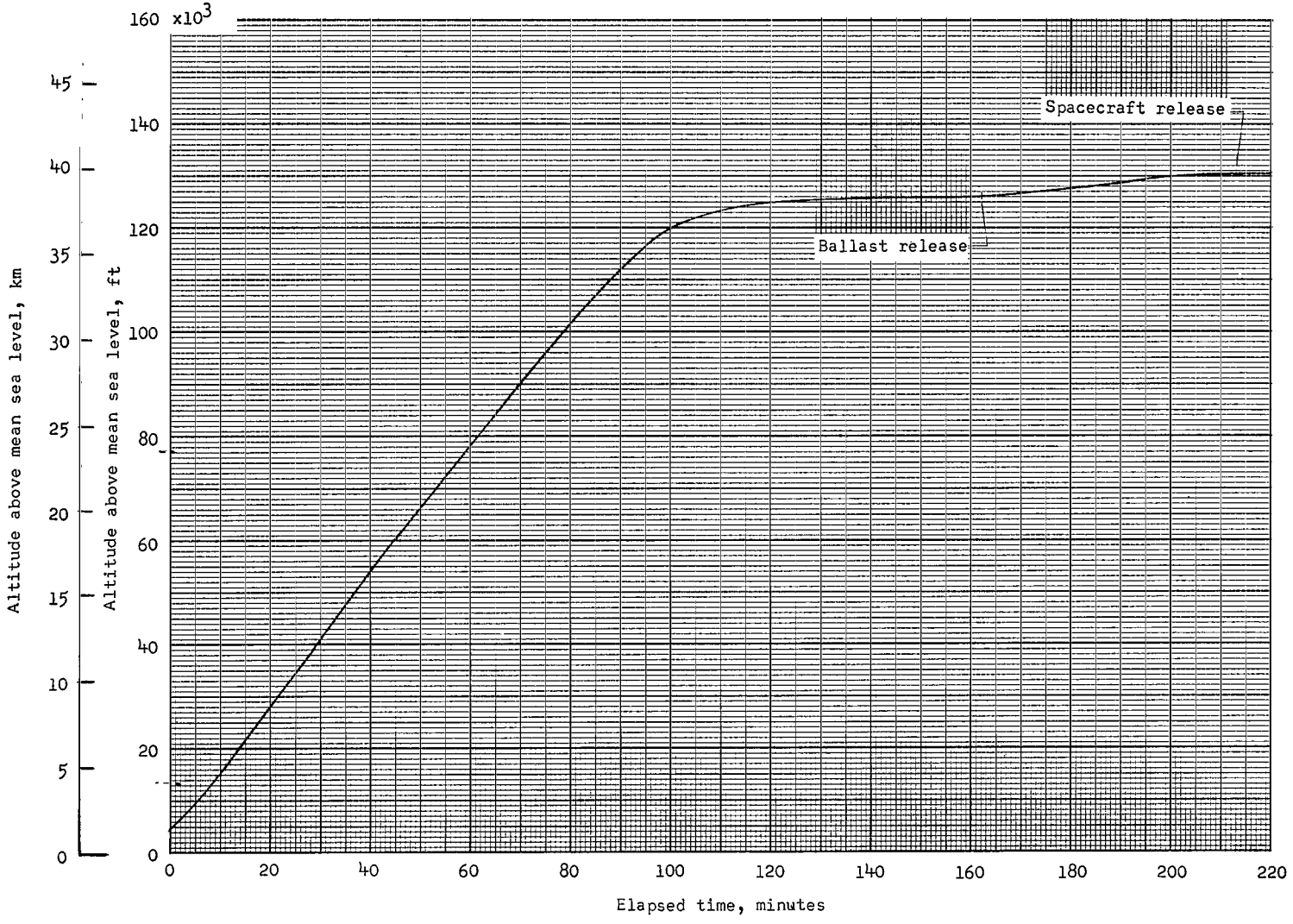

Figure 12.- Altitude time history of balloon system from launch.

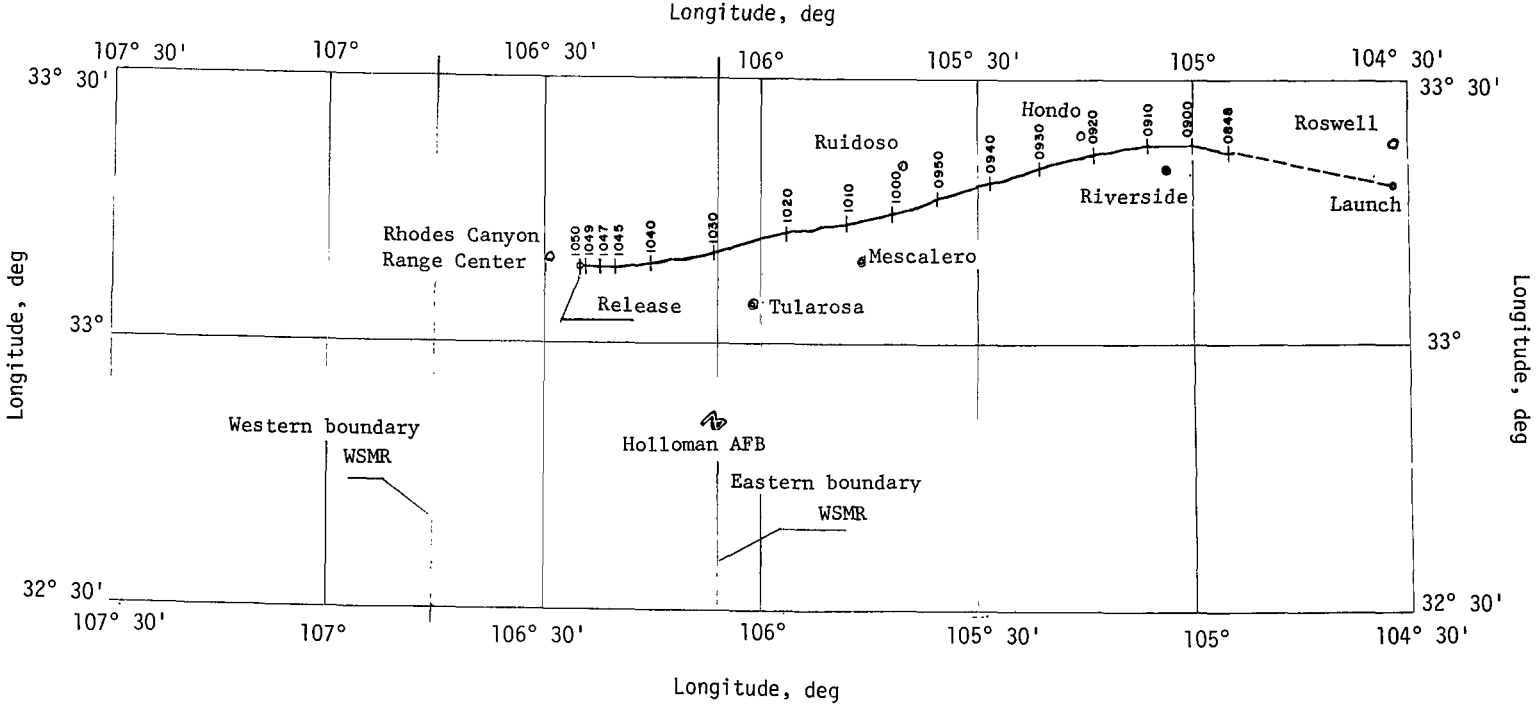

Figure 13.- Ground track of balloon from launch to spacecraft release. Labeled tick marks are mountain standard time.

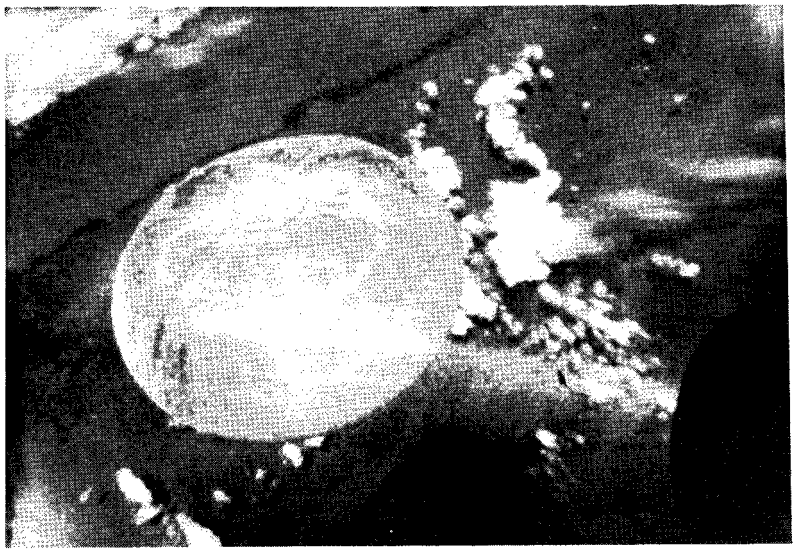

Figure 14.- Photograph of balloon after spacecraft release taken from on-board camera. L-67-6643

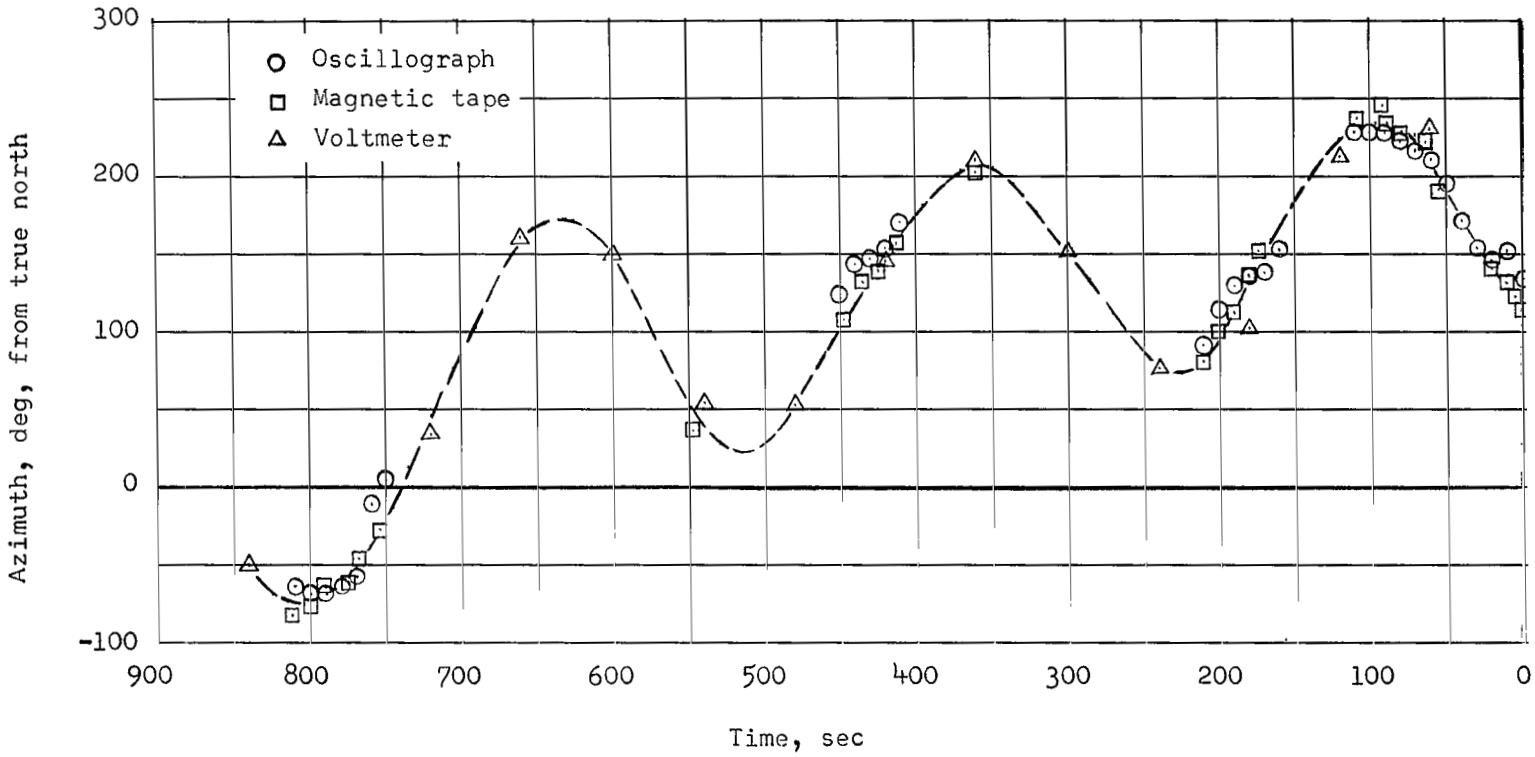

Figure 15.- Spacecraft pointing azimuth variation with time before release (t = 0) from the balloon.

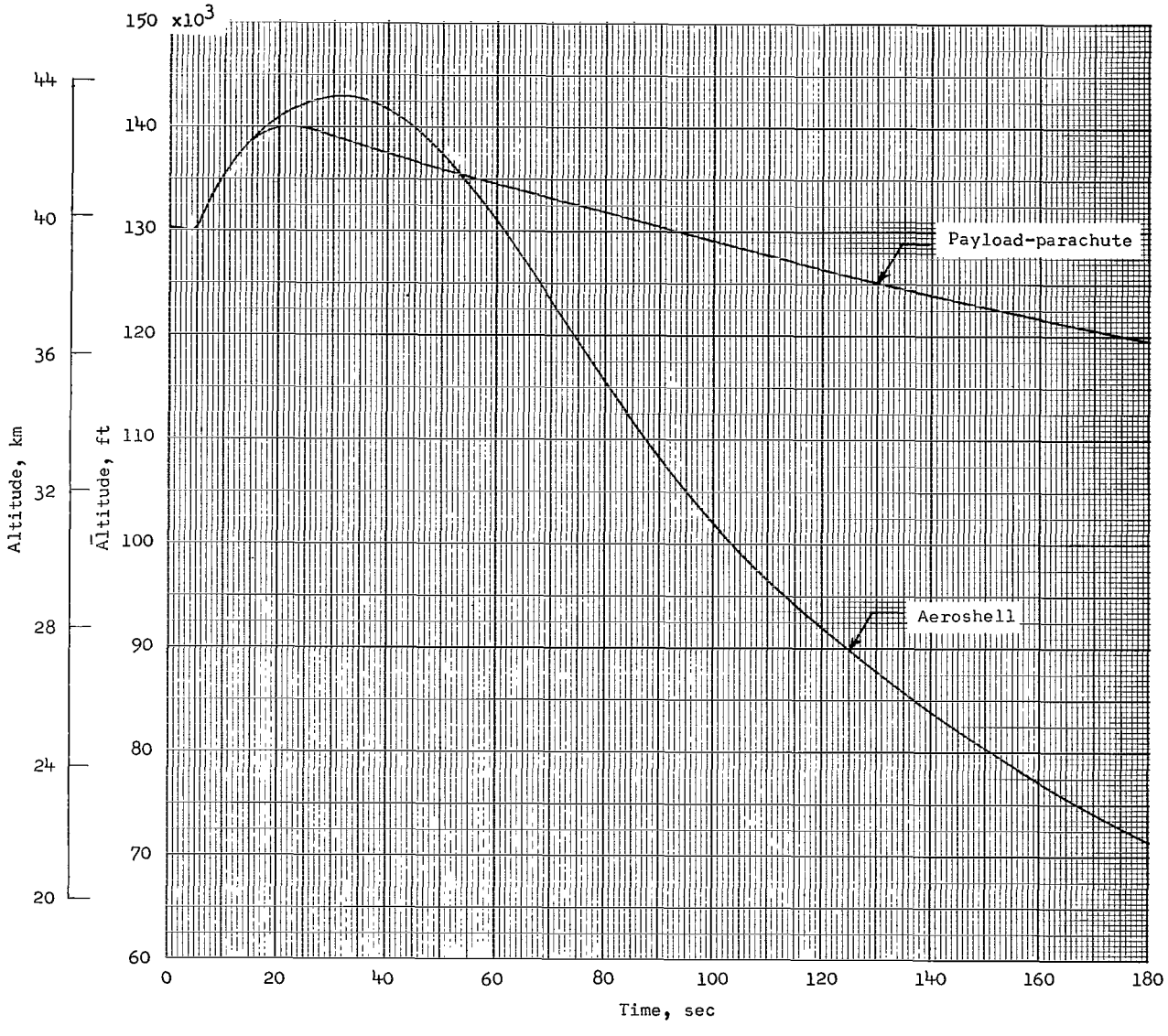

Figure 16.- Variation of altitude with time for the aeroshell and payload-parachute.

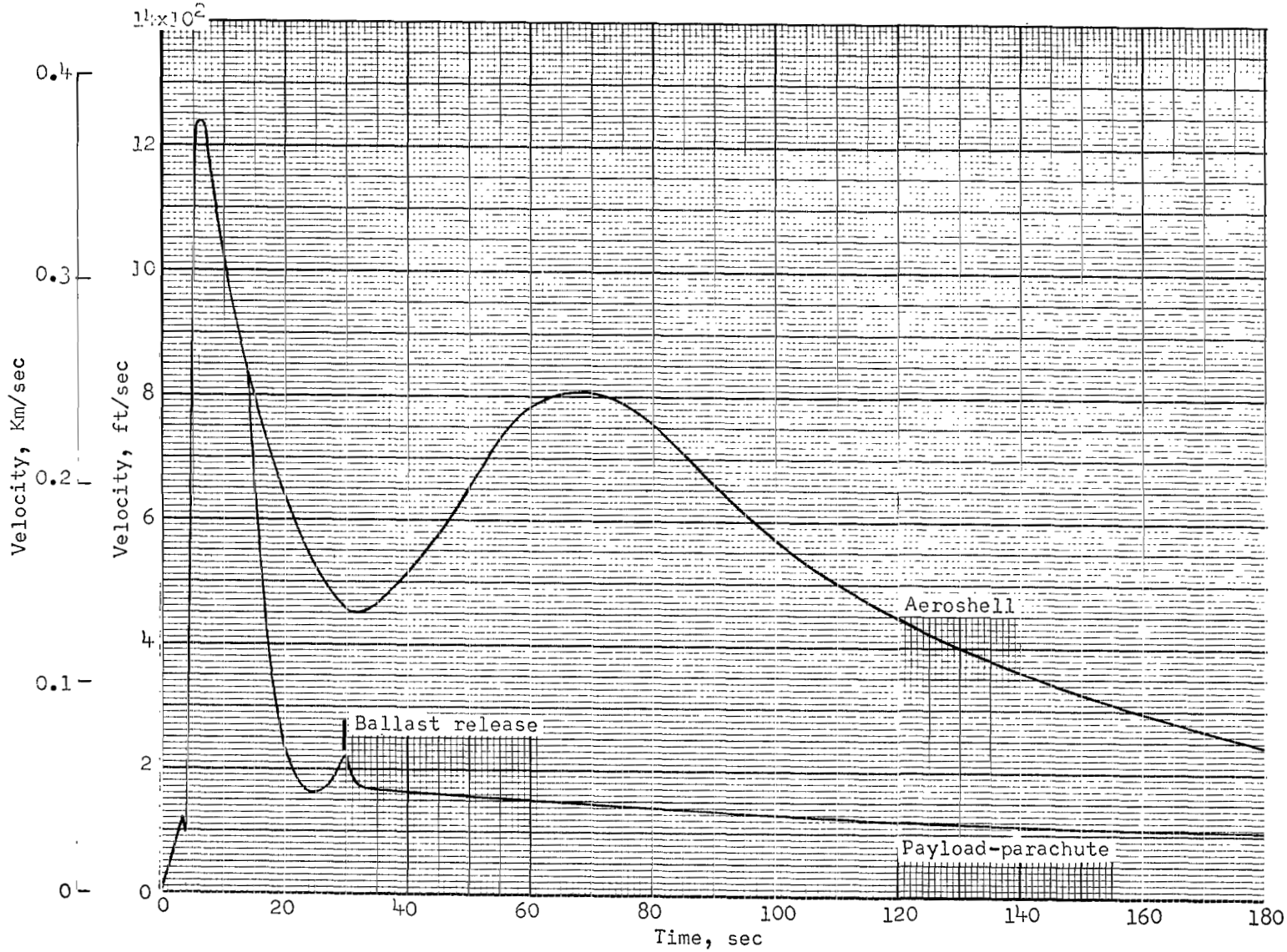

Figure 17.- Variation of the velocity with time of the aeroshell and payload-parachute from 0 to 180 seconds.

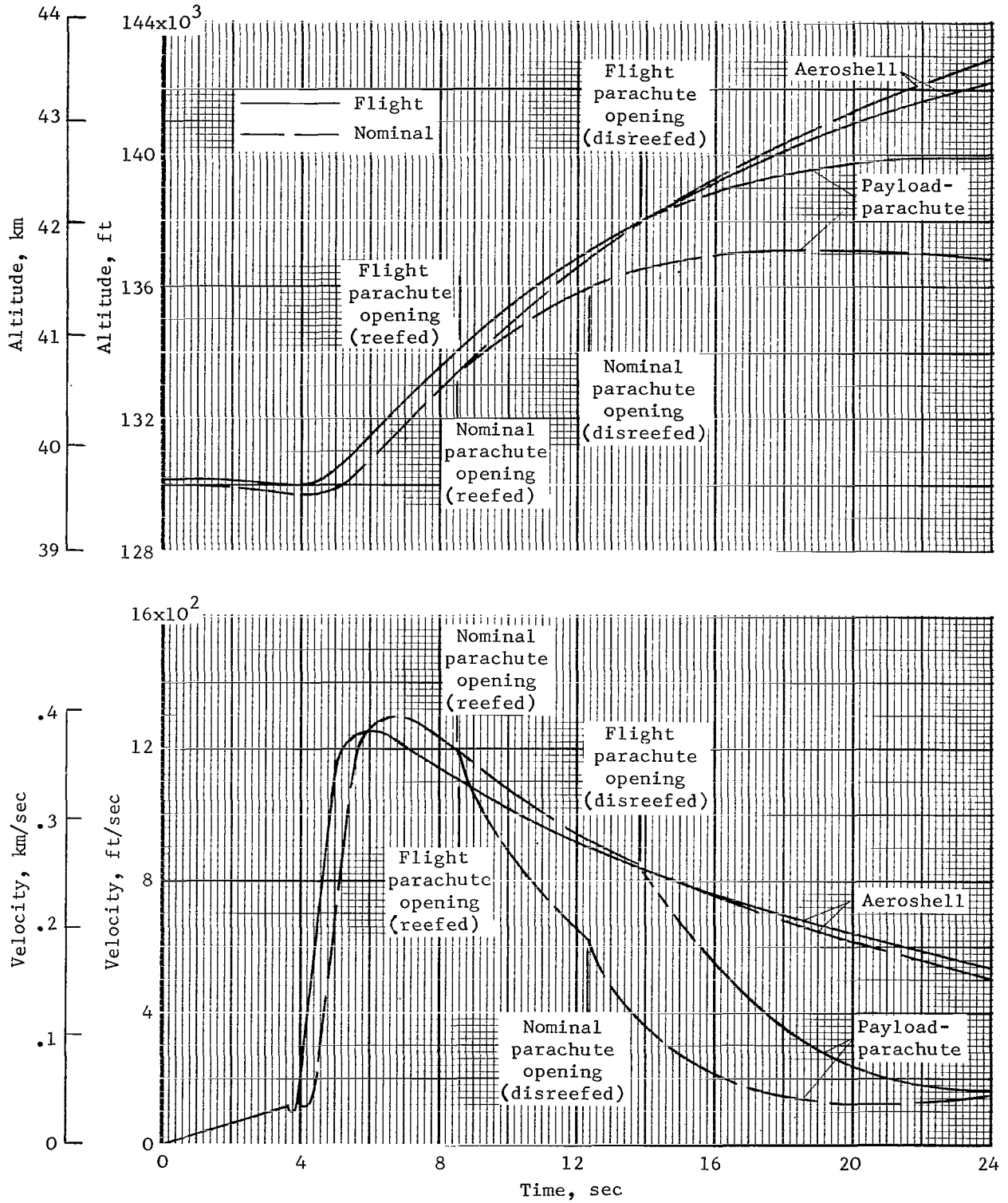

Figure 18.- Variation of altitude and velocity with time for the aeroshell and payload-parachute during the prime test period.

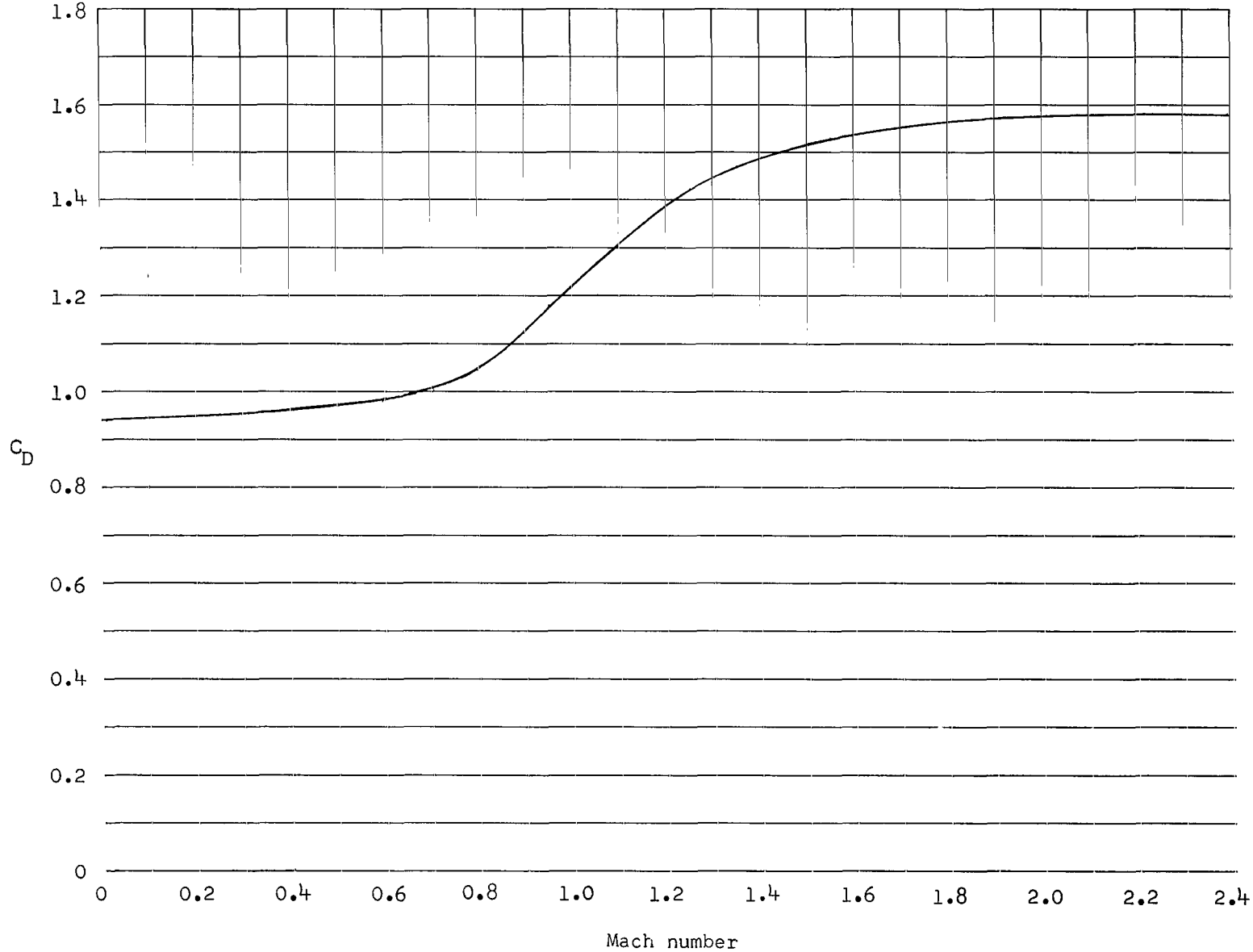

Figure 19.- Variation of drag coefficient with Mach number for 120° blunt cone configuration at zero angle of attack.

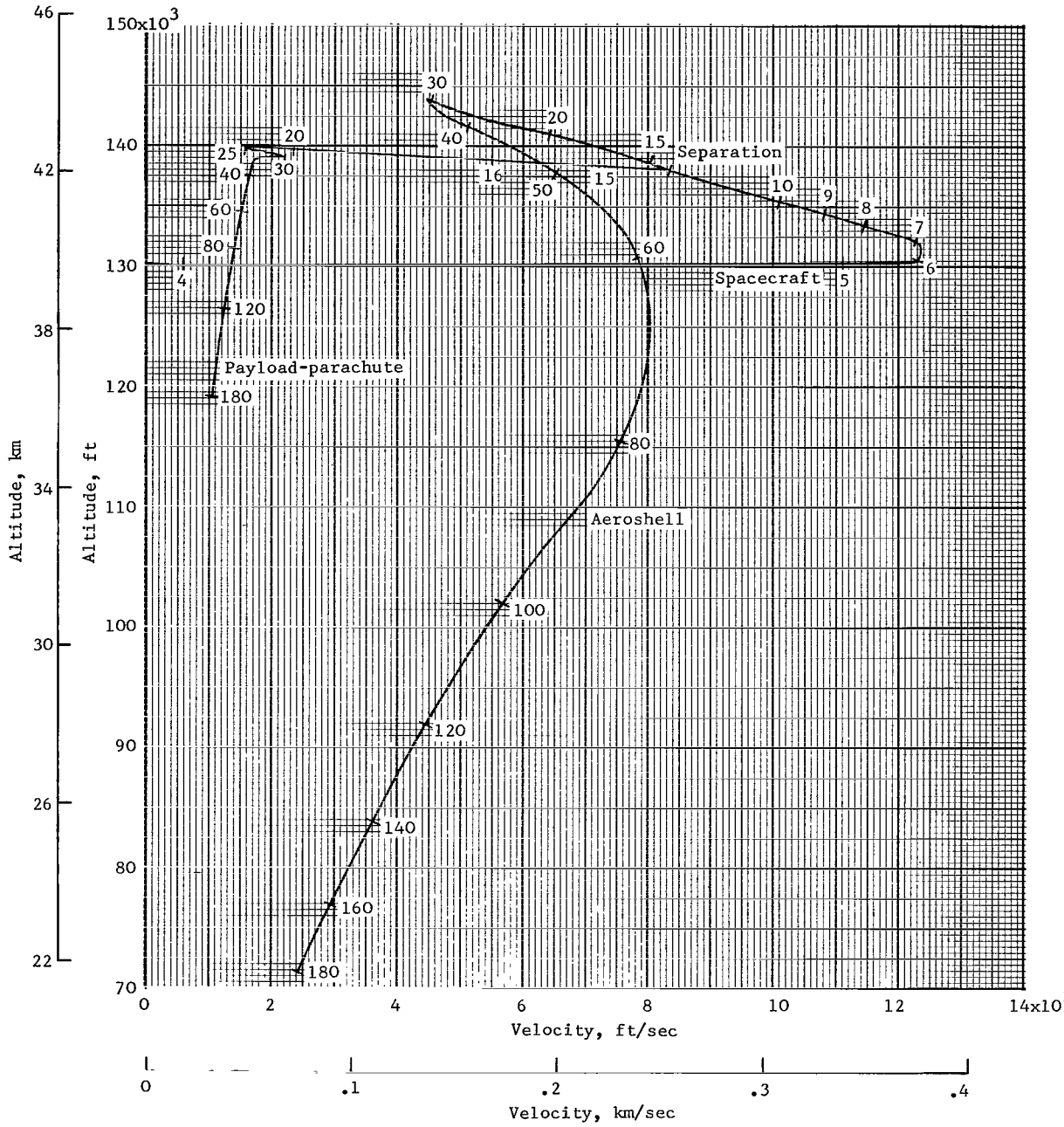

Figure 20.- Variation of the altitude with velocity of the aeroshell and payload-parachute. Tick marks indicate time from release in seconds.

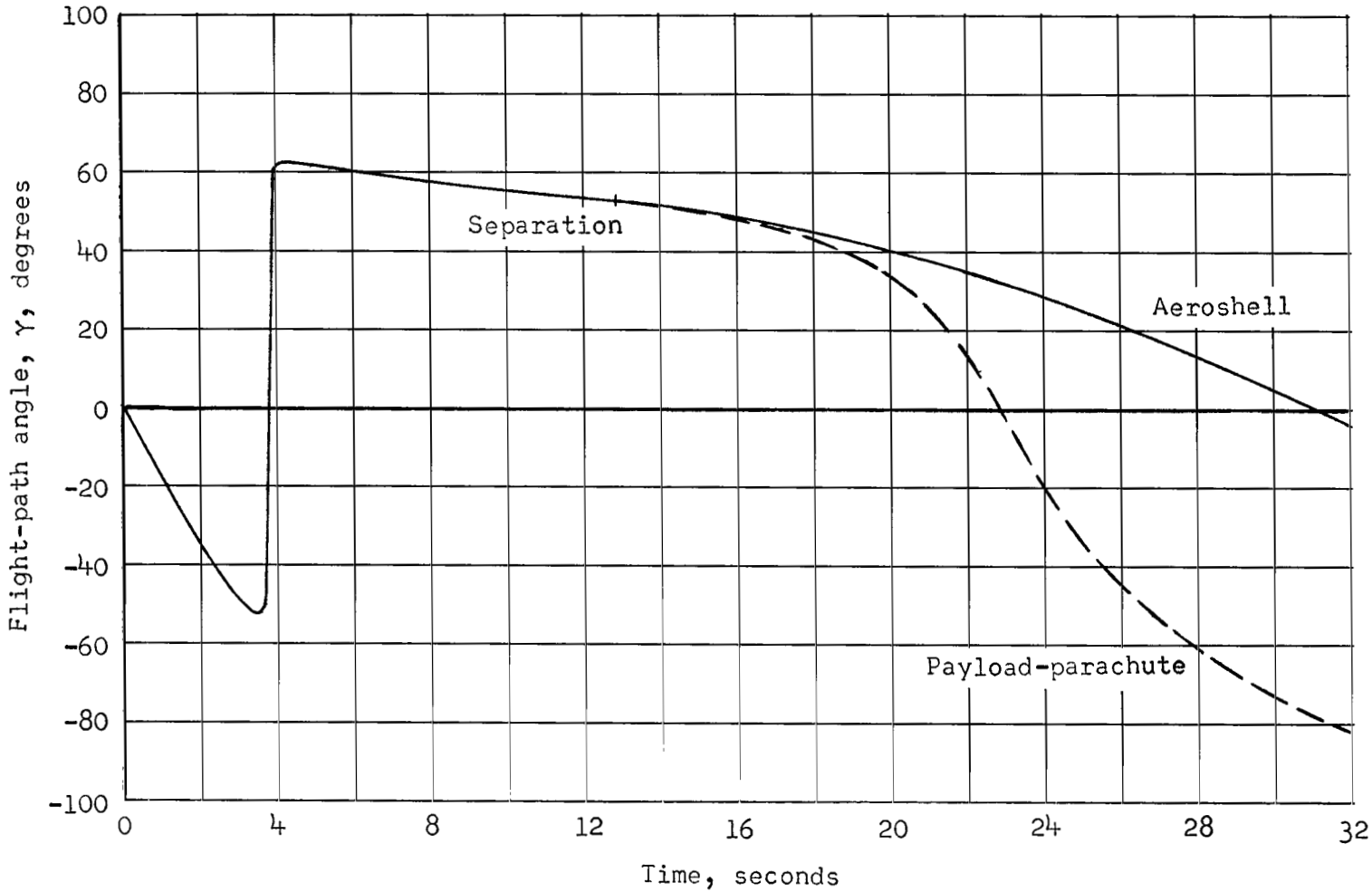

Figure 21.- Variation of flight-path angle with time.

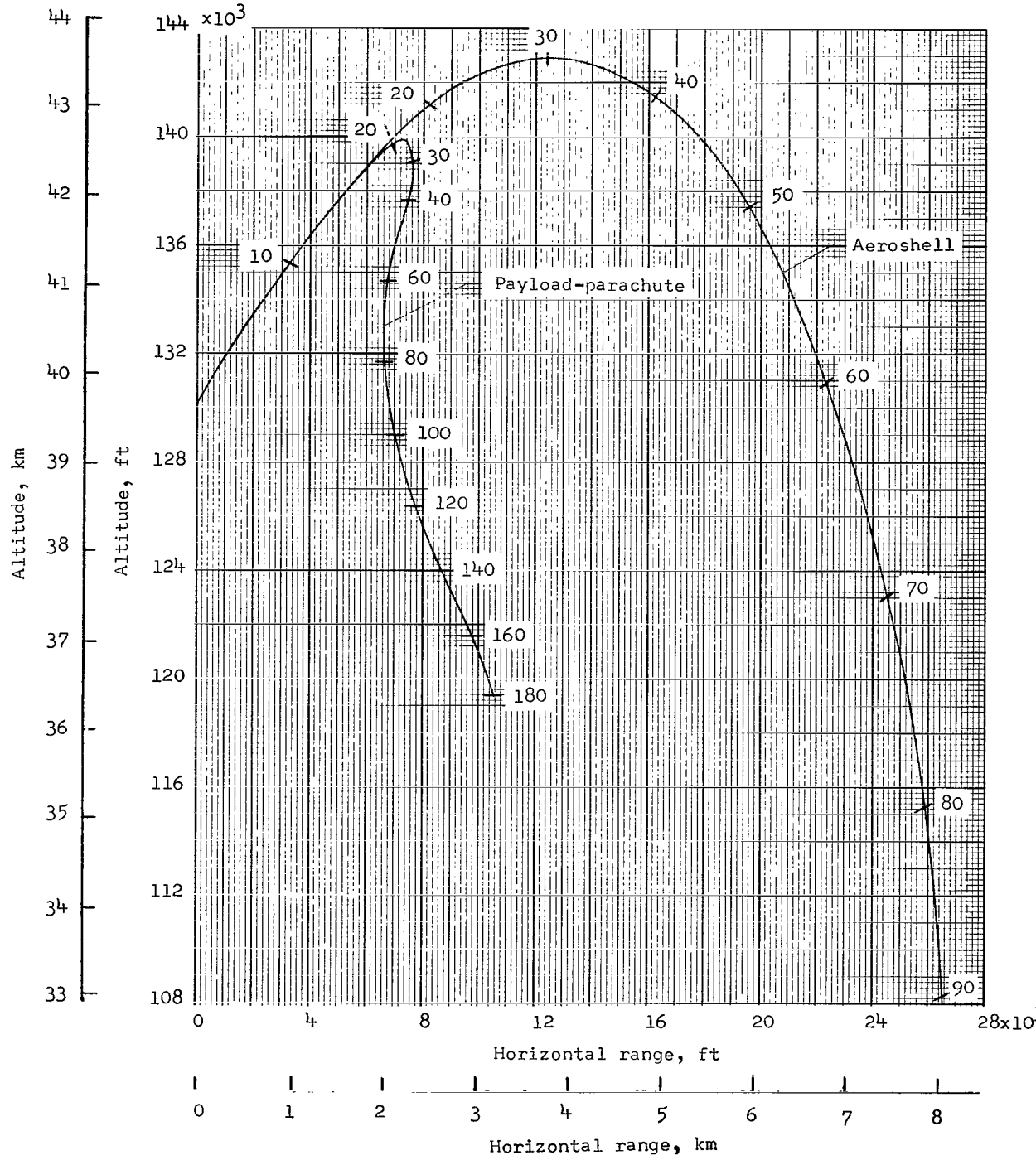

Figure 22.- Variation of altitude with horizontal range of the aeroshell and payload-parachute. Ticks mark time in seconds.

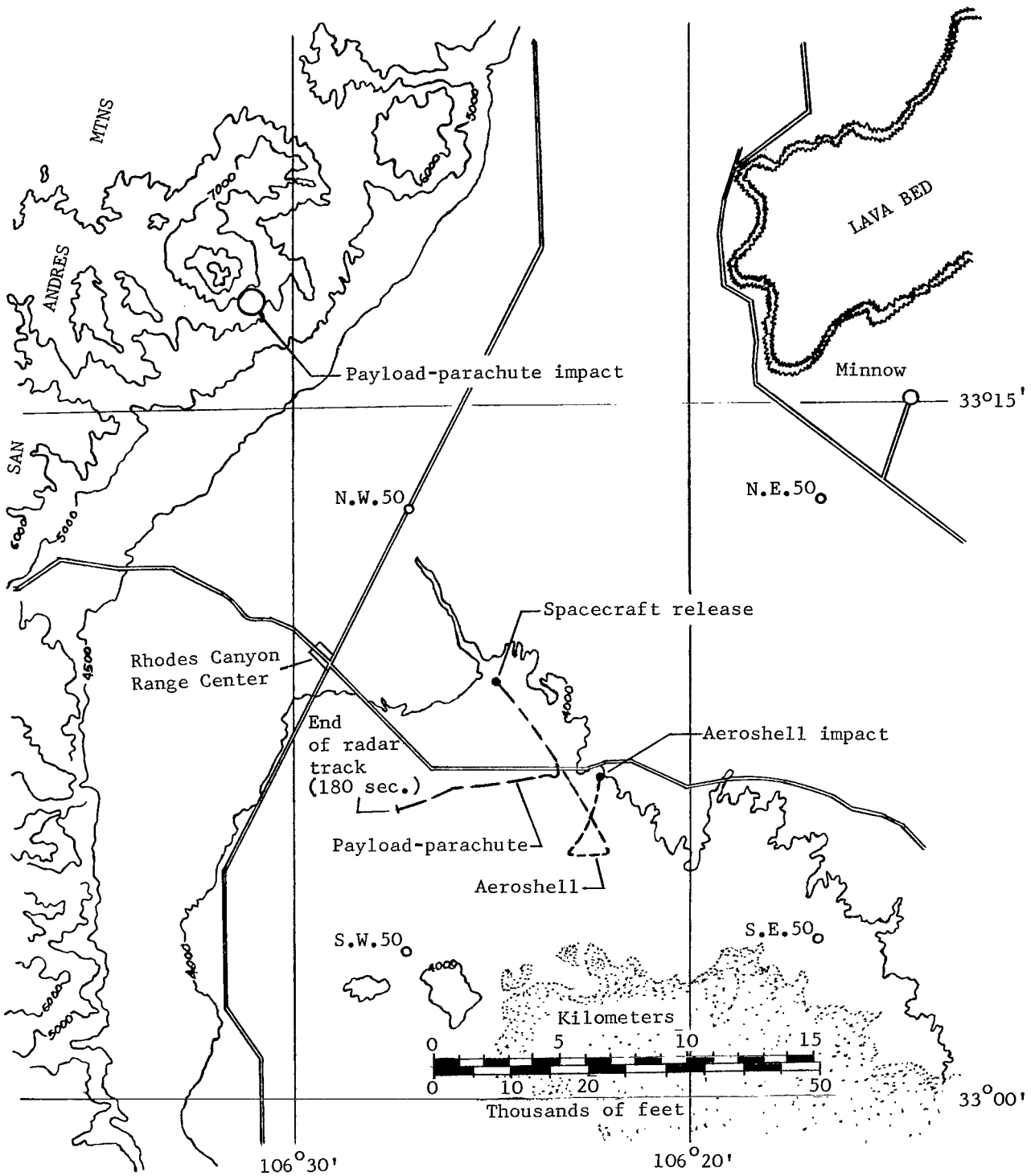

Figure 23.- Ground track of aeroshell and payload-parachute.

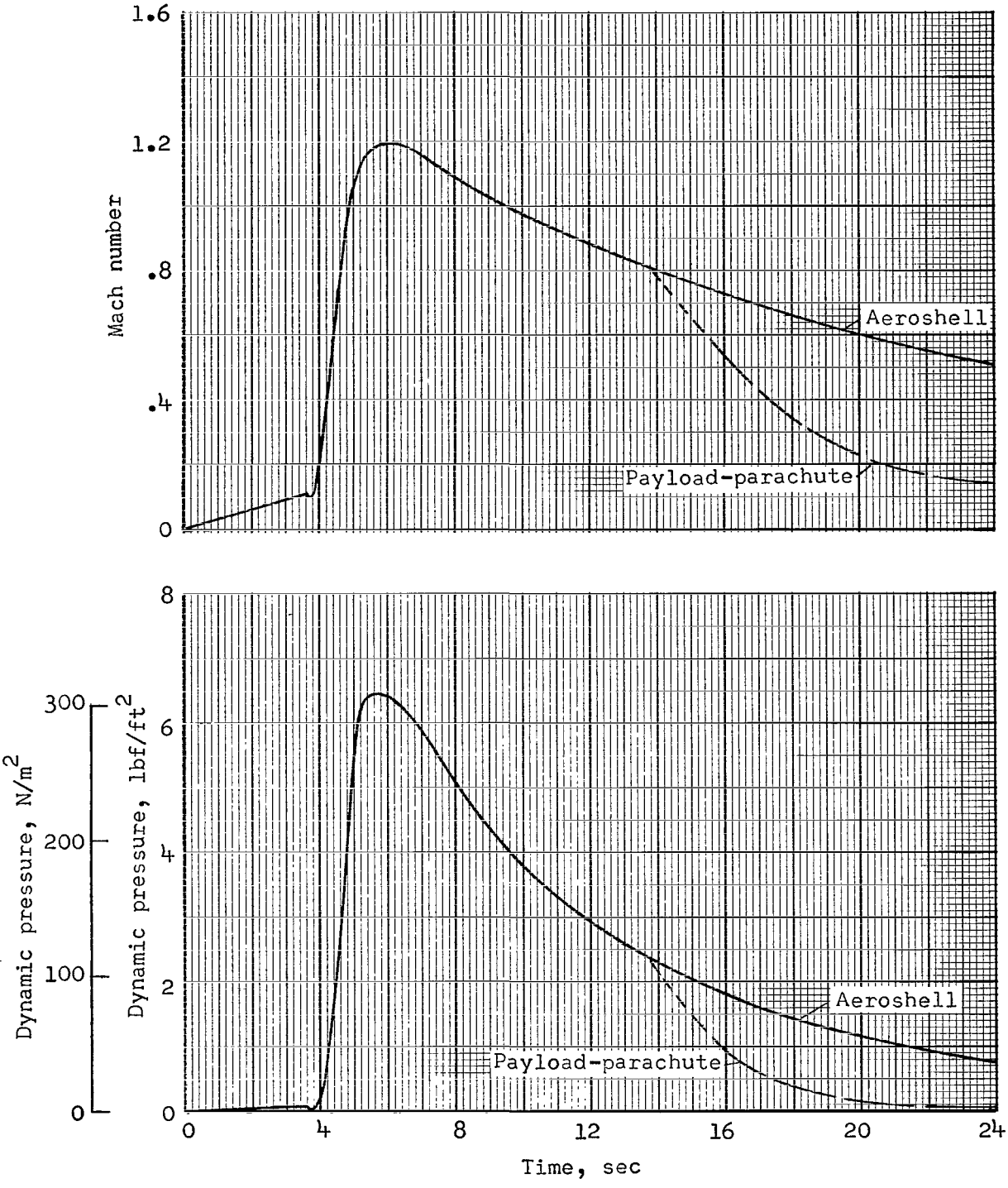

Figure 24.- Variation of Mach number and dynamic pressure with time for the aeroshell and payload-parachute.

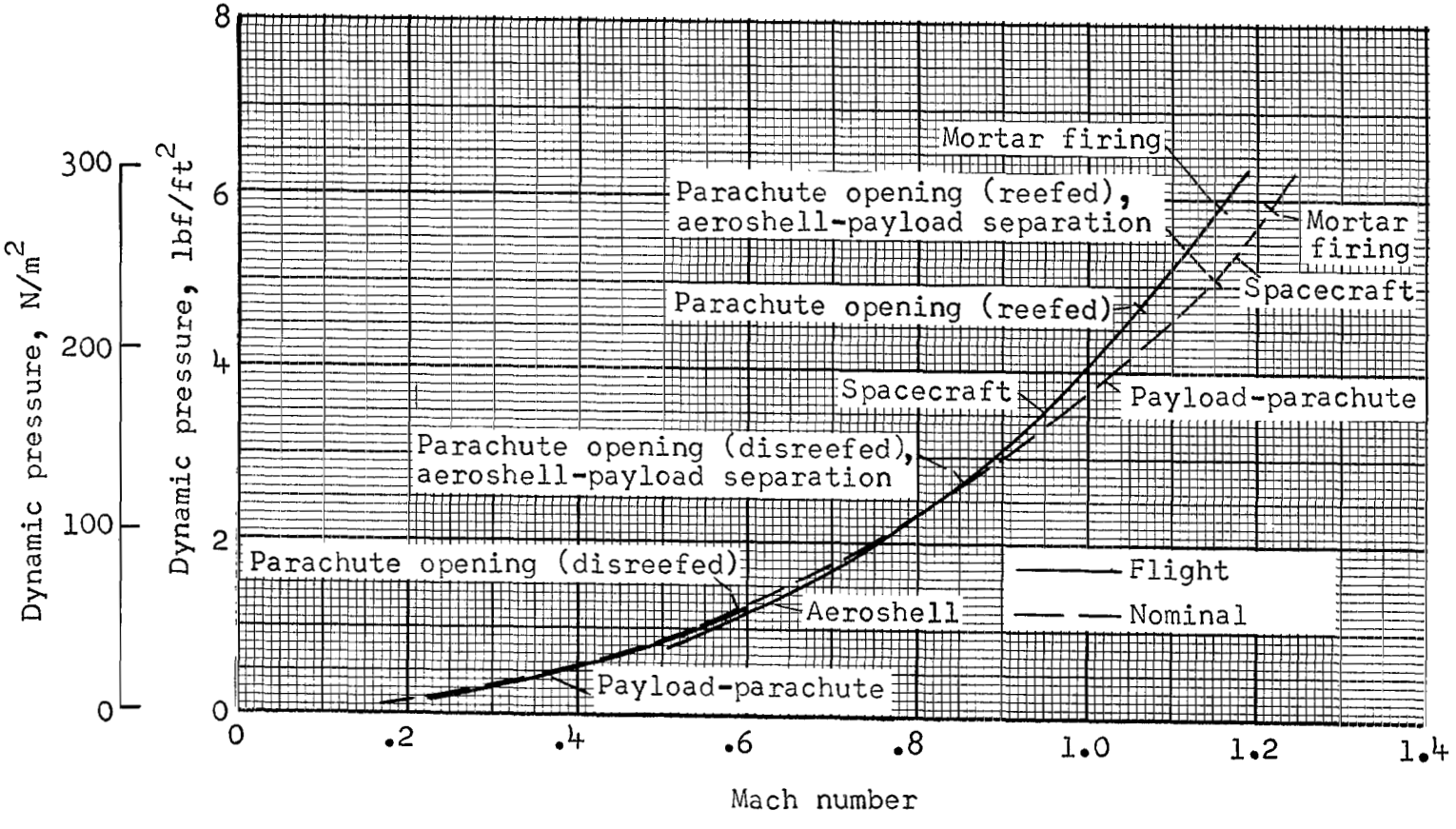

Figure 25.- Variation of dynamic pressure with Mach number comparing flight data with nominal data. Tick marks indicate the occurrence of flight events.

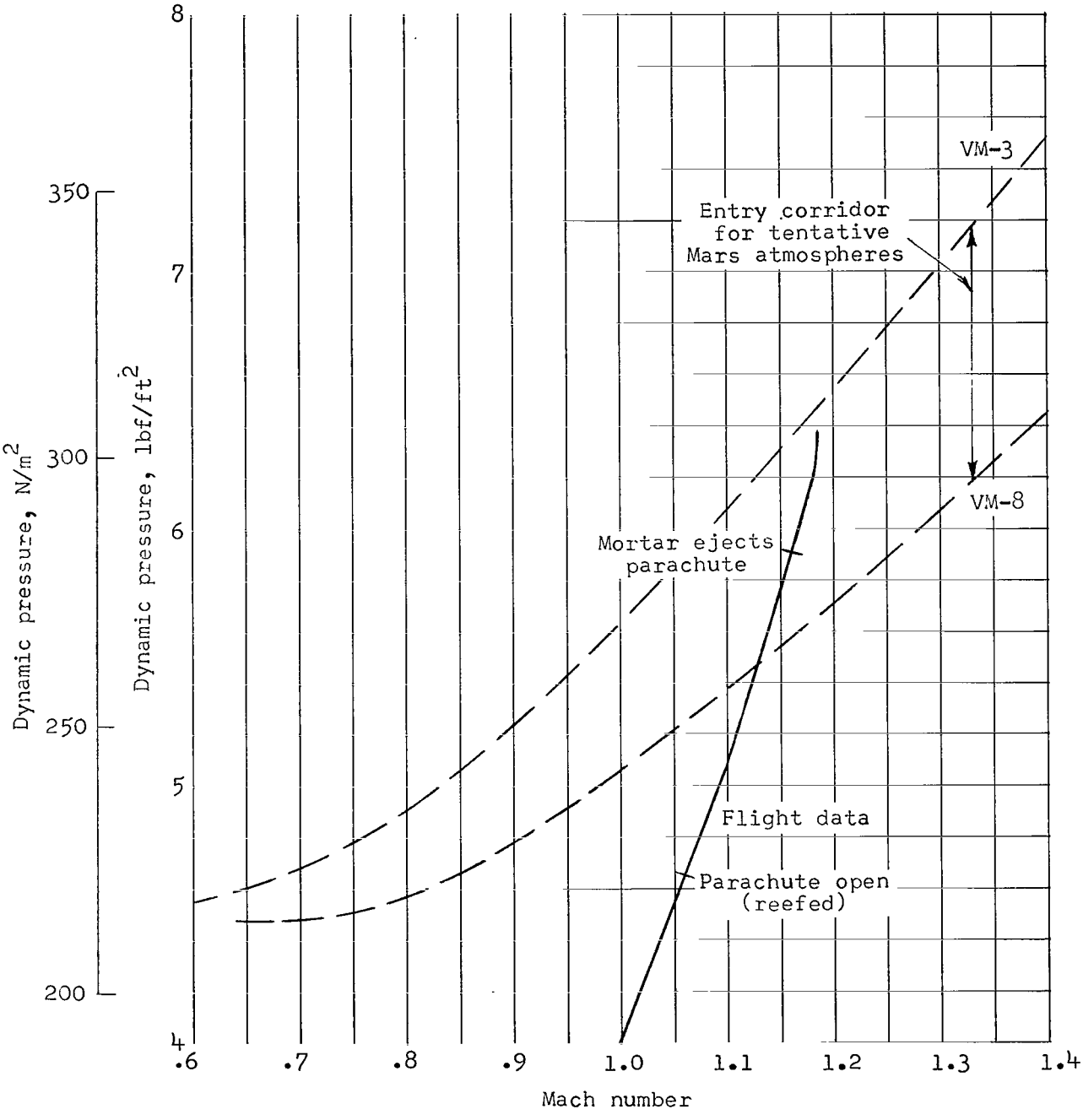

Figure 26.- Dynamic pressure variation with Mach number for the flight as compared with that for the entry corridor defined by the tentative Mars atmosphere (see fig. 1).

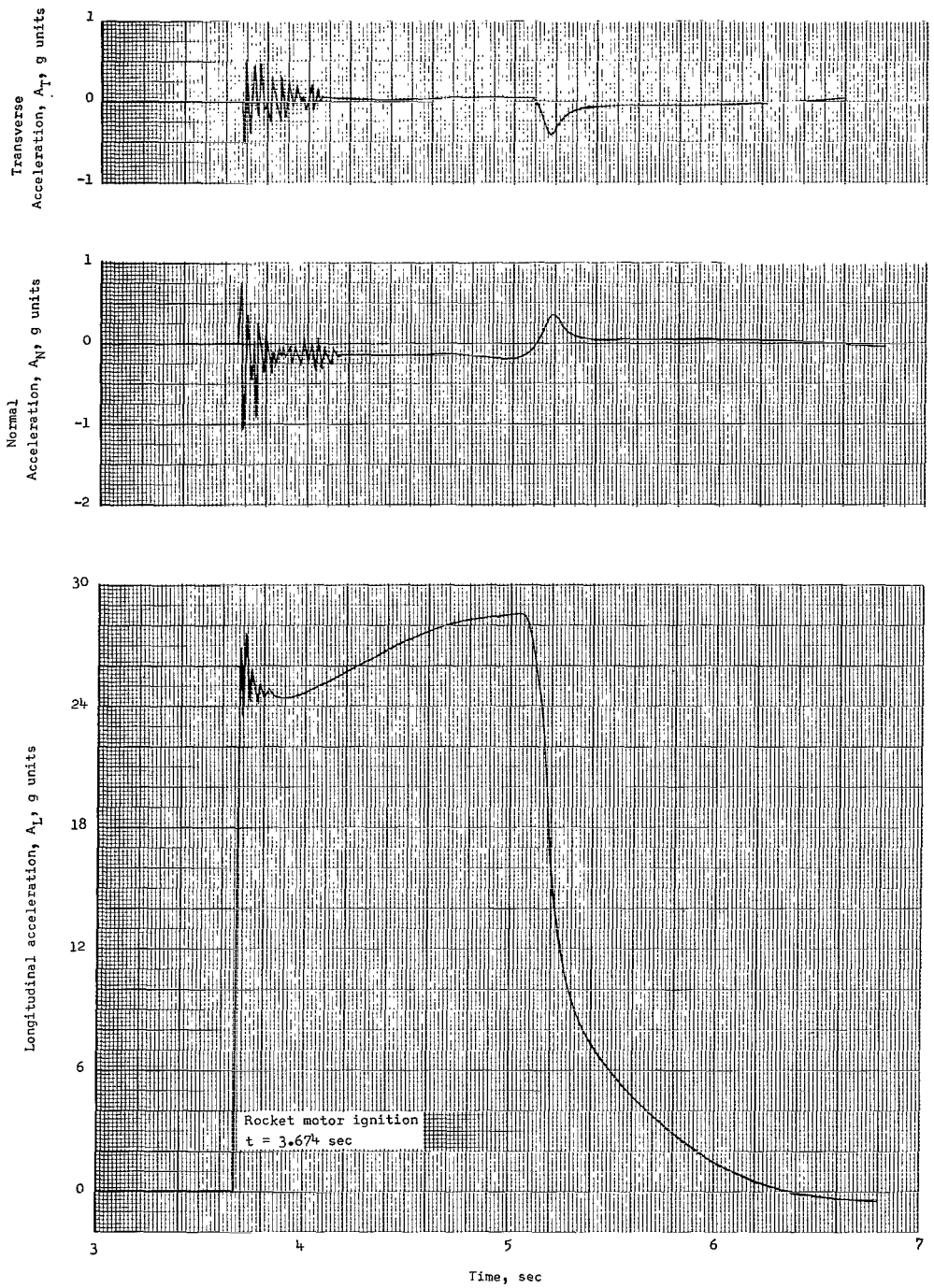

(a) t = 3 to 7 sec.

Figure 27.- Time history of the longitudinal, normal, and transverse acceleration measured in the payload.

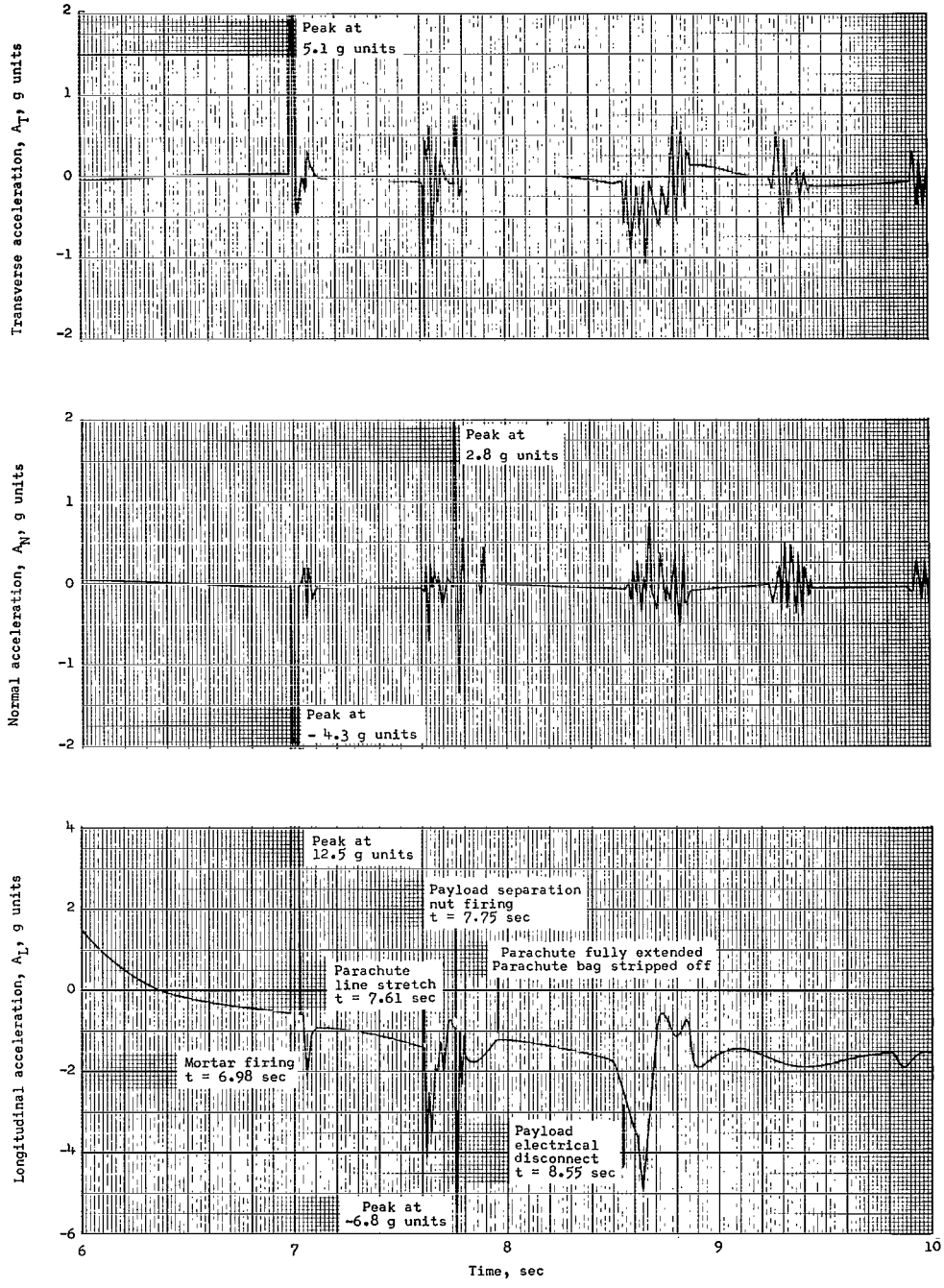

(b) t = 6 to 10 sec.

Figure 27.- Continued.

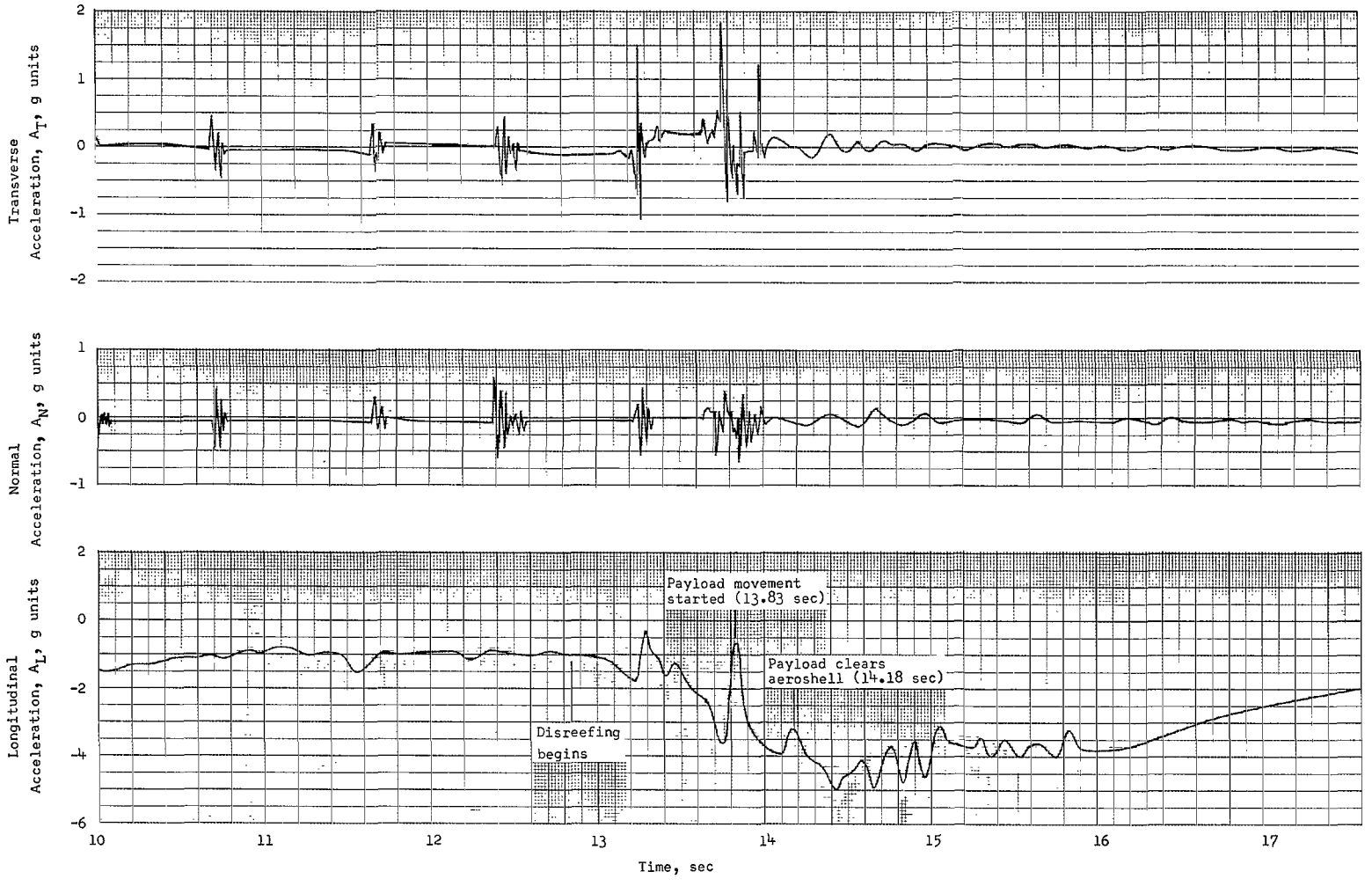

(c) t = 10 to 17.6 sec.

Figure 27.- Continued.

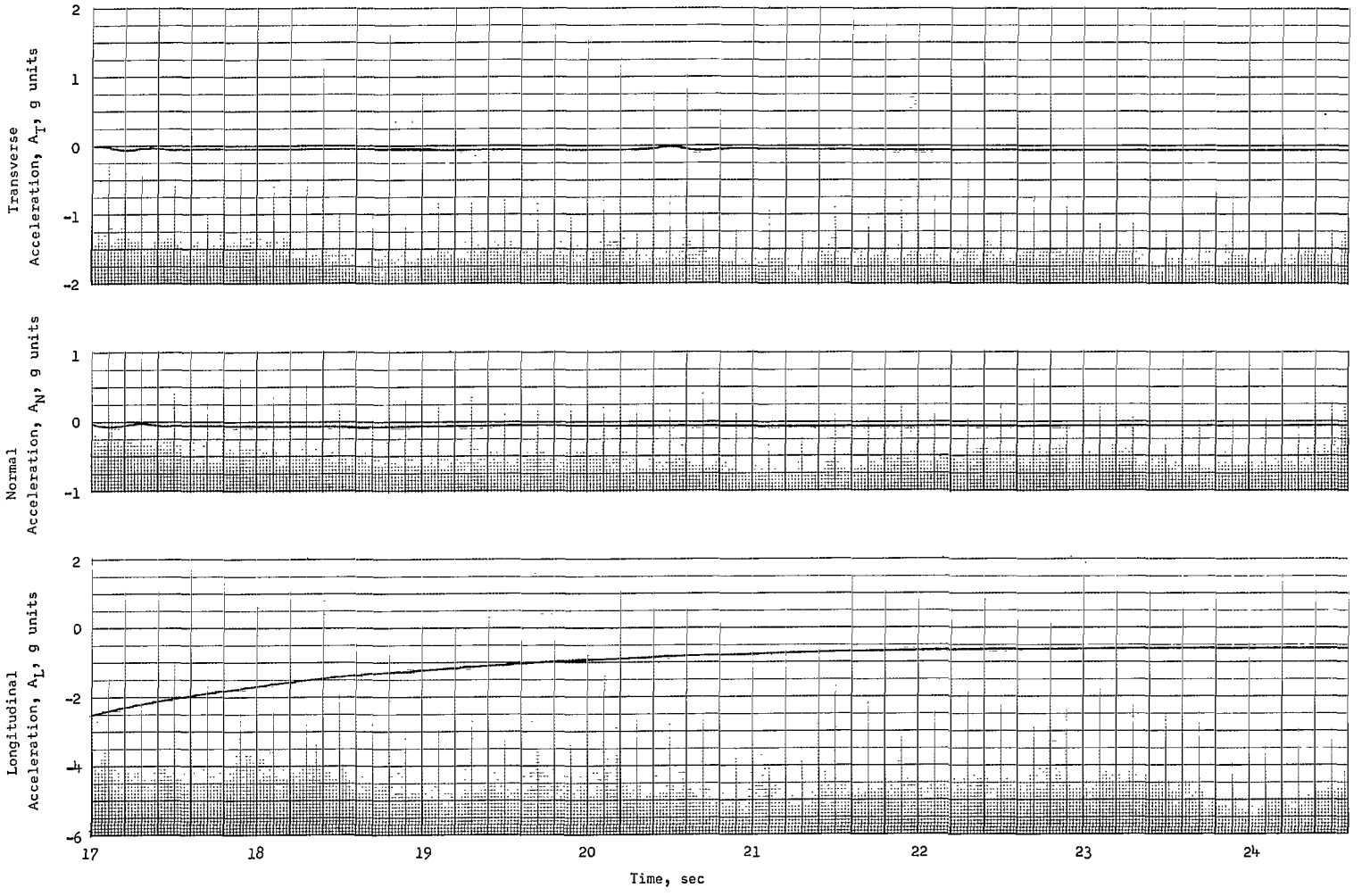

(d) t = 17 to 24.6 sec.

Figure 27.- Continued.

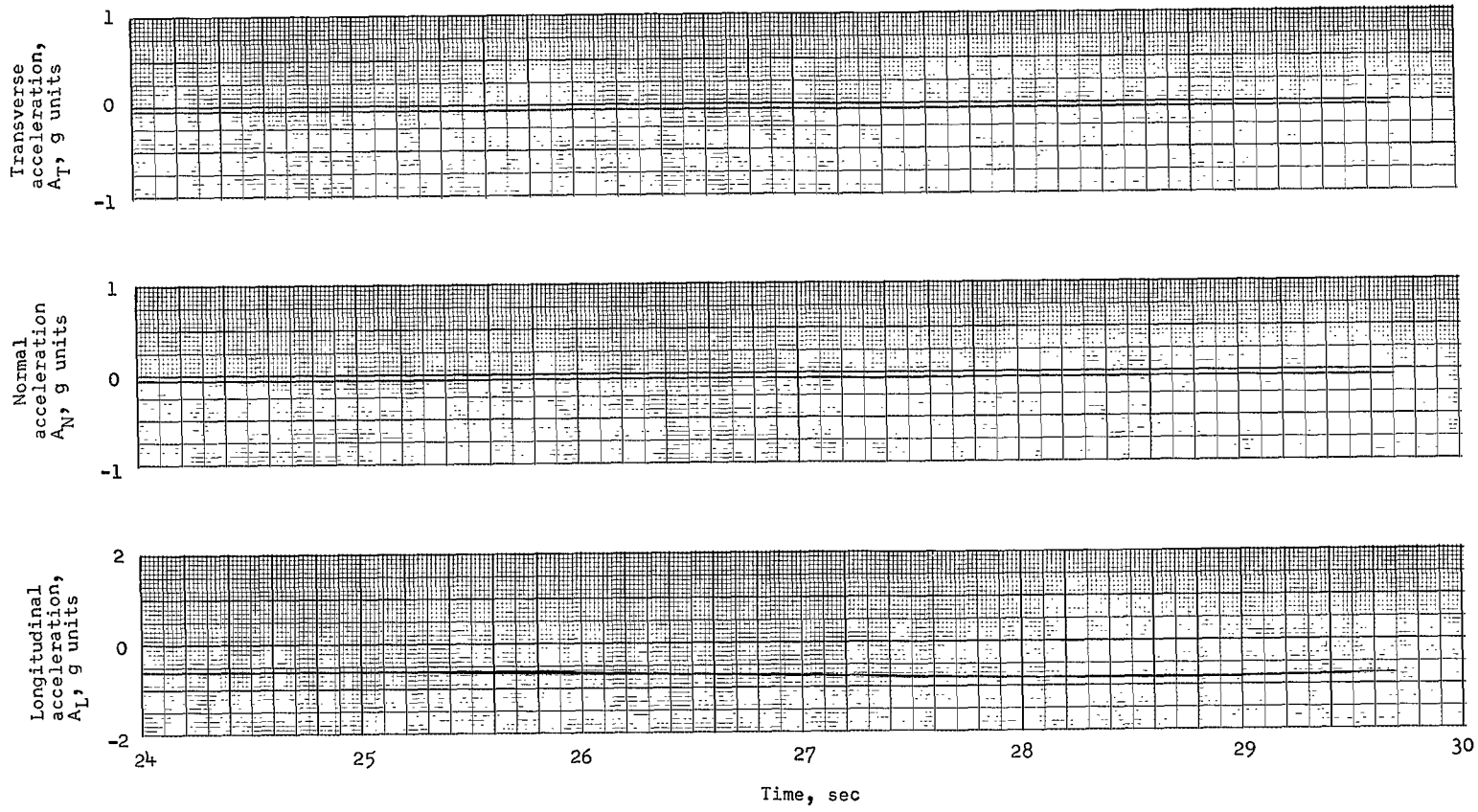

(e) t = 24 to 30 sec.

Figure 27.- Concluded.

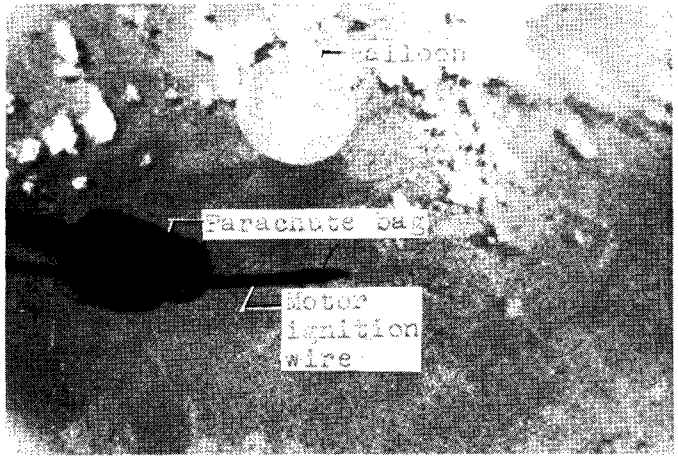

(a) Parachute bag after leaving mortar.

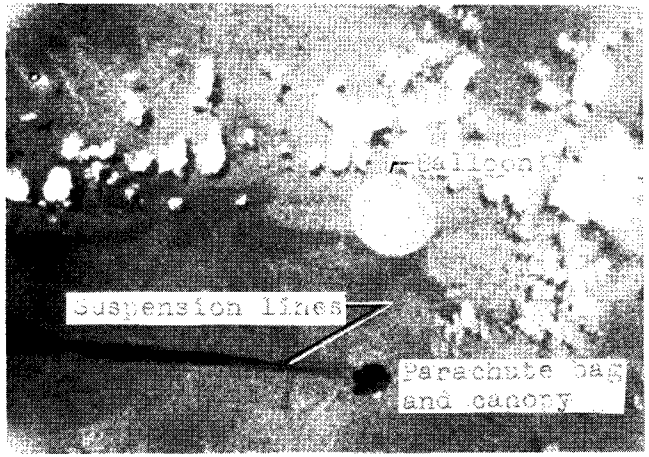

(b) Ringsails emerging from bag.

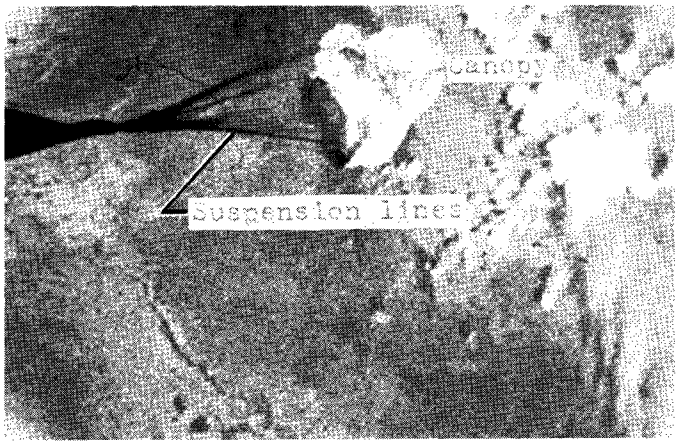

(c) Reefed inflation of parachute.

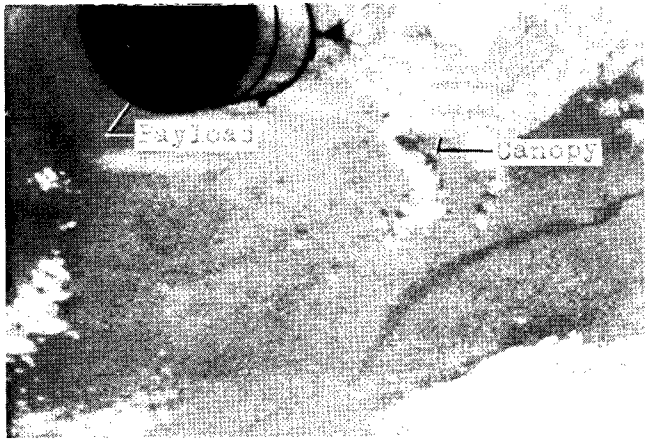

(d) Payload leaving aeroshell.

Figure 28.- View of parachute deployment from aeroshell camera 1. L-67-6644

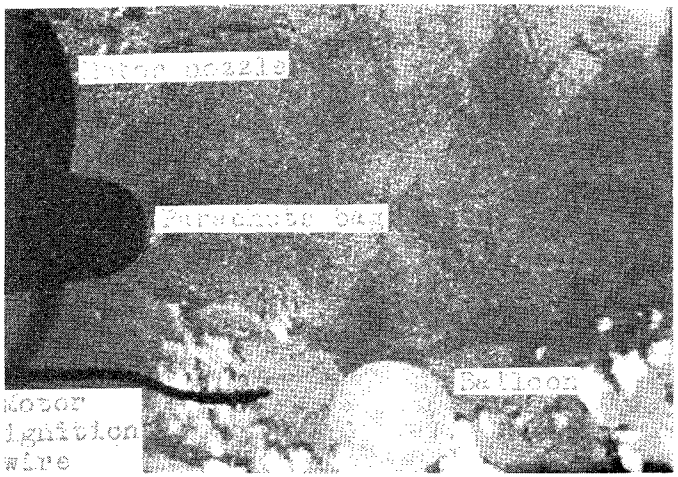

(a) Parachute bag emerging from mortar.

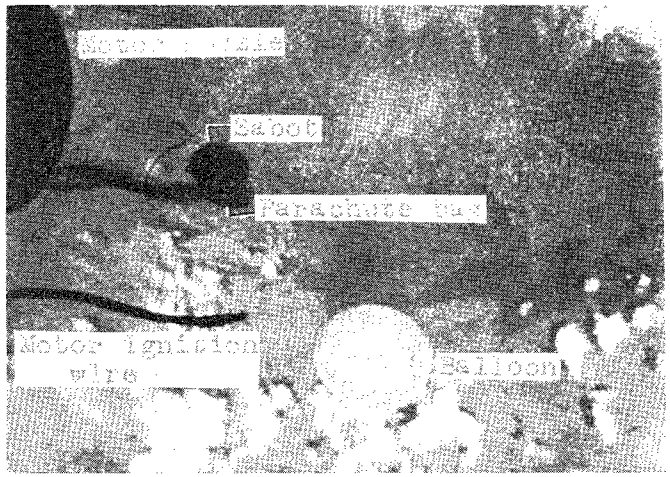

(b) Parachute bag leaving sabot.

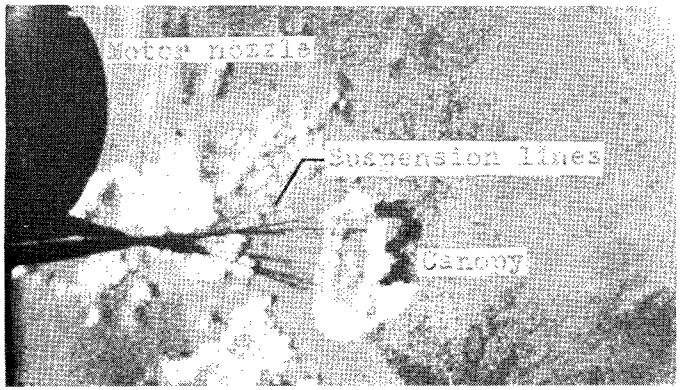

(c) Parachute opening to reefed condition.

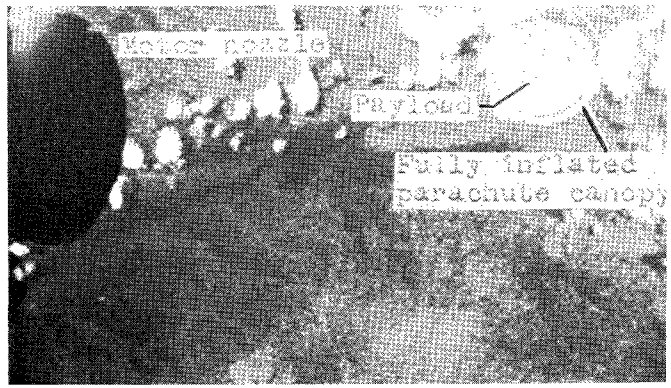

(d) Parachute disreefed.

Figure 29.- View of parachute deployment from aeroshell camera 2. L-67-6645

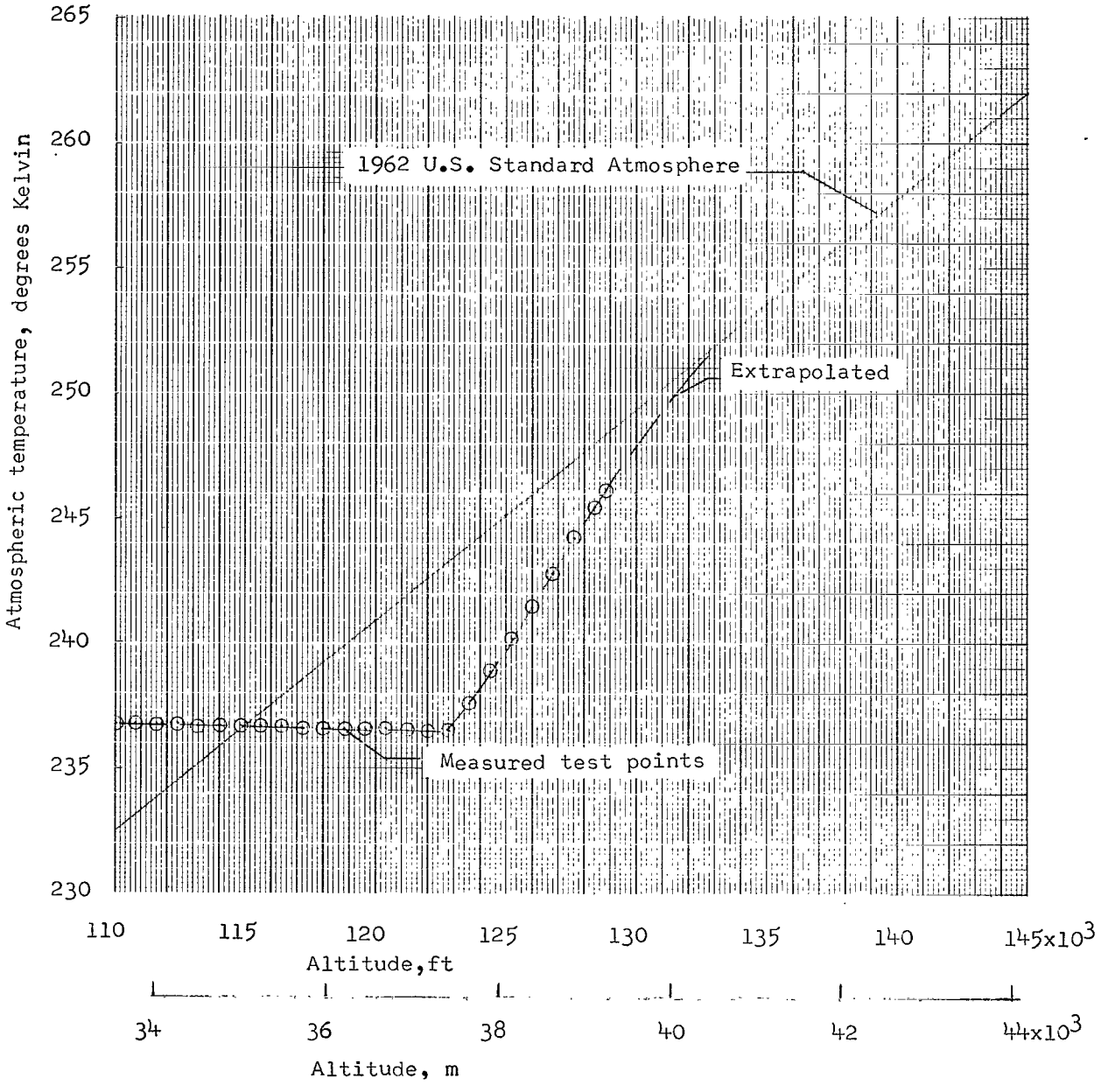

(a) Atmospheric temperature variation with altitude.

Figure 30.- Atmospheric conditions as measured by rawinsonde.

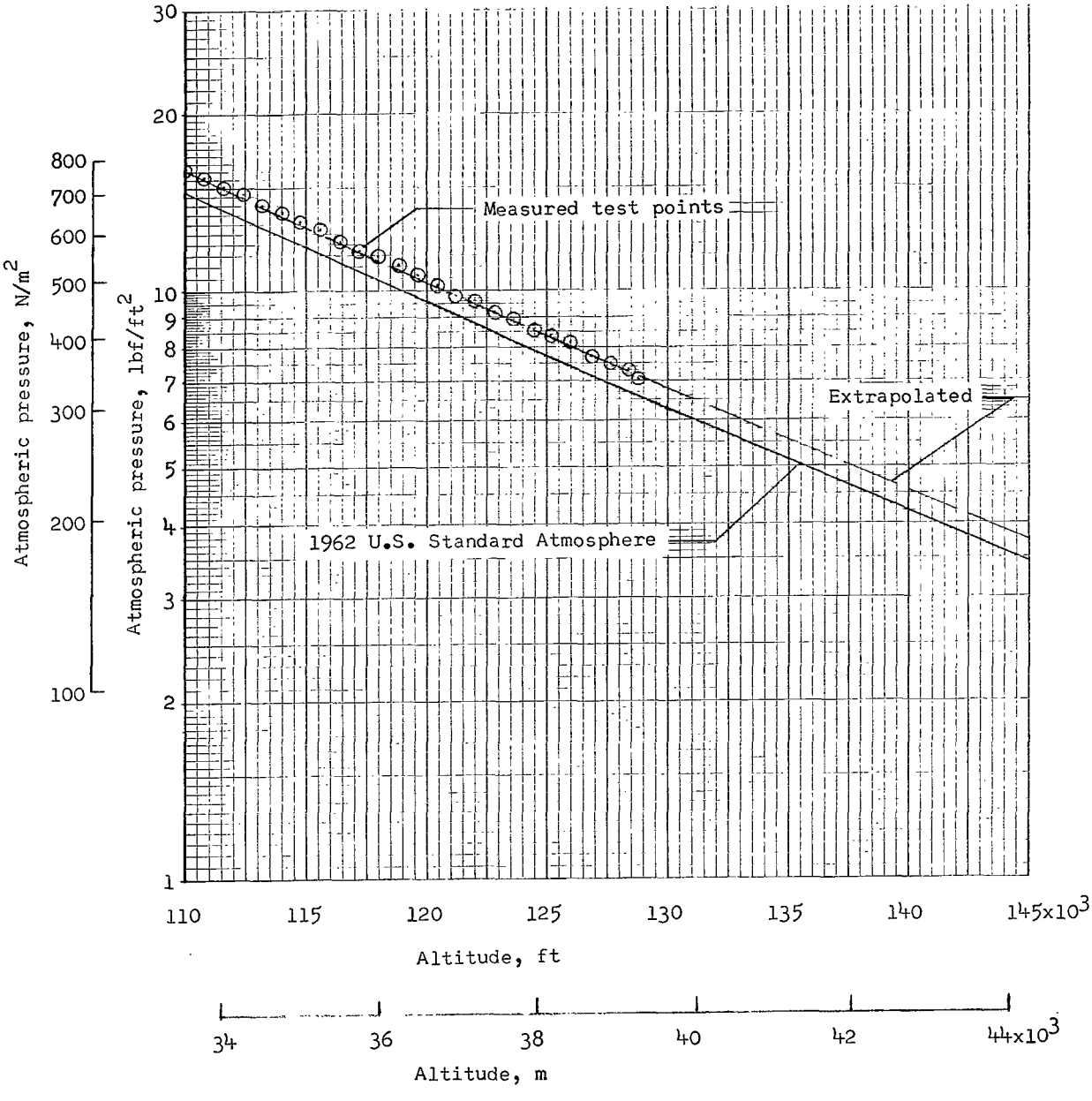

(b) Atmospheric pressure variation with altitude.

Figure 30.- Concluded.

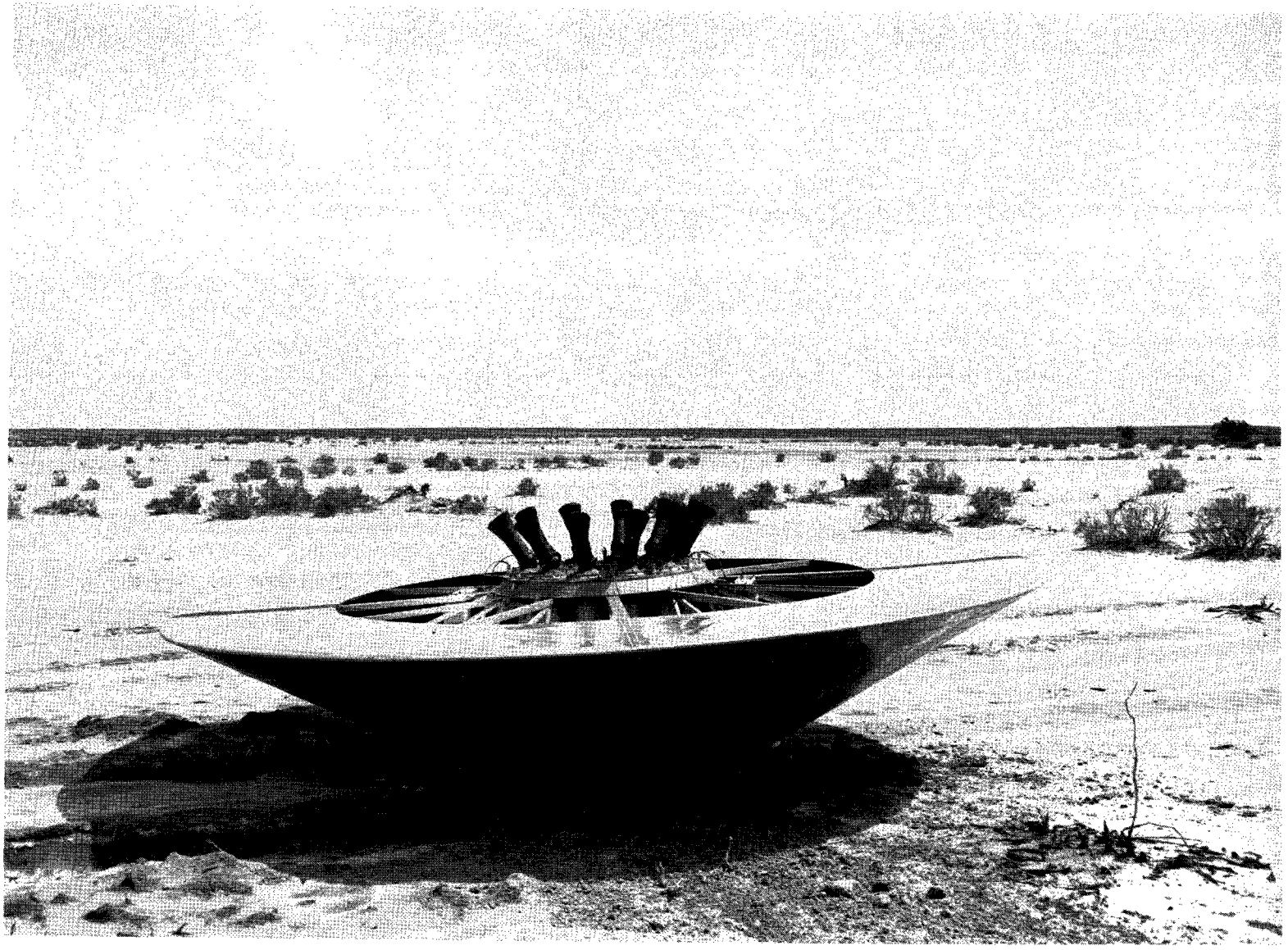

Figure 31.- Photograph of aeroshell after impact.

L-67-6646

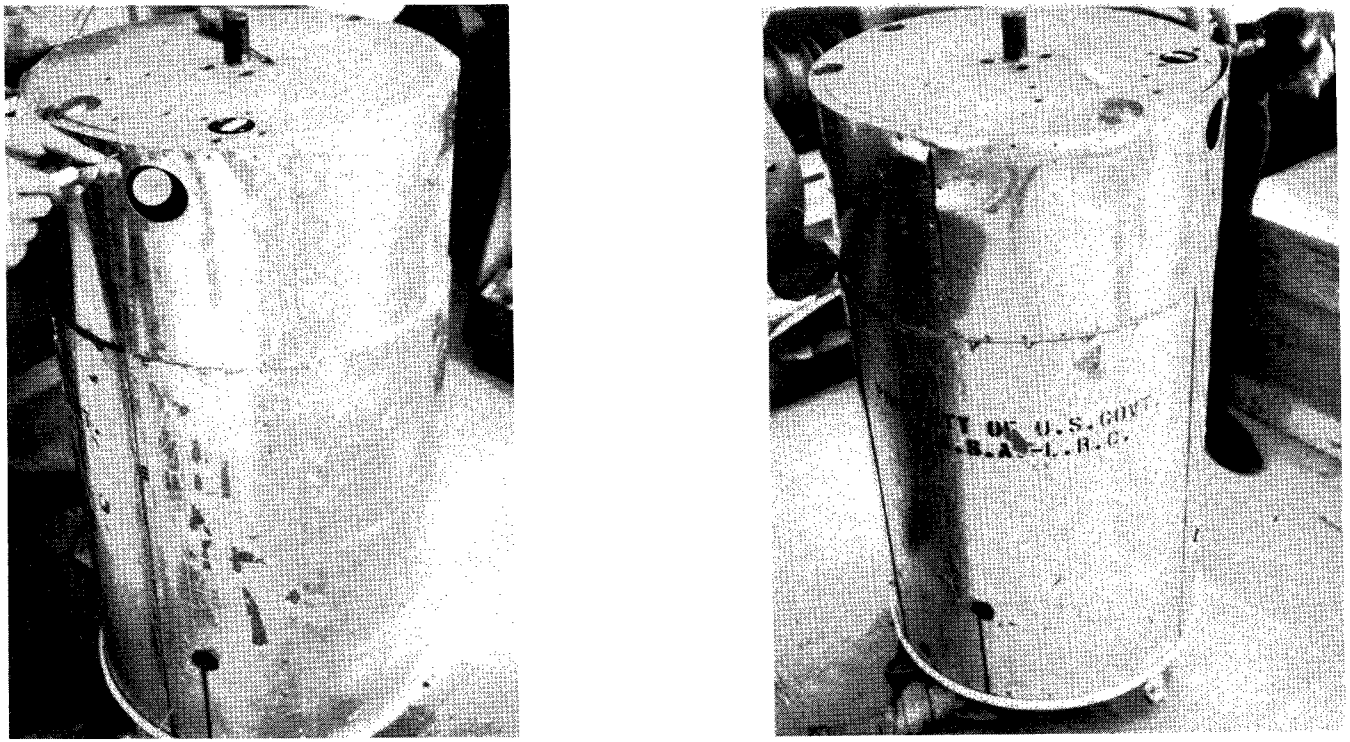

Figure 32.- Photographs of recovered payload.

L-67-6647

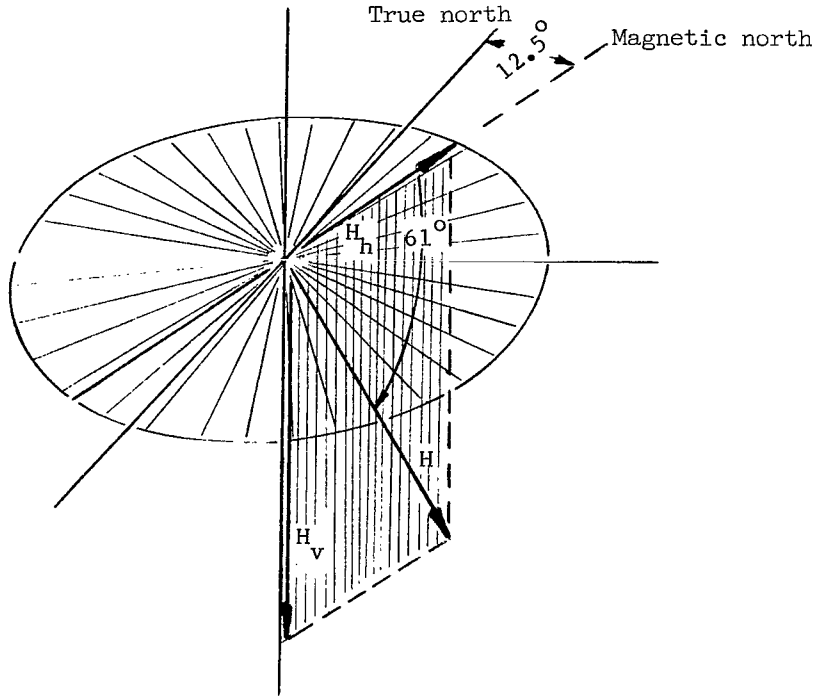

(a) Magnetic field vector H and its components (H_h, horizontal; H_v, vertical).

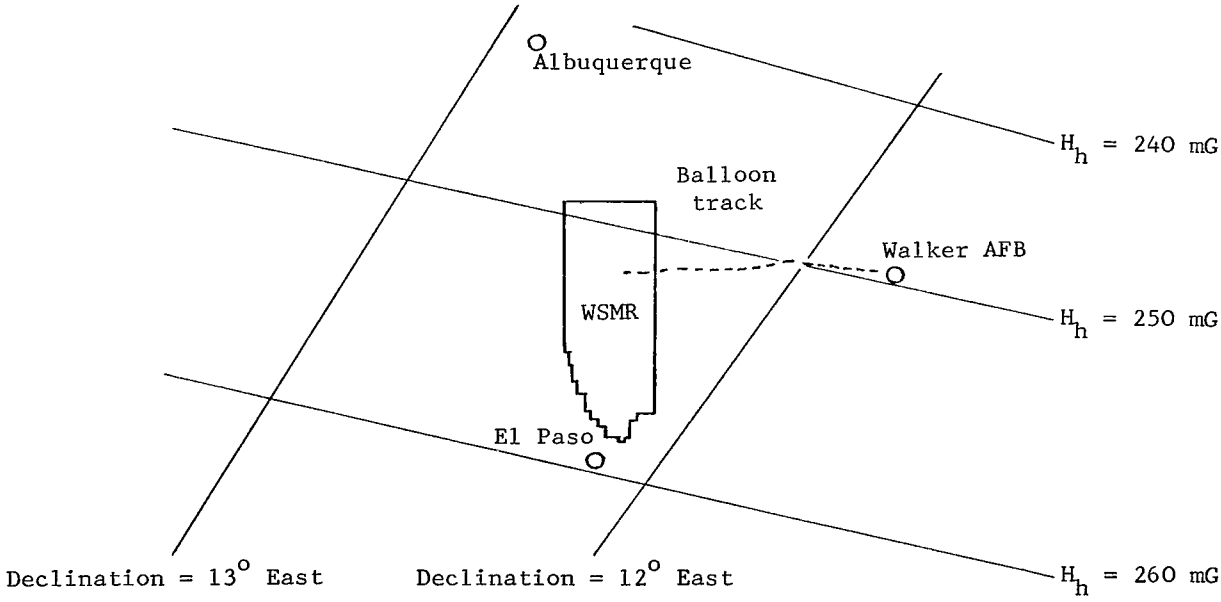

(b) Horizontal magnetic field lines at earth surface plane.

Figure 33.- Characteristic magnetic field conditions for area of WSMR.

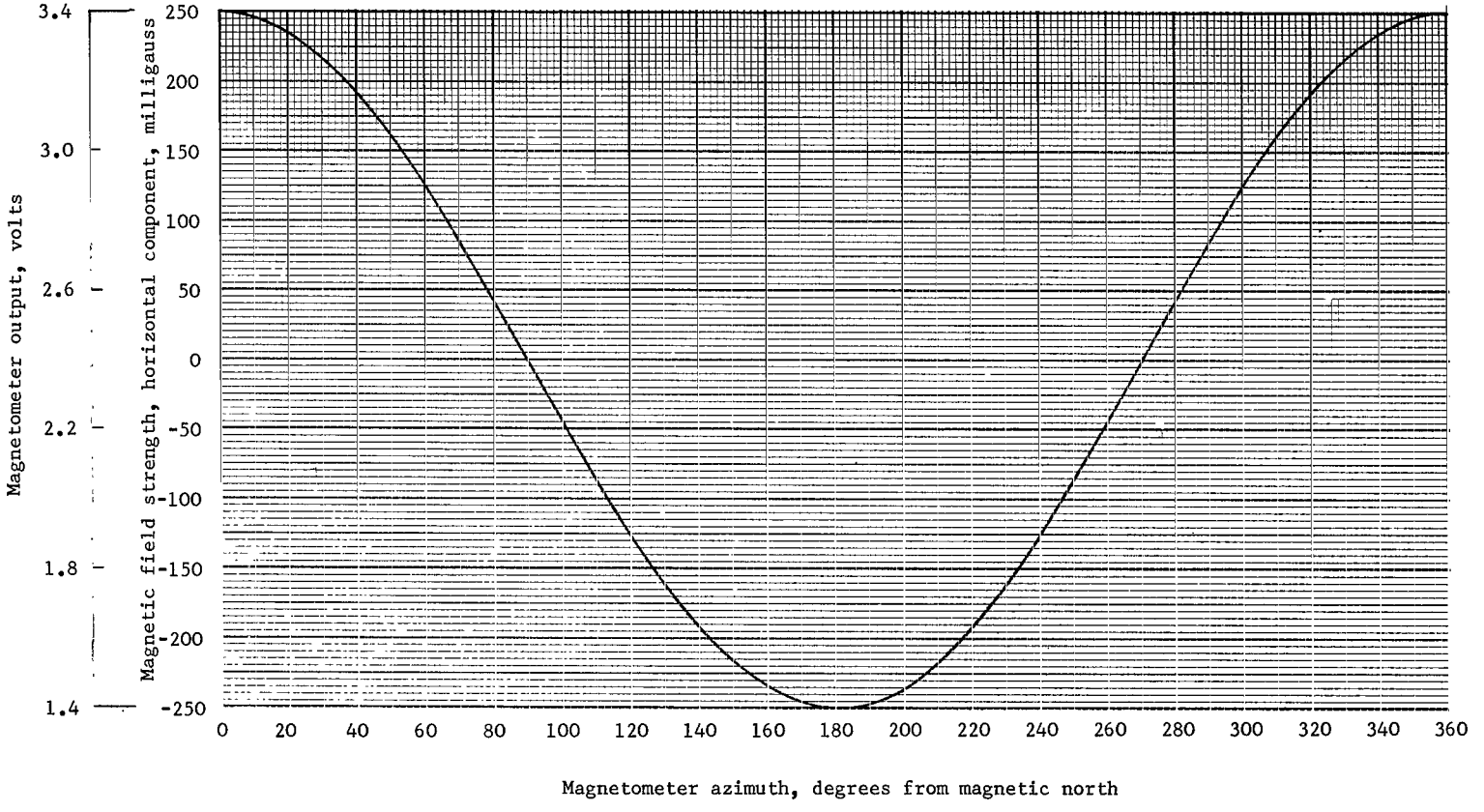

Figure 34.- Variation of horizontal component of magnetic field strength and magnetometer voltage with the azimuth of a magnetometer probe in a typical magnetic field in the general area of WSMR.

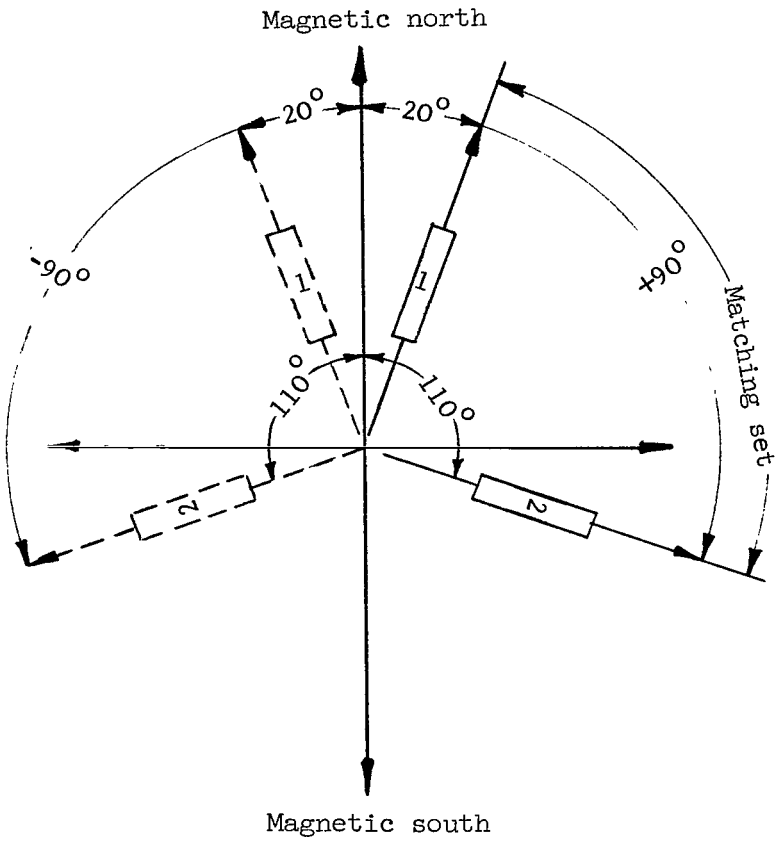

Figure 35.- Example of graphic method used to determine the proper matching set of azimuth valves from the four possibilities indicated by magnetometers. Azimuth of probe 2 should be chosen to lie 90° clockwise from the probe 1 value.

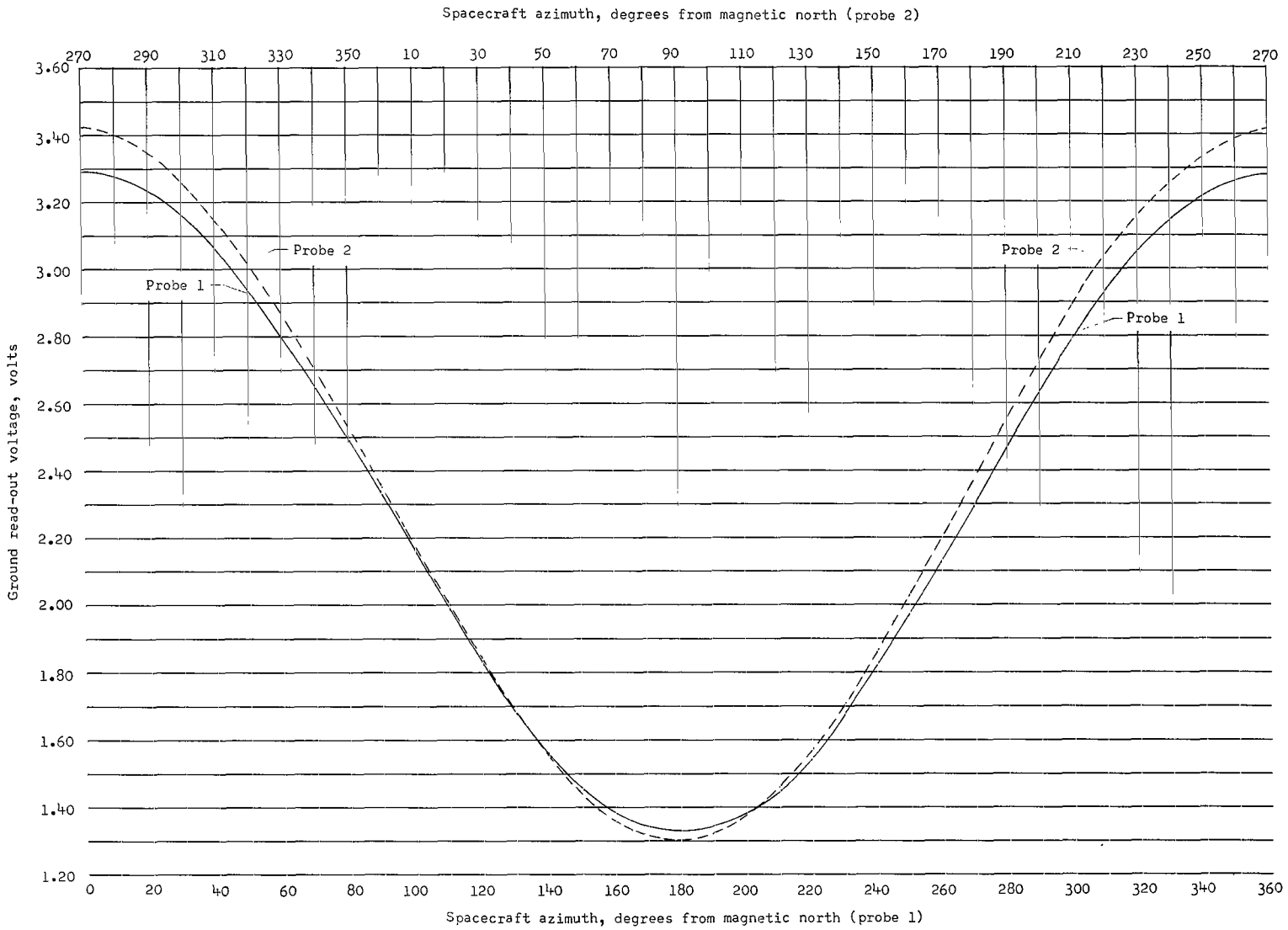

Figure 36.- Calibration curve made during ground checkout for flight data use.

"The aeronautical and space activities of the United States shall be conducted so as to contribute . . . to the expansion of human knowledge of phenomena in the atmosphere and space. The Administration shall provide for the widest practicable and appropriate dissemination of information concerning its activities and the results thereof."

—NATIONAL AERONAUTICS AND SPACE ACT OF 1958

NASA SCIENTIFIC AND TECHNICAL PUBLICATIONS

TECHNICAL REPORTS: Scientific and technical information considered important, complete, and a lasting contribution to existing knowledge.

TECHNICAL NOTES: Information less broad in scope but nevertheless of importance as a contribution to existing knowledge.

TECHNICAL MEMORANDUMS: Information receiving limited distribution because of preliminary data, security classification, or other reasons.

CONTRACTOR REPORTS: Scientific and technical information generated under a NASA contract or grant and considered an important contribution to existing knowledge.

TECHNICAL TRANSLATIONS: Information published in a foreign language considered to merit NASA distribution in English.

SPECIAL PUBLICATIONS: Information derived from or of value to NASA activities. Publications include conference proceedings, monographs, data compilations, handbooks, sourcebooks, and special bibliographies.

TECHNOLOGY UTILIZATION PUBLICATIONS: Information on technology used by NASA that may be of particular interest in commercial and other non-aerospace applications. Publications include Tech Briefs, Technology Utilization Reports and Notes, and Technology Surveys.

Details on the availability of these publications may be obtained from:

SCIENTIFIC AND TECHNICAL INFORMATION DIVISION

NATIONAL AERONAUTICS AND SPACE ADMINISTRATION

Washington, D.C. 20546